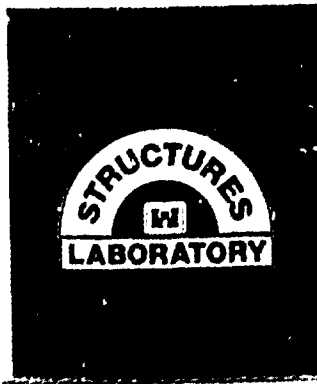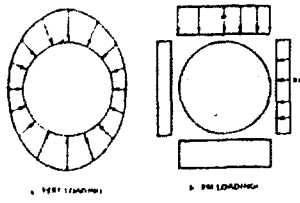TECHNICAL REPORT SL-80-4

# STRENGTH DESIGN OF REINFORCED CONCRETE HYDRAULIC STRUCTURES

## Report 7
## STRENGTH OF CIRCULAR REINFORCED CONCRETE CONDUITS, ANALYSIS AND DESIGN

by

Kurt H. Gerstle

Department of Civil, Environmental
and Architectural Engineering
University of Colorado
Boulder, Colorado   80302

**US Army Corps of Engineers**

AD-A199 894

DTIC
ELECTE
OCT 3 1 1988
S    D
H

September 1988

Report 7 of a Series

88 10 31 085

# REPORT DOCUMENTATION PAGE

Form Approved
OMB No 0704-0188
Exp Date Jun 30 1986

| 1a REPORT SECURITY CLASSIFICATION | 1b RESTRICTIVE MARKINGS |
|---|---|
| Unclassified | |

| 2a SECURITY CLASSIFICATION AUTHORITY | 3 DISTRIBUTION/AVAILABILITY OF REPORT |
|---|---|
| | Approved for public release; |
| 2b DECLASSIFICATION/DOWNGRADING SCHEDULE | distribution unlimited. |

| 4 PERFORMING ORGANIZATION REPORT NUMBER(S) | 5 MONITORING ORGANIZATION REPORT NUMBER(S) |
|---|---|
| | Technical Report SL-80-4 |

| 6a NAME OF PERFORMING ORGANIZATION | 6b OFFICE SYMBOL (If applicable) | 7a NAME OF MONITORING ORGANIZATION |
|---|---|---|
| University of Colorado | | USAEWES Structures Laboratory |

| 6c ADDRESS (City, State, and ZIP Code) | 7b ADDRESS (City, State, and ZIP Code) |
|---|---|
| Boulder, CO 80302 | PO Box 631 Vicksburg, MS 39180-0631 |

| 8a NAME OF FUNDING/SPONSORING ORGANIZATION | 8b OFFICE SYMBOL (If applicable) | 9 PROCUREMENT INSTRUMENT IDENTIFICATION NUMBER |
|---|---|---|
| US Army Corps of Engineers | | |

| 8c ADDRESS (City, State, and ZIP Code) | 10 SOURCE OF FUNDING NUMBERS | | | |
|---|---|---|---|---|
| | PROGRAM ELEMENT NO | PROJECT NO | TASK NO | WORK UNIT ACCESSION NO |
| Washington, DC 20314-1000 | | | | |

11 TITLE (Include Security Classification)
Strength Design of Reinforced Concrete Hydraulic Structures; Strength of Circular Reinforced Concrete Conduits - Analysis and Design

12 PERSONAL AUTHOR(S)
Gerstle, Kurt H.

| 13a TYPE OF REPORT | 13b TIME COVERED | 14 DATE OF REPORT (Year, Month, Day) | 15 PAGE COUNT |
|---|---|---|---|
| Report 7 of a series | FROM Dec 86 TO Aug 87 | September 1988 | 106 |

16 SUPPLEMENTARY NOTATION
Available from National Technical Information Service, 5285 Port Royal Road, Sringfield, VA 22161.

| 17 | COSATI CODES | | 18 SUBJECT TERMS (Continue on reverse if necessary and identify by block number) |
|---|---|---|---|
| FIELD | GROUP | SUB-GROUP | Circular conduits          Strength design |
| | | | Hydraulic structures |
| | | | Reinforced concrete |

19 ABSTRACT (Continue on reverse if necessary and identify by block number)

Various analytical and experimental aspects of the US Army Engineer Waterways Experiment Station concrete pipe test program were studied in an effort to maximize the returns from this project.

Methods of flexural strength prediction, based on both elastic and plastic approaches, are presented and applied to the test specimens. Different approaches to determination of flexural strength are critically discussed, and the applicability of each approach is checked by comparison with test results.

Graphical longhand design methods and uses are presented and explained by examples. These approaches are intended to provide the basis for future computerized design tools.

The shear strength of concrete rings under various loading conditions is explored, using several available methods. Since these methods seem unable to predict the shear

(Continued)

| 20 DISTRIBUTION/AVAILABILITY OF ABSTRACT | 21 ABSTRACT SECURITY CLASSIFICATION |
|---|---|
| ☒ UNCLASSIFIED/UNLIMITED ☐ SAME AS RPT ☐ DTIC USERS | Unclassified |

| 22a NAME OF RESPONSIBLE INDIVIDUAL | 22b TELEPHONE (Include Area Code) | 22c OFFICE SYMBOL |
|---|---|---|
| | | |

**DD FORM 1473, 84 MAR**      83 APR edition may be used until exhausted
All other editions are obsolete

19. ABSTRACT (Continued).

strength of rings under distributed loads, the need for further study along these lines might be helpful. However, the apparent fact that shear will not be critical in concrete pipe in the ground may deem this in fact a "nonproblem."

Further necessary research directions for optimal design of concrete pipe are noted.

PREFACE

This study was conducted during the period December 1986 through August 1987 by the Department of Civil, Environmental, and Architectural Engineering (CEAE), University of Colorado, under the sponsorship of Headquarters, US Army Corps of Engineers (HQUSACE). The Technical Monitor was Dr. Tony Liu.

This work was monitored by the US Army Engineer Waterways Experiment Station (WES) under the supervision of Messrs. Bryant Mather, Chief, Structures Laboratory (SL), James T. Ballard, Assistant Chief, SL; and Dr. Jimmy P. Balsara, Chief, Structural Mechanics Division (SMD), SL. Dr. Robert L. Hall, SMD, monitored the study. Mr. Stanley C. Woodson, SMD, coordinated the publication of the work with final editing by Mmes. Gilda Miller and Chris Habeeb, Information Products Division, Information Technology Laboratory, WES.

Dr. Kurt H. Gerstle, CEAE, was the Principal Investigator. Dr. Nevis Cook, CEAE, and Mr. Hik Peng Lim, Graduate Assistant, CEAE, completed many of the calculations and prepared computer programs used in the analysis. Mr. Russ Preuit, Chief Engineer, American Concrete Pipe Association, Vienna, Virginia, provided valuable advice and reference material.

COL Dwayne G. Lee, EN, is Commander and Director of WES. Dr. Robert W. Whalin is Technical Director.

1

## CONTENTS

CONVERSION FACTORS, NON-SI TO SI (METRIC)
UNITS OF MEASUREMENT

Non-SI units of measurement used in this report can be converted to SI
(metric) units as follows:

| Multiply | By | To Obtain |
|---|---|---|
| degrees (angle) | 0.01745329 | radians |
| feet | 0.3048 | metres |
| inches | 25.4 | millimetres |
| kips (force) | 4.448222 | kilonewtons |
| kip-inches | 112.9848 | newton-metres |
| kips (force) per inch | 0.1751269 | kilonewtons per millimetre |
| kips (force) per square inch | 6.894757 | kilopascals |
| kips (force) per square foot | 47.88026 | megapascals |
| pounds per square inch | 0.006894757 | megapascals |
| square inches | 6.4516 | square centimetres |

STRENGTH OF CIRCULAR REINFORCED CONCRETE CONDUITS
ANALYSIS AND DESIGN

PART I: INTRODUCTION

1. The series of reinforced concrete rings tested under applied radial loads at the US Army Engineer Waterways Experiment Station (WES) provided a large amount of experimental data about the behavior of such structures under load. In an effort to maximize the returns from this test series, an earlier analytical study (Gerstle 1985) attempted to explain the ring response by use of finite element analysis. That report also contained suggestions for applying limit, or plastic, analysis for strength prediction and as a possible design tool.

2. Following Gerstle (1985), the goals of the present study were initially set as follows:

a. To provide the theoretical basis for determination of the strength of circular reinforced concrete culvert sections on the basis of plastic theory.

b. To verify the applicability of this method by comparison of analytical predictions with results of the WES test program.

c. To develop design methods based on a and b, leading to simple procedures suitable for office practice using longhand design aids or computer programs.

3. During a meeting in March 1987, the thrust of the study was slightly changed. Not only the plastic approach, but also elastic methods were to be studied for applicability to the prediction of flexural strength of rings under load and as design tools. Further, shear strength was identified as a major problem to be studied within the scope of this report. Accordingly, the results of the study are presented in the following sequence:

a. Part II covers plastic, or limit, analysis of concrete rings under external loads, along with ductility considerations.

b. Part III is the elastic counterpart of Part II, laying the bases for elastic analysis as well as for the deflection calculations necessary for ductility determination.

c. Part IV uses the methods outlined in the first two parts to compare strength predictions with data from the WES test program. It also contains a critical comparison of the different analysis methods.

d. Part V uses the concepts of Parts II and III to develop tools for flexural design of rings under distributed loads. While in current form these are graphical longhand design methods, and the intent is to outline computer approaches to be implemented at a future time.

e. Part VI considers shear strength of these rings. Available methods from the literature are applied, and a number of conclusions of theoretical and practical interest are drawn.

f. Part VII summarizes the work, draws conclusions, and contains suggestions for further study to arrive at optimal design of pipe structures.

PART II: LIMIT ANALYSIS OF RINGS

## Strength of Rings

### General approach

4. Rings tested at WES collapsed in general by discrete hinge formation at critical sections (Wright and Chiarito 1987). Plastic analysis assuming hinge formation at crown and springing sections (Hodge 1959) (Figure 1) appears to be a useful approach to the rational determination of the collapse loads on these rings.

5. Because of the simplicity of this method, the effect of various parameters such as geometric proportions, steel content, and load distribution can be easily explored. It may also offer a straightforward design approach, which is the goal of this study.

6. Plastic analysis as suggested here presumes ductile failure. If this assumption is not satisfied, the plastic collapse load provides an upper bound, or unsafe overestimation, of the actual ring strength. A ductility check must be an integral part of the analysis.

7. Plastic analysis must satisfy two basic conditions:

   a. The lower-bound theorem: Equilibrium must be satisfied without exceeding section strength at any point, which means, "if the structure can stand up, it will."

   b. The upper-bound theorem: The member strength must be reached at a sufficient number of sections to permit collapse, which means, "if the structure can collapse, it will."

8. A correct solution must satisfy both lower- and upper-bound theorems. These aspects, equilibrium, member strength, and structure strength, will be considered separately in the following paragraphs.

### Equilibrium

9. Two distinct loading conditions must be considered here: the radial jack loads applied during the WES tests, for purposes of verification of the approach, and the loads prescribed in Engineer Manual (EM) 1110-2-2902 (Headquarters, Department of the Army 1969) which are to be used for the design of culvert sections. The former of these two loading conditions can be handled as a special case of the latter, as shown in the next paragraphs.

10. The loading (EM 1110-2-2902) (referred to herin as EM loading) consists of uniform vertical pressure, $w$ , and uniform lateral pressure,
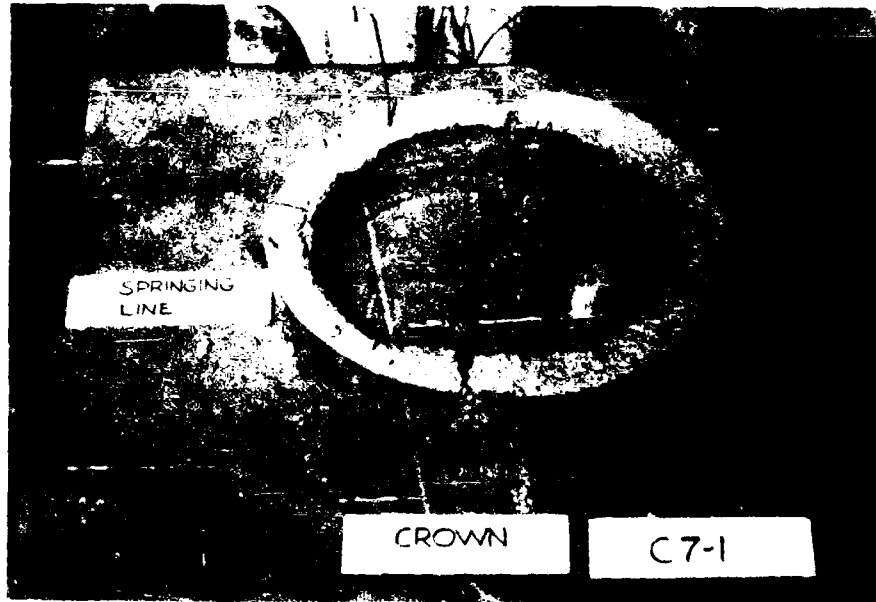
a. WES test specimen
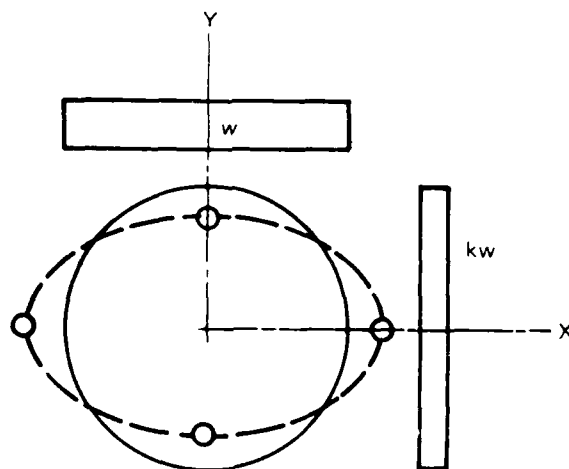


b. Collapse mechanism

Figure 1. Plastic ring collapse

7

$k \cdot w$ , as shown in Figure 2. The radial, or normal pressure, variation on the ring due to both loads is, according to calculations shown in Appendix A,

$$p_N = \frac{w}{2} [(1 + k) - (1 - k) \cos 2\theta] \qquad (1)$$

where

$p_N$ = radial pressure acting on unit length of ring

$k$ = ratio of lateral earth pressure to vertical earth pressure

and the tangential, or shear, traction on the ring is

$$p_T = \frac{w}{2} (1 - k) \sin 2\theta \qquad (2)$$

where

$p_T$ = tangential traction acting on a unit length of ring

$w$ = uniform vertical pressure

The distributions of the load components along the ring are shown in Figure 3.
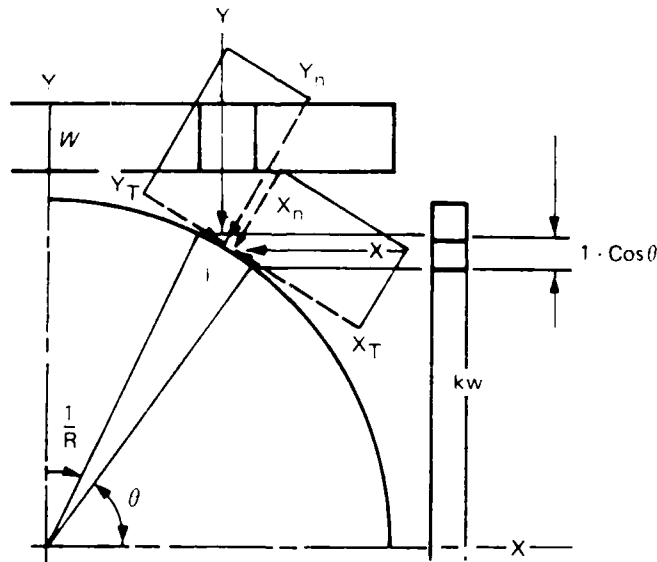


Figure 2. Loads

11. The vertical and horizontal resultants of the radial pressure, $p_N$ , on the quarter ring and, therefore, the axial forces, $N_{sp}$ and $N_{cr}$ , on the springing and crown sections, due to the radial pressure only (the test

8
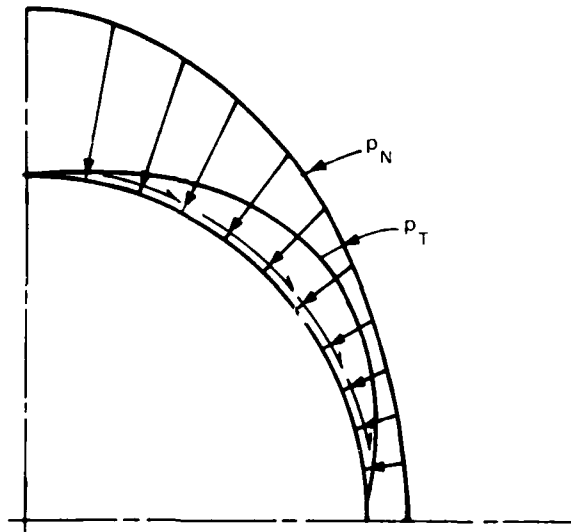
Figure 3. Surface tractions

loading) are, by integration of the Y- and X-components of $p_N$,

$$N_{sp}^N = \frac{wR}{3} (2 + k) = \frac{8}{3\pi} P_{cr} (2 + k) \tag{3a}$$

$$N_{cr}^N = \frac{wR}{3} (2k + 1) = \frac{8}{3\pi} P_{cr} (2k + 1) \tag{3b}$$

where

$N_{sp}$ = internal thrust at springing acting on a cross section of width b , pounds/foot

R = outer radius of conduit

$P_{cr}$ = concentrated crown load in a 16-point test loading, pounds

12. In Equations 1 through 3, the concentrated crown load $P_{cr}$ for the 16-point test loading is calculated by multiplying the distributed load w by the tributary length $2\pi R/16$ .

13. The vertical and horizontal resultants of the tangential tractions, $p_T$ , on the quarter ring and, therefore, the axial springing and crown forces, due to these shears, are

$$N_{sp}^T = \frac{wR}{3} (1 - k) \tag{4a}$$

9

$$N^T_{cr} = \frac{wR}{3}(k - 1) \tag{4b}$$

where

T = tangential component of $N_{sp}$ or $N_{cr}$

$N_{cr}$ = internal thrust at springing acting on a cross section of width b , pound/foot

The sums of Equations 3 and 4 are the axial forces at these sections under EM loading

$$N^N_{sp} + N^T_{sp} = wR \tag{5a}$$

$$N^N_{cr} + N^T_{cr} = k \cdot wR \tag{5b}$$

14. Referring to the free body of Figure 4a of the quarter ring under loads set forth in EM 1110-2-2902, moment equilibrium requires that

$$M_{cr} + M_{sp} = \frac{wR^2}{2}(1 - k) \tag{6}$$

where

$M_{cr}$ = internal moment at crown acting on a cross section of width b , foot pounds/foot

$M_{sp}$ = internal moment at springing acting on a cross section of width b , foot pounds/foot

For radial components only, applied in the test loading, moment equilibrium of the free body of Figure 4b requires that

$$M_{cr} + M_{sp} = \frac{wR^2}{3}(1 - k) = \frac{8}{3\pi} \cdot P_{cr} R(1 - k) \tag{7}$$

15. Any solution, elastic or inelastic, must satisfy Equations 3 and 7 for the test loading, and Equations 5 and 6 for the loading specified in EM 1110-2-2902.

10

a.  EM loading                          b.  Test loading
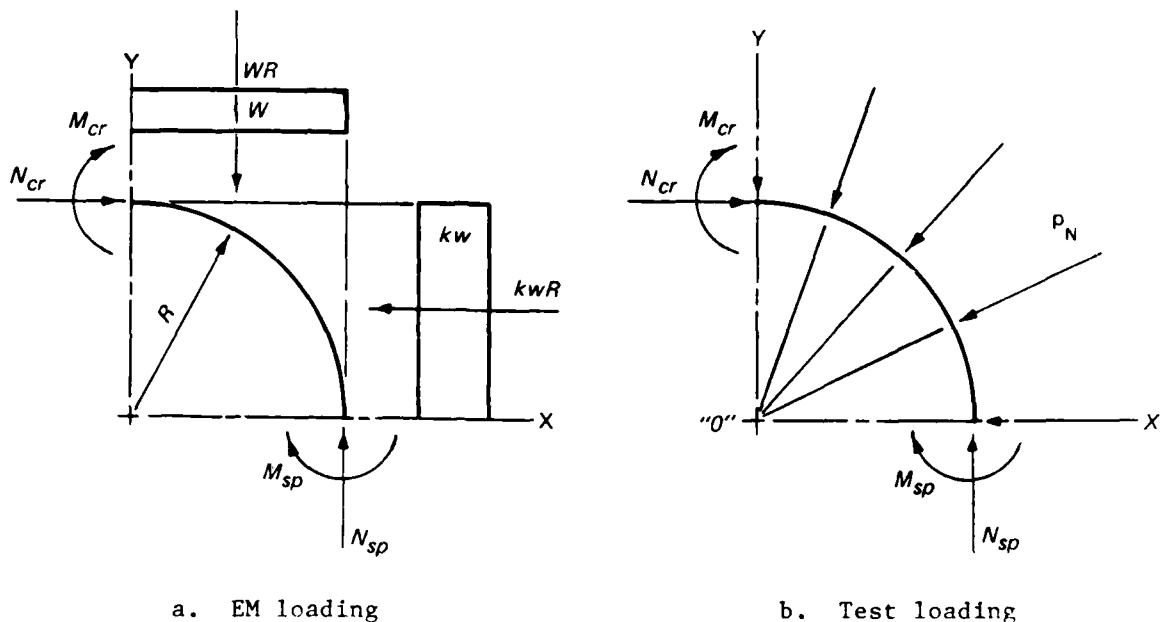
Figure 4.  Free bodies

## Section strength

16.  The strength of reinforced concrete sections of specified materials
under axial force and moment, as in these rings, can be determined by well
known methods of structural mechanics, assuming uniaxial stress states and
plane sections (Park and Paulay 1975).  The effects of initial curvature of
these rings, which leads to a nonlinear strain distribution across the sec-
tion, have been considered for these rings (Chiarito and Mlakar (1984)).  It
was concluded that initial curvature is a minor effect which can be ignored in
the analysis of these rings.

17.  Such analyses lead to strength interaction envelopes as shown in
Figure 5a covering section strength under conditions ranging from pure axial
force to pure bending.  The balance point separates the regime in which fail-
ure is initiated by brittle compressive concrete crushing, labeled "compres-
sion failure," from the regime where yielding of the tension steel precedes
concrete crushing, or "tension failure."

18.  The upper-bound theorem states that collapse will occur when the
moment-axial force combinations at the crown and springing sections satisfying
equilibrium lie on the strength envelope of Figure 5a.

11
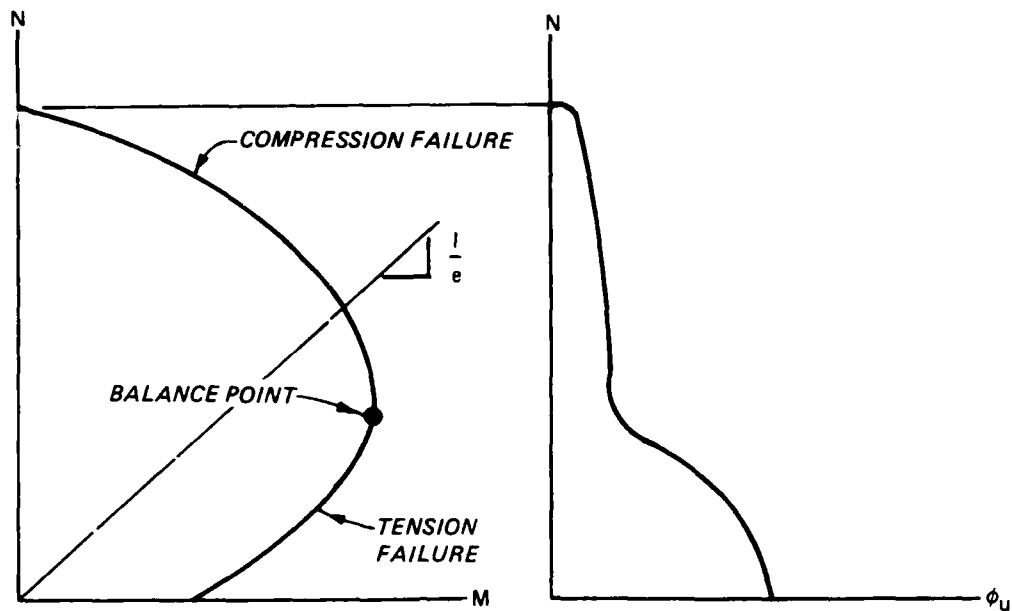
a. Strength envelope          b. Ultimate curvature

Figure 5. Section strength and ductility

19. For the specimens tested under the WES program, such interaction curves are available (Wright and Chiarito 1987). For design purposes, it will be necessary to establish dimensionless strength curves, similar to those provided by the American Concrete Institute (ACI) (1985).

## Ring strength

20. This study considers only the plastic strength of rings under the radial test loading, since the current results will serve only the purpose of verification by comparison with results of the WES test series. Procedures for loading (EM 1110-2-2902) will be entirely analogous.

21. According to the upper-bound theorem of plasticity, a proper solution for the collapse load must satisfy equilibrium and strength conditions.

22. Equilibrium requires, from Equations 3a and 3b,

$$N_{sp} = \frac{8}{3\pi} (2 + k)P_{cr} \qquad (8a)$$

$$N_{cr} = \frac{8}{3\pi} (2k + 1)P_{cr} \qquad (8b)$$

12

where $P_{cr}$ is the force exerted by the crown jack of the 16-jack test apparatus. Collapse loads, discussed by Wright and Chiarito (1987), are given in terms of $P_{cr}$.

23. Moment equilibrium according to Equation 7 requires that

$$M_{sp} + M_{cr} = \frac{8}{3\pi} (1 - k) P_{cr} R \qquad (9)$$

24. The axial force $N_{sp}$ and the moment $M_{sp}$, at the springing, and $N_{cr}$ and $M_{cr}$, at the crown, must fall on the strength envelope at the instant of plastic collapse. Satisfaction of these conditions requires a trial-and-error procedure, for which the following average quantities are introduced:

$$N_{avg} = \frac{1}{2} (N_{sp} + N_{cr}) \qquad (10)$$

where $N_{avg}$ is average of internal thrust at springing and crown acting on cross section of width $b$, pounds/foot, and

$$M_{avg} = \frac{1}{2} (M_{sp} + M_{cr}) \qquad (11)$$

where $M_{avg}$ is average of internal moments at springing and crown acting on a cross section of width $b$, foot pounds/feet.

25. Substituting Equations 3 and 7 into Equations 10 and 6 and dividing Equation 11 by Equation 10, we get the average eccentricity $(e_{avg})$

$$e_{avg} = \frac{M_{avg}}{N_{avg}} = \frac{1}{3}\left(\frac{1 - k}{1 + k}\right) \cdot R \qquad (12)$$

where $e_{avg}$ is eccentricity based on average of moment and thrust values at crown and springing.

26. Equations 3 and 10 permit expression of the axial forces and the crown load at collapse in terms of the average force $N_{avg}$:

$$N_{sp} = \frac{2}{3}\left(\frac{2 + k}{1 + k}\right)N_{avg} \qquad (13)$$

13

$$N_{cr} = \frac{2}{3}\left(\frac{2k+1}{1+k}\right)N_{avg} \qquad (14)$$

$$P_{cr} = \frac{\pi}{4}\left(\frac{1}{1+k}\right)N_{avg} \qquad (15)$$

27. With given strength envelope, Equations 12 through 15 permit solution for the collapse load by graphical or iterative means, as is illustrated in the cases listed in the following paragraphs.

Straight-line strength envelope

28. If the relevant region of the strength envelope is a straight line, as shown in Figure 6, these steps should be taken:

   a. Draw the radial line of slope $1/e_{avg}$ , using Equation 12, from the origin and intersect it with the straight-line strength envelope at point $(N_{avg}$ , $M_{avg})$. The force-moment combinations at springing and crown, as calculated from Equations 11, 13, and 14 and shown in Figure 6, lie on the linear strength envelope.

   b. Compute the collapse load $P_{cr}$ by Equation 15.

Curved strength envelope

29. In the more common case where the strength envelope is curved (Figure 7), an iterative approach is needed, and these steps should be taken:

   a. Draw the radial line of slope $1/e_{avg}$ from the origin, using Equation 12. The point $(N_{avg}$ , $M_{avg})$ will lie at an unknown location along this line, not necessarily on the strength envelope. The points $(N_{sp}$ , $M_{sp})$ and $(N_{cr}$ , $M_{cr})$ form the intercepts with the strength envelope of a straight line with midpoint on the point $(N_{avg}$ , $M_{avg})$. These intercept points must satisfy two conditions:

   (1) N-coordinates must satisfy Equations 13 and 14.

   (2) M-coordinates must be equidistant from the $M_{avg}$ coordinate.

   b. Assume a point $(N_{avg}$ , $M_{avg})$ on the radial line of slope $1/e_{avg}$ drawn in step a. Mark the points on the strength envelope satisfying condition a, and connect them with a straight line. If this line passes through the point $(N_{avg}$ , $M_{avg})$, condition b is also satisfied and the collapse load $P_{cr}$ can be determined by Equation 15.
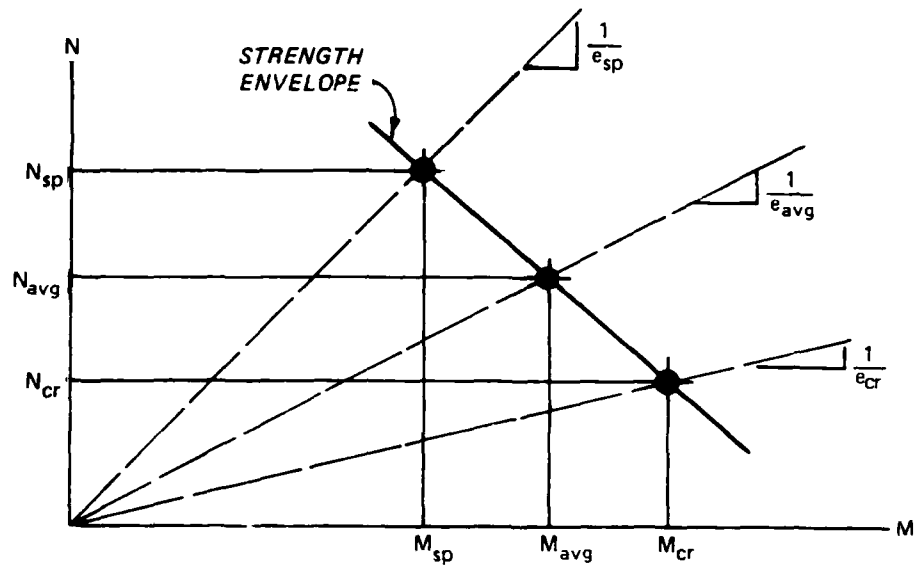
Figure 6.  Ring strength, straight-line strength envelope
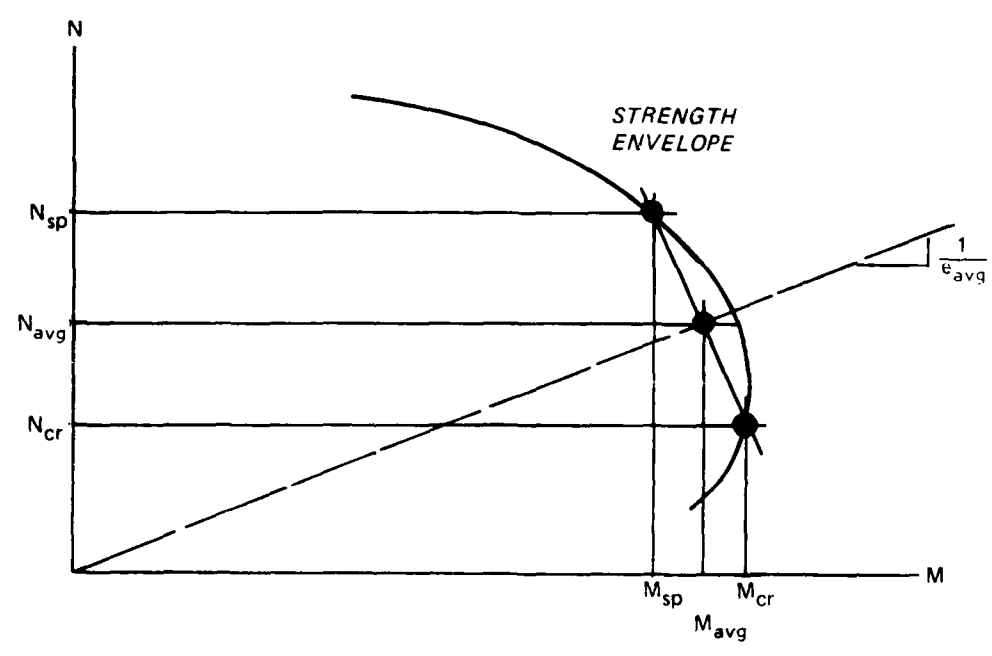


Figure 7.  Ring strength, curved strength envelope

15

<u>c</u>. In the more common case when the straight-line segment connecting the intercepts does not pass through the point ($N_{avg}$, $M_{avg}$), take the intersection with the radial line of slope $1/e_{avg}$ as the new point ($N_{avg}$, $M_{avg}$), and repeat step b.

<u>d</u>. Repeat step c to convergence, and determine the collapse load $P_{cr}$ by Equation 15.

30. One or two iterations are usually sufficient for engineering accuracy. A convenient way of satisfying the equilibrium conditions of step a and strength conditions of step b graphically is illustrated in Figure 8, which uses radial lines of slopes $N_{sp}/N_{avg} \cdot 1/e_{avg}$ and $N_{cr}/N_{avg} \cdot 1/e_{avg}$ to satisfy Equations 13 and 14.
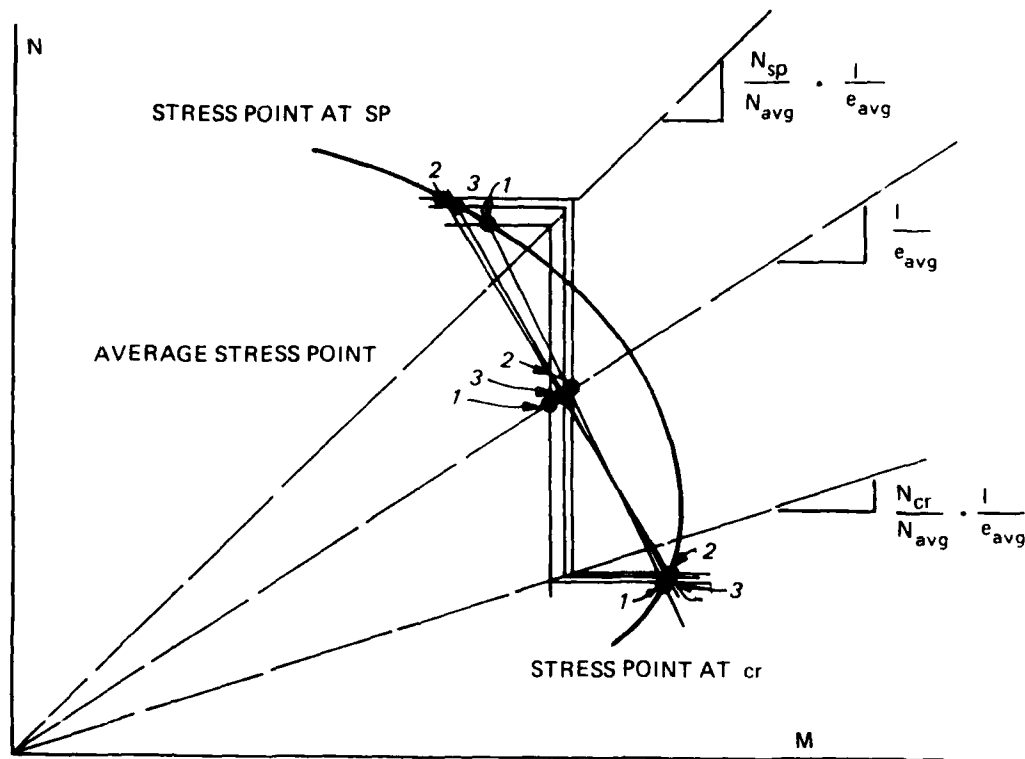


Figure 8. Graphical solution technique

Example 1

31. Model 2-1 of the WES test series (Wright and Chiarito 1987), is a thick ring under a load of ratio $k = 1/3$. The strength envelope shown in Figure 9 is based on straight-beam theory. All graphical and numerical

$$\frac{N_{sp}}{N_{avg}} \cdot \frac{1}{e_{avg}}$$

$$\frac{1}{e_{avg}}$$

$$\frac{N_{cr}}{N_{avg}} \cdot \frac{1}{e_{avg}}$$

R = 7.47 in.

k = 1/3

Equation 12:  $e_{avg} = 1.25$ in.

Equation 13:  $N_{sp} = 1.167 \, N_{avg}$

Equation 14:  $N_{cr} = 0.833 \, N_{avg}$

Equation 15:  $P_{cr} = 0.589 \, N_{avg}$

$$\frac{N_{sp}}{N_{cr}} = 1.40$$

| $N_{avg}^k$ | $N_{sp}^k$ | $N_{cr}^k$ | $P_{cr}^k$ |
|---|---|---|---|
| 48 | 56.0 | 40.0 | |
| 49 | 57.2 | 40.8 | 28.8 |

Figure 9.   Strength analysis, specimen 2-1,
straight-beam strength envelope

17

calculations are shown in Figure 9. Only one iteration is required to attain the collapse load to within an accuracy of 0.1 kip.*

## Separate strength envelopes for crown and springing

32. In the WES study (Wright and Chiarito 1987), curved-beam theory was followed to evaluate the section strengths, leading to different strength envelopes for the springing (tension outside) and the crown (tension inside), as shown in the following example. The same approach as in the preceding case applied here, but now using the appropriate strength envelope for each section.

## Example 2

33. Model 2-1 of the WES test series is again considered, now using the two different strength envelopes for springing and crown sections given by Wright and Chiarito (1987), and shown in Figure 10. Again, only one iteration (Figure 10) is needed.

## Comparison of results of straight- and curved-beam strengths

34. Comparing the results of the preceding examples, using the single straight-beam strength envelope, the failure load is $P_{cr}$ = 28.8 kips; and using the two separate curved-beam strength envelopes, the failure load is $P_{cr}$ = 29.2 kips, a difference of 1.4 percent is found. It appears that use of section strength based on straight-beam theory is adequate for design purposes, as already predicted by Chiarito and Mlakar (1984). Further analysis and design procedures will be based on single envelopes based on conventional straight-beam reinforced concrete theory.

## Ductility

35. The plastic theory presumes that the hinging sections have enough rotation capacity to permit redistribution of internal forces without premature brittle failure. This requires that the available ductility equals or exceeds the rotation required to permit formation of the last hinge leading to collapse.

---

* A table of factors for converting non-SI units of measurement to SI (metric) units is presented on page 3.
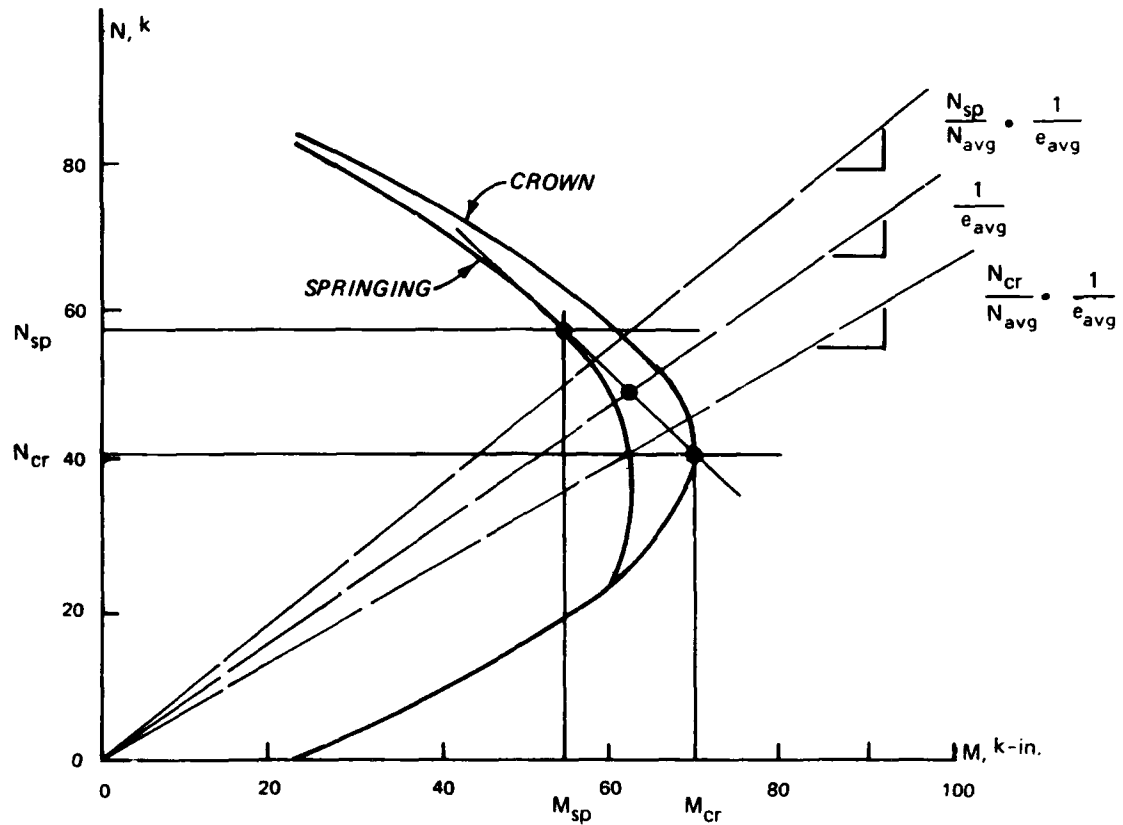
$$R = 7.47 \text{ in.} \quad \text{Equation 12:} \quad e_{avg} = 1.25 \text{ in.}$$

$$k = 1/3 \quad \text{Equation 13:} \quad N_{sp} = 1.167\, N_{avg}$$

$$\text{Equation 14:} \quad N_{cr} = 0.833\, N_{avg}$$

$$\text{Equation 15:} \quad P_{cr} = 0.589\, N_{avg}$$

| $N^k_{avg}$ | $N^k_{sp}$ | $N^k_{cr}$ | $P^k_{cr}$ |
|-------------|------------|------------|------------|
| 49          | 57.2       | 40.8       |            |
| 49.5        | 57.7       | 41.2       | 29.2       |

Figure 10. Strength analysis, specimen 2-1,
curved-beam strength envelopes

36.  The available ductility at a section is plotted in Figure 5b in terms of the ultimate curvature, or rotation capacity per unit length.  It will be discussed further in the next section.

37.  The rotation demand at each hinge can be computed by a series of piecewise-linear analyses permitting determination of the plastic hinge rotations to be compared to the available rotation capacity.  In the rings under doubly symmetrical loading, plastic hinges may occur at crown and springing sections.  A series of elastic analyses, as outlined in Part III, will lead to load-deflection and load-hinge rotation curves (Figure 11).  These are the hinge rotations which are to be compared to the available rotation capacity. Results of such analyses are presented later.



a.  Load deflection                          b.  Load rotation
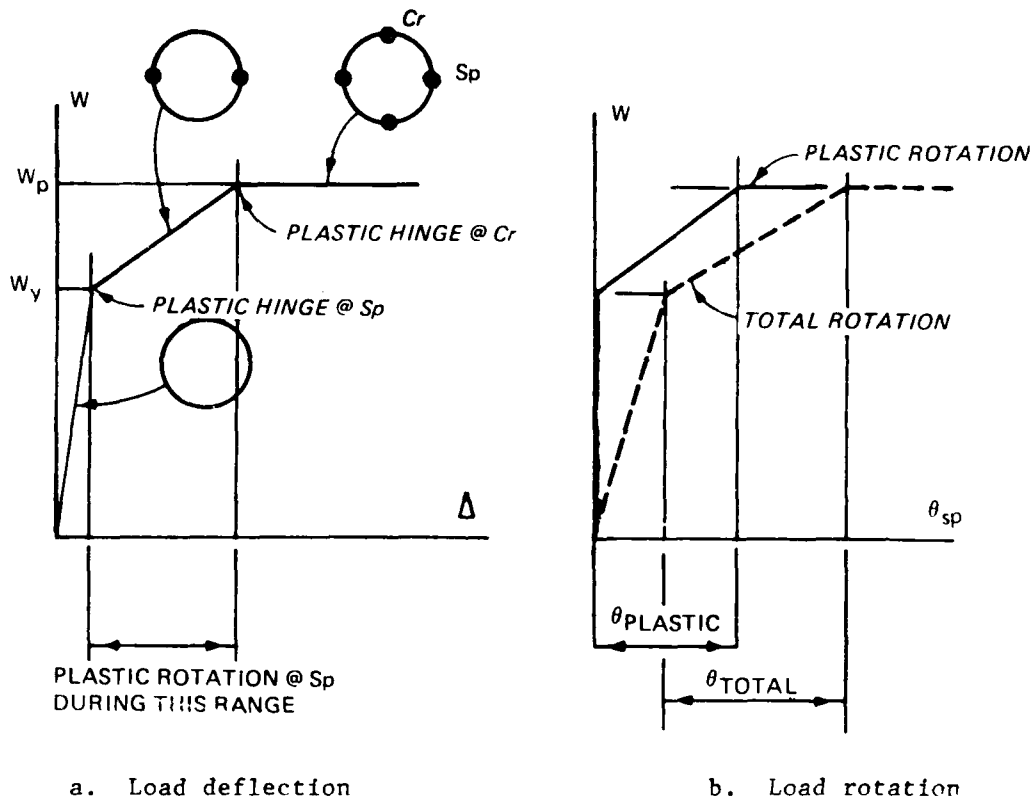
Figure 11.  Piecewise-linear analysis

## Rotation capacity of hinges

38.  The ultimate curvatures shown in Figure 5b were calculated from the strain distribution across the critical section at the instant of compressive concrete crushing due to attainment of the ultimate compressive strain $\varepsilon_u$ , assumed at $\varepsilon_u = 0.003$ .  Thus, assuming plane sections, $\phi_u = \varepsilon_u/c$ , where  c

20

is the distance from the extreme compression fiber to the neutral axis. This rotation capacity per unit length is to be integrated over an effective hinge length to obtain the available rotation capacity of the hinge.

39. A number of empirical methods are available to this end (Park and Paulay 1975), based on tests carried out on straight beams under various moment gradients. The applicability of these results to the case of initially curved members, such as these rings, may be doubted. The presence of a bi-axial stress field due to radial stresses, along with diagonal tension, is likely to have a severe impact on the ductility, as evidenced by many of the failure modes of the rings in the WES test program.

40. Here, based on observation of hinging modes in the WES test specimens, a hinge length equal to the section depth  h  is assumed, so that the rotation capacity of the hinge will be

$$\theta_u = \phi_u \cdot h \tag{16}$$

where

$\theta_u$ = rotation capacity

$\phi_u$ = ultimate curvature

A special test program may be needed to verify and improve on this formulation.

## Rotation demand

41. Results of piecewise-linear analysis for the test loading and for the EM loading will be presented separately. Details of the analysis are presented in Part III.

## Test loading

42. Elastic analysis of the closed ring under test loading ($p_T = 0$), as shown in Part III, results in the springing and crown moments:

$$M_{sp} = - \frac{wR^2}{6} (1 - k) = - \frac{4}{3\pi} P_{cr}R(1 - k)$$

$$\tag{17}$$

$$M_{cr} = + \frac{wR^2}{6} (1 - k) = + \frac{4}{3\pi} P_{cr}R(1 - k)$$

that is, moments at the critical sections are equal in magnitude, a result

21

which seems surprising but is explained in Part III by symmetry of structure and antisymmetry of loading.

43. The axial loads at these critical sections due to the test load are given by Equation 3 as

$$N_{sp}^N = \frac{wR}{3}\ (2 + k) = \frac{8}{3\pi}\ P_{cr}(2 + k)$$

$$(18)$$

$$N_{cr}^N = \frac{wR}{3}\ (2k + 1) = \frac{8}{3\pi}\ P_{cr}(2k + 1)$$

These different axial forces will affect the section strength so that, in spite of the equal moments of Equation 17, unequal section strengths will lead to sequential, rather than simultaneous, hinge formation, as shown in Figure 11. The specifics depend on the shape of the strength envelope, so that each ring will require separate calculation of its ductility demand.

44. For instance, in Figure 12, specimen 2.1 shows the same strength envelope as in Figure 9, along with the stress paths of springing and crown sections. The strength envelope is first reached at the springing, under $N_{sp}$ = 55 kips, corresponding to $P_{cr}$ = 27.9 kips. Plastic rotation of the springing section will occur as the applied load increases from the elastic limit load $P_{cr}$ = 27.8 kips to the collapse load computed in Figure 9 of $P_{cr}$ = 28.8 kips, and is computed in Part III as

$$\Delta\theta_{sp} = \Delta P_{cr} \cdot \frac{R^2}{EI} \cdot \frac{4}{3}\ (1 - k) \qquad (19)$$

According to the calculations of Part III, this results in $\Delta\theta_{sp}$ = 0.20 $\cdot 10^{-3}$ rad. The rotation capacity computed is $3.5 \cdot 10^{-3}$ rad.

45. The movement of the stress point for the springing section along the strength envelope after hinging indicates that, contrary to the analysis assumption, $\Delta M \neq 0$. This secondary effect is neglected in the engineering approach.

46. It appears that, for this ring, the rotation capacity vastly exceeds the demand, so full redistribution might be expected, and the collapse load based on plastic analysis might be realistic. In fact, the observed failure load (Wright and Chiarito 1987) of this ring was 38.5 kips, or

22
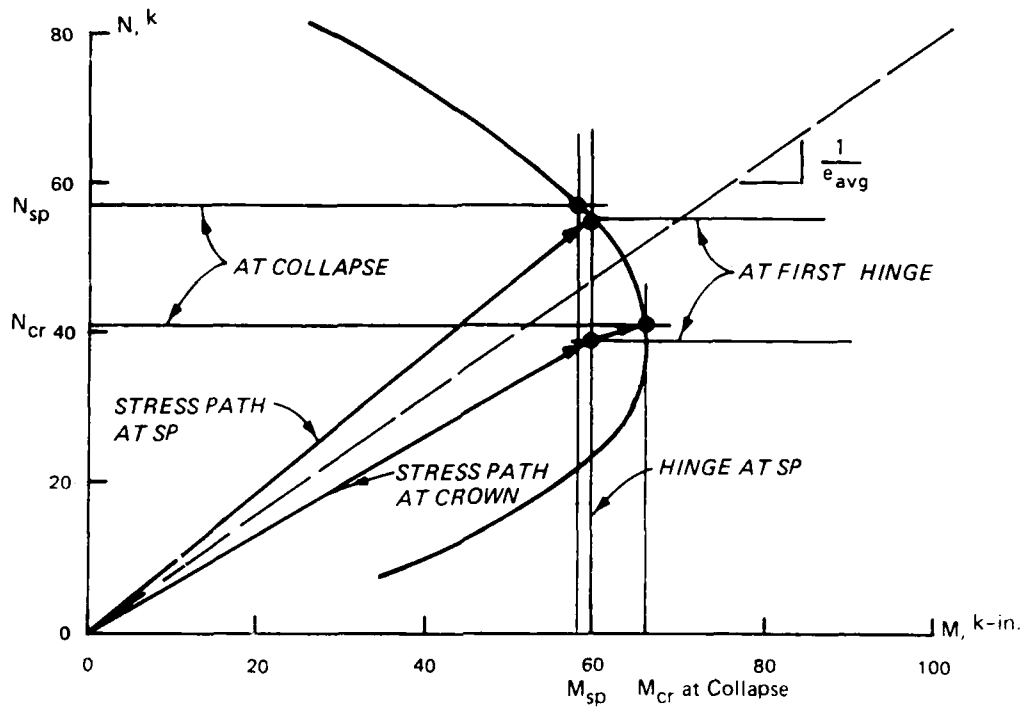
R = 7.47 in.

k = 1/3

Plastic hinge at SP when: $-M_{sp} = +M_{cr} = 59$ k-in.

$$N_{sp} = 55 \text{ k}$$

By Equation 17 or 18:

$$P_{cr} = 27.8 \text{ k}$$

Collapse of ring from Figure 9 when:

$$P_{cr} = 28.8 \text{ k}$$

Figure 12.   Piecewise-linear stress paths at springing
and crown sections

23

34 percent stronger than predicted. It appears that the strength envelope computed by Wright and Chiarito (1987) is conservative.

EM loading

47. The EM loading, according to the elastic analysis of Part III, again results in moments of equal magnitude at springing and crown:

$$M_{sp} = - \frac{wR^2}{4} (1 - k) \tag{20a}$$

$$M_{cr} = + \frac{wR^2}{4} (1 - k) \tag{20b}$$

a conclusion which results from the antisymmetry of loading.

48. The axial loads at these critical sections due to the EM loading are given by Equation 5:

$$N_{sp} = wR \tag{21a}$$

$$N_{cr} = k \cdot wR \tag{21b}$$

and these different axial loads will affect the section strength so that in spite of the equal moments given by Equations 20a and 20b, unequal section strengths will lead to sequential hinge formation. The calculations in Part III indicate a rotation demand at the springing section of

$$\Delta\theta_{sp} = \Delta w \cdot \frac{R^3}{EI} \cdot \frac{5\pi}{6} (1 - k) \tag{22}$$

49. The steps necessary for comparison of rotation capacity and rotation demand are identical to those considered for the test loading.

24

PART III:  ELASTIC ANALYSIS AND DEFORMATIONS OF RINGS

## Introduction

50.  In Part II it is noted that elastic analysis is necessary for ductility calculations, even if not for perfectly plastic strength determination. Further, with the availability of efficient computer programs for elastic analysis of arbitrary structures (Harter, Bricher, and Wilson 1980), the earlier work done on elastic analysis and design of culvert shapes (Anderson, Haelsig, and Reifel 1966), and the precedent set by ACI (1983) in its strength design method (which will be discussed further in Part IV), it seems appropriate to explore elastic analysis of these rings.

51.  In this part, the prismatic elastic rings under radial (test) loading and EM 1110-2-2902 loading (Headquarters, Department of the Army 1969) are considered to stress the simplicity of the solution of this case and to make available results for use in Part II (ductility), Part IV (comparison), and Part VI (shear strength).

## Elastic Analysis of Rings Under Doubly Symmetric Loads

52.  For this analysis, the consideration is a circular ring subjected to load which is symmetric about the X- and Y-axes shown in Figure 13a for the first quadrant.  This load can be decomposed into a rotationally symmetric, or hydrostatic, part (Figure 13b), and the remaining part, symmetric with respect to the X- and Y-axes or antisymmetric with respect to the 45-deg axes (Figure 13c).  The latter will be called the "antisymmetric part" in the text that follows.

53.  Due to the hydrostatic part, moment and shear are zero.  The axial force due to this loading is constant:

$$N_{Hydro} = \frac{wR}{2} (1 + k) \qquad (23)$$

54.  Due to the antisymmetric part, the moments at the springing ($\theta = 0$) and at the crown ($\theta = 90°$) must be equal in magnitude and opposite in

25
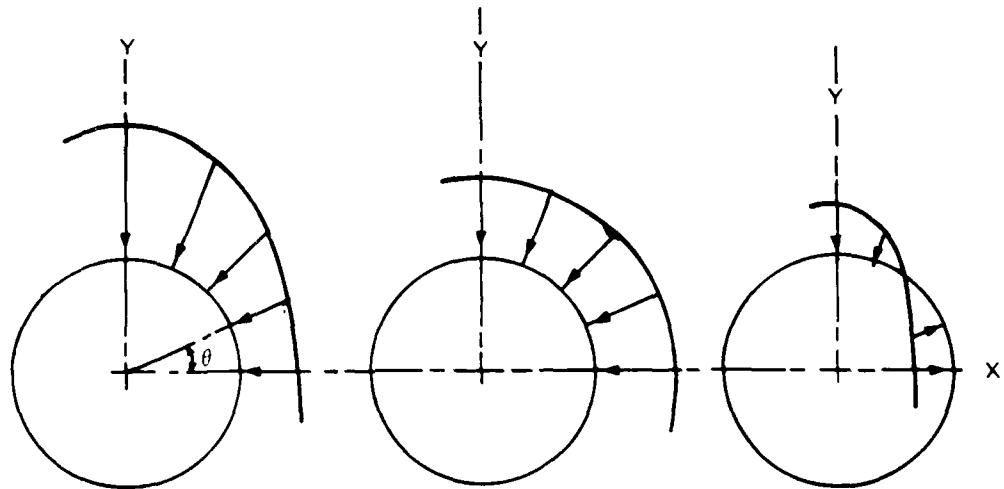
$$p_{Total} = p_{Hydrostatic} + p_{Antisymmetric}$$

For test loading:

$$p = \frac{w}{2}\left[(1 + k) - (1 - k)\cos 2\theta\right] = \frac{w}{2}(1 + k) \qquad - \frac{w}{2}(1 - k)\cos 2\theta$$

For EM loading:

$$p_N = \frac{w}{2}\left[(1 + k) - (1 - k)\cos 2\theta\right] = \frac{w}{2}(1 + k) \qquad - \frac{w}{2}(1 - k)\cos 2\theta$$

$$p_T = \frac{w}{2} \cdot (1 - k)\sin 2\theta = 0 \qquad + \frac{w}{2}(1 - k)\sin 2\theta$$

Figure 13. Decomposition of load

26

direction, that is, $M_{sp} = M_{cr}$ . Invoking the equilibrium Equation 7 for test loading, it follows that

$$M_{cr} + M_{sp} = 2M_{cr} = 2M_{sp} = \frac{wR^3}{3} (1 - k)$$

or

$$M_{cr} = M_{sp} = \frac{wR^2}{6} (1 - k) \tag{24}$$

Similarly, Equation 6 for EM loading results in

$$M_{cr} = M_{sp} = \frac{wR^2}{4} (1 - k) \tag{25}$$

55.  With these redundants determined by considerations of equilibrium and symmetry, the internal forces along the ring can be found by statics alone.  Using appropriate free bodies, the following result (Anderson, Haelsig and Reifel 1966):

Test loading:

$$N = \frac{wR}{2} \left[ (1 + k) + \frac{1}{3} (1 - k) \cos 2\theta \right] \tag{26}$$

$$V = \frac{wR}{3} (1 - k) \sin 2\theta \tag{27}$$

$$M = \frac{wR^2}{6} (1 - k) \cos 2\theta \tag{28}$$

EM loading:

$$N = \frac{wR}{2} \left[ (1 + k) + (1 - k) \cos 2\theta \right] \tag{29}$$

27

$$V = \frac{wR}{2} (1 - k) \sin 2\theta \qquad (30)$$

$$M = \frac{wR^2}{4} (1 - k) \cos 2\theta \qquad (31)$$

In both cases, because of antisymmetry, the maximum shear occurs at $\theta = 45$ deg, and maximum moments occur at $\theta = 0$ deg and $\theta = 90$ deg.

## Plastic Hinge Rotation

56.  It will be recalled from Part II that the calculation of the ductility demand at a plastic hinge requires a piecewise-elastic analysis of the structure. To this end, the computation of the rotation of a plastic hinge at the springing section of the ring due to an increment $\Delta w$ of test loading will be demonstrated.

57.  Assume a perfectly plastic set of hinges at the springing sections, with the remainder of the ring perfectly elastic of flexural stiffness $EI$, (Figure 14) with only flexural deformations considered.

58.  The hinge rotation is computed by the principle of virtual forces (Gerstle 1974):

$$\theta_{sp} = 2 \int_{\theta=0}^{\pi/2} \phi \cdot m \, ds = 2 \int_{0}^{\pi/2} \frac{M}{EI} \cdot m \cdot R d\theta \qquad (32)$$

where $m$ is nondimensionalized moment in which the real curvature $\phi = M/EI$ is due to the applied increment of load on the ring with hinges, and $m$ is due to a pair of virtual unit moments at the hinge:

$$\phi = \frac{M}{EI} = \frac{\Delta wR^2}{6EI} (1 - k)(1 - \cos 2\theta)$$

$$m = 1$$

28

SYMMETRICAL ABOUT

$\phi = \dfrac{M}{EI}$

$\theta$

SYMMETRICAL ABOUT
X
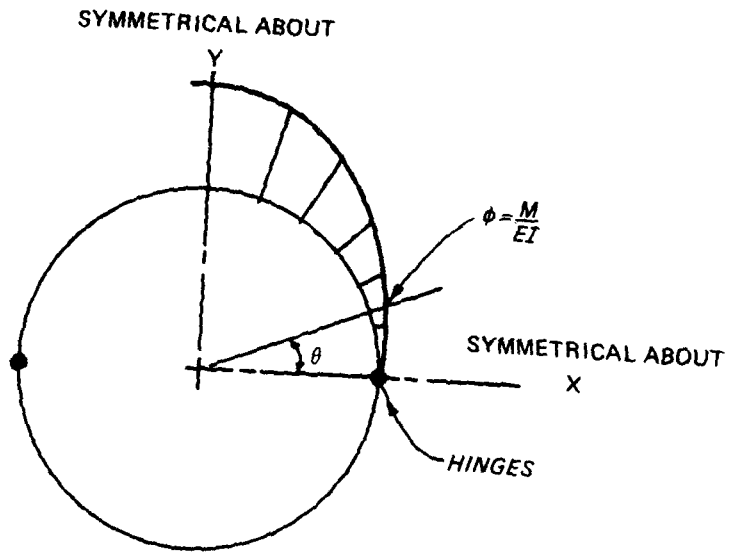
HINGES

a. Real displacement system

SYMMETRICAL ABOUT

$m = 1$

$\theta$

SYMMETRICAL ABOUT
X
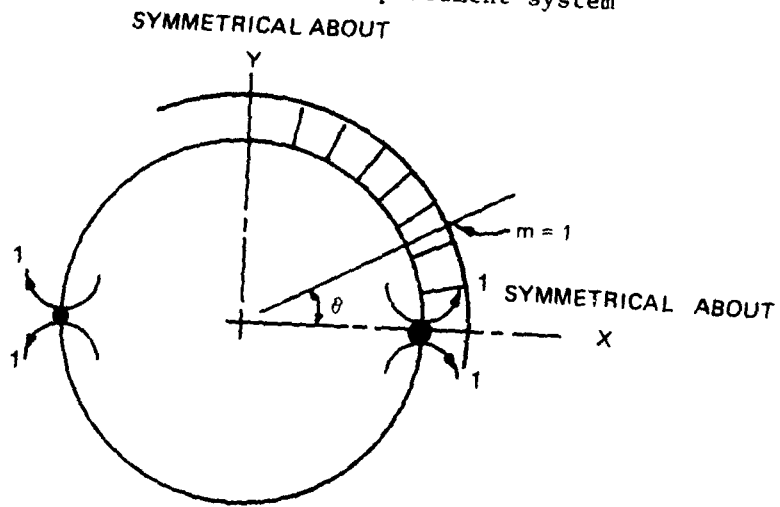
b. Virtual force system

Figure 14. Computation of hinge rotation

59.  Substituting these values into Equation 32 and integrating results in

$$\theta_{sp} = \frac{\Delta wR^3}{EI} \cdot \frac{\pi}{6} (1 - k) = \Delta P_{cr} \cdot \frac{R^2}{EI} \cdot \frac{4}{3} (1 - k) \tag{33}$$

60.  Similar calculations for the EM loading result in plastic hinge rotations due to a load increment $\Delta w$ of

$$\theta_{sp} = \frac{\Delta wR^3}{EI} \cdot \frac{5\pi}{6} (1 - k) \tag{34}$$

61.  Sample calculations for the EM loading are shown in Appendix B.

## Elastic Strength of Rings

62.  Strength design according to ACI (1983) combines elastic structure analysis as outlined in this part with ultimate capacity of sections as given by the strength envelopes shown in Part II.  Critical sections will be at the springing or the crown section, depending on loading and ring characteristics. In Figure 12, for instance, section capacity under increasing load is first reached at the springing, under a combination of axial load $N_{sp}$ = 55 kips, moment $M_{sp}$ = 60 kip/in.  According to strength design philosophy, this constitutes the structure strength.  Any force redistribution due to plastification is neglected.

63.  The radial lines defining the force paths at springing and crown have slopes computed from the results of the preceding elastic analysis.  For test loading from Equations 3a and 3b and 24:

$$e_{sp} = \frac{M_{sp}}{N_{sp}} = \frac{1 - k}{2(2 + k)} \cdot R \tag{35}$$

where $e_{sp}$ is eccentricity at springing, and

$$e_{cr} = \frac{M_{cr}}{N_{cr}} = \frac{1 - k}{2(1 + 2k)} \cdot R \tag{36}$$

where $e_{cr}$ is eccentricity at crown. For EM loading from Equations 5a and 5b and 25:

$$e_{sp} = \frac{M_{sp}}{N_{sp}} = \frac{1 - k}{4} \cdot R \tag{37}$$

$$e_{cr} = \frac{M_{cr}}{N_{cr}} = \frac{1 - k}{4k} \cdot R \tag{38}$$

64. Application of the ACI (1983) strength design method to the analysis of the WES test specimens is illustrated in Part IV.

## PART IV: VERIFICATION OF ANALYTICAL PREDICTIONS

65. In Part II, the plastic method of analysis for strength of rein-
forced concrete pipes was stressed, while the elastic method was outlined in
Part III. In Part IV, a more general look at the various alternatives for
strength determination will be taken to arrive at specific recommendations for
analytical approaches. Following this, the results of these recommended analy-
ses will be compared with the results of the WES ring tests for verification
to arrive at conclusions regarding the validity of these approaches.

## Types of Ring Analysis

66. Strength prediction of reinforced concrete culvert sections depends
in any case on the equilibrium equations, Equations 1 through 15. Beyond this
the section strength and the structure strength can be defined and combined in
different ways, as discussed in the next paragraphs.

### Section strength

67. The concrete stress-strain curve, shown dashed in Figure 15, can be
idealized in different ways:

    <u>a</u>.  The ascending compression branch, of peak strain
        $\varepsilon = 0.002$ in./in., is represented by a linearly elastic curve,
        as shown in Figure 15a.



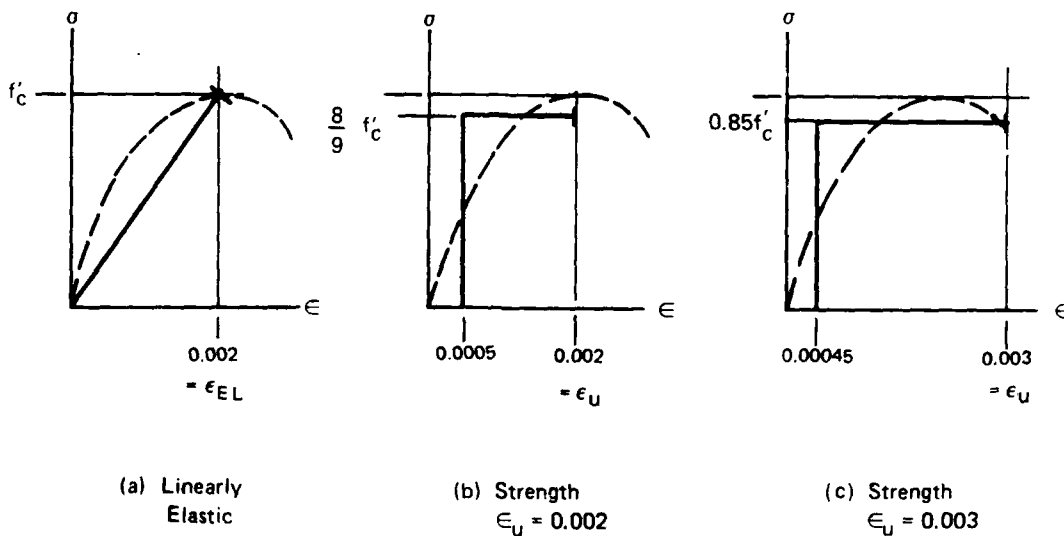|  |  |  |
|---|---|---|
| (a) Linearly Elastic | (b) Strength $\epsilon_u = 0.002$ | (c) Strength $\epsilon_u = 0.003$ |

Figure 15. Concrete stress-strain relations

32

b. The compression branch is represented by a Whitney-type rectangular stress block, of $\epsilon_u = 0.002$ . Assuming a parabolic dashed stress-strain curve, equilibrium considerations determine the rectangular stress block constants as $\alpha = 8/9$ , $\beta = 0.75$ , as shown in Figure 15b.

c. The conventional ACI-Whitney stress block of $\epsilon_u = 0.003$ , $\alpha = 0.85$ , and $\beta = 0.85$ , as shown in Figure 15c.

68. Concrete tension strength is in any case ignored, and steel is considered elastic, perfectly plastic of yield strength $f_y$ . Conventional flexural theory assuming plane section, and using the concrete properties of Figure 15 will lead to three different strength envelopes as shown in Figures 16 and 17. The one labeled "Elastic" defines the section strength by attainment of concrete strain $\epsilon_u = 0.002$ or steel stress $f_y$ . No stress redistribution is considered. This is the allowable or working stress approach used by ACI prior to 1963. Strength theory using the rectangular concrete stress block of Figures 15b and 15c leads to the strength envelopes labeled $\epsilon_u = 0.002$ and $\epsilon_u = 0.003$ in Figures 16 and 17. We see relatively little difference between the two, whereas the elastic limit curve indicates vastly reduced strength.

## Structure strength

69. Two criteria for the determination of the structure strength are considered:

a. The elastic method defines the structure strength by attainment of the section strength at any one section, as already covered in Part III and Figure 12. Elastic analysis of rings under doubly symmetrical loading predicts equal moments at the critical crown and springing sections.

b. Plastic, or limit analysis, presumes redistribution of forces so that ring collapse requires attainment of the full section strength at both crown and springing sections, as outlined in Part II.

70. Figures 6 through 12 show techniques for determination of structure strength according to both methods. The different approaches to the determination of section and structure strength can be combined in different ways, as shown in Table 1.

## Ring strength

71. In order to assess the effect of the different approaches on the prediction of ring strength, we have followed the techniques of Parts II and III to predict the strength of two specimens of the WES test series: the

33

BETA 1 = 3/4, GAMMA = 8/9, Eu = 0.002

LEGEND
+ ELASTIC
● PLASTIC

$\epsilon_u = 0.002$

$\epsilon_u = 0.003$

ELASTIC
$\epsilon_u = 0.002$

62.8 k

64.8 k

62.2 k

55.2 k

53.5 k

MOMENT, KIP-INCH

THRUST, KIPS
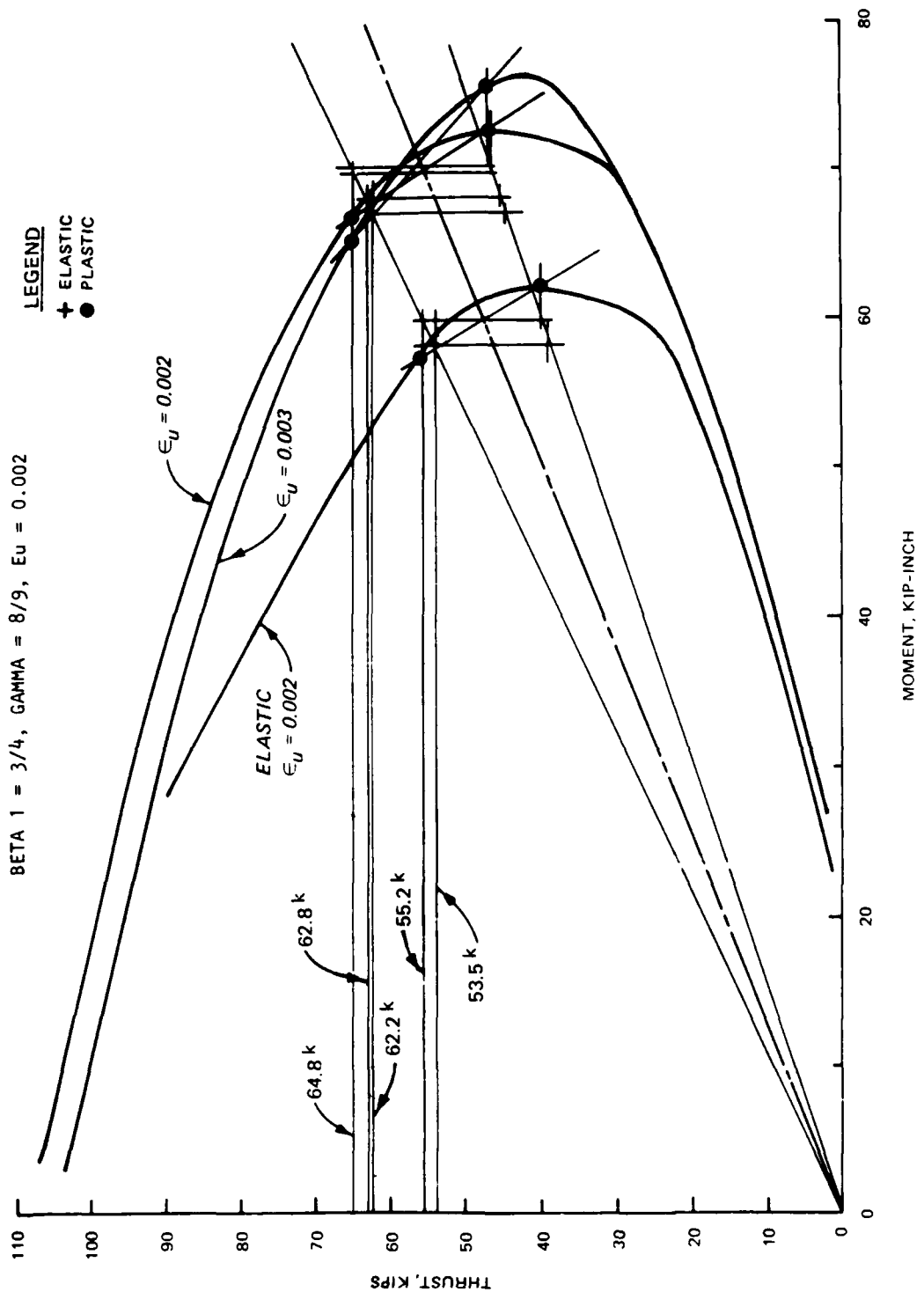
Figure 16.  Analysis of Model C 2-1

34

BETA 1 = 3/4, GAMMA = 8/9, Eu = 0.002

+ ELASTIC
● PLASTIC

$\epsilon_u = 0.003$

$\epsilon_u = 0.002$

ELASTIC
$\epsilon_u = 0.002$

THRUST, KIPS

MOMENT, KIP-IN.

8.9 k
9.0 k
9.6 k
7.7 k
7.9 k
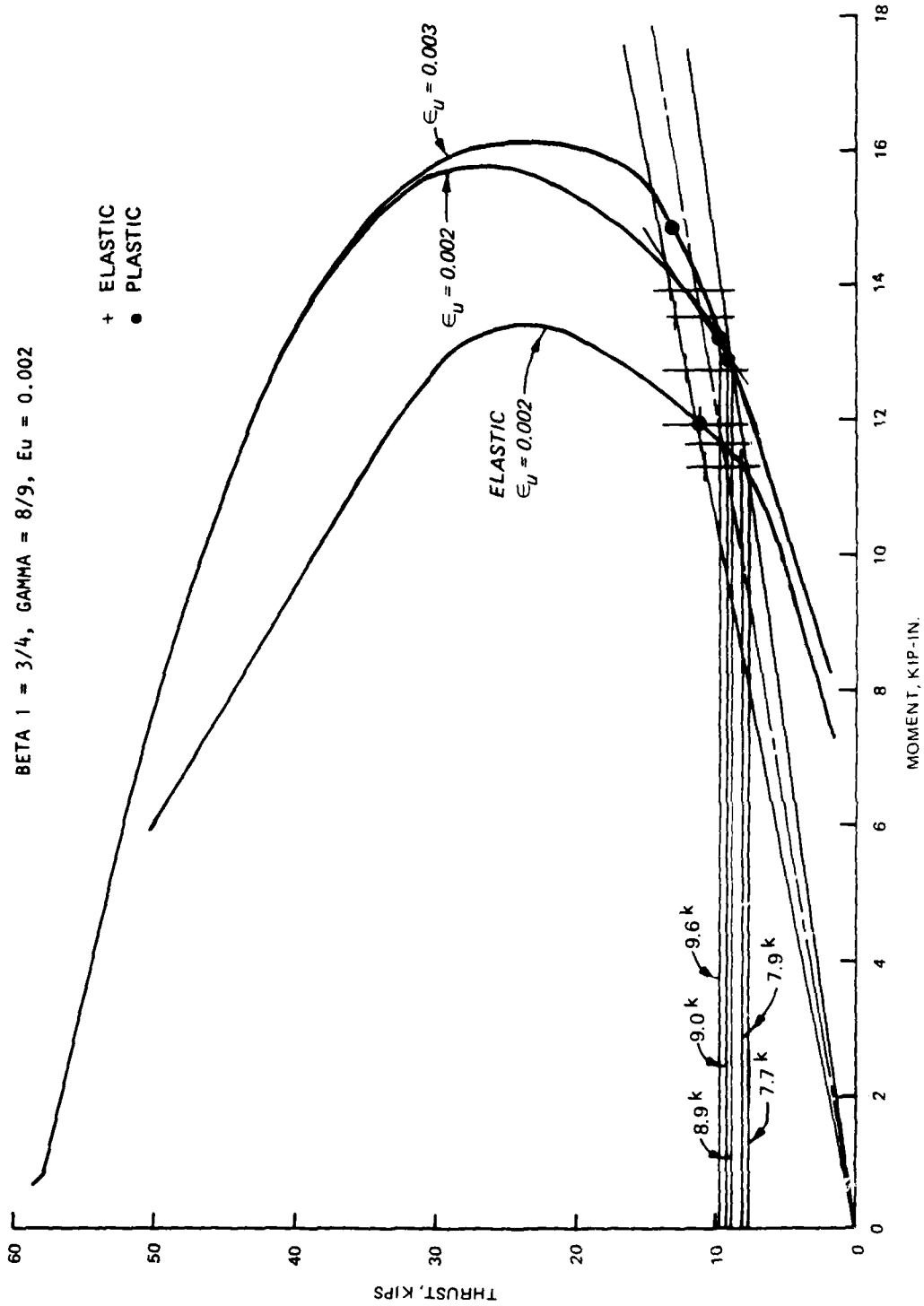
Figure 17. Analysis of Model C 8-2

35

Table 1

Methods of Ring Analysis

| Structure Strength; | Method | |
| Section Strength | Elastic | Plastic |
| --- | --- | --- |
| Elastic | Elastic analysis | Not reasonable |
| Plastic | Strength analysis (ACI 1983) | Limit analysis |

thick Model C 2-1 (R/h = 1.5) and the thin Model C 8-2 (R/h = 4.2). The graphical computations are shown in Figures 15 and 16, and the results for the test loading are summarized in Table 2.

72. The following observations can be made from the strength envelopes of Figures 16 and 17 and from the results of Table 2:

a. The effect of ultimate concrete strain $\varepsilon_u$ is minor when rectangular stress blocks are assumed.

b. Strength computed by linearly elastic theory is much less than that according to strength theory for compression failure. The difference is insignificant for tension failure. It therefore appears that linearly elastic theory will not result in rings which are notably safer against cracking than strength theory.

c. The difference between the ring strengths computed according to strength theory and according to limit analysis is relatively minor.

d. All strength predictions are conservative for Model C2-1, which failed in compression. Test strength of Model C8-2 is suspect because of unknown $f_y$ and possible inaccuracy of steel placement in the very thin section.

Table 2

Comparison of Predictions and Test Results

| | Ultimate Crown Jack Load, kips | | | | | |
| | | Strength | | Limit | | |
| Model | Elastic | $\varepsilon_u = 0.002$ | $\varepsilon_u = 0.003$ | $\varepsilon_u = 0.002$ | $\varepsilon_u = 0.003$ | Test |
| --- | --- | --- | --- | --- | --- | --- |
| C 2-1 | 27.7 | 32.5 | 32.2 | 33.6 | 33.6 | 38.5 |
| C 8-2 | 5.0 | 5.1 | 5.1 | 5.8 | 6.2 | 5.2 |

73. On the basis of these observations, it appears that the well known strength approach according to ACI (1983), using $\varepsilon_u = 0.003$, or limit

analysis using the same strength envelope, may be appropriate design methods for these rings. Purely elastic analysis assesses the ring strength too low. Limit analysis may require force redistribution involving tensile concrete cracking which may be undesirable in a pipe. It may also be observed that with these curved strength envelopes, the strength theory, which requires matching internal forces with strength at only one critical section, is considerably simpler than limit analysis, which requires this match at two critical sections.

74. In the systematic comparison between predicted and observed strengths of the WES rings, the strength and limit analysis based on $\varepsilon_u = 0.003$ will be used.

## Comparison of Predictions and WES Test Results

75. In this section, predicted strengths for the 18 specimens tested in the WES series calculated according to strength and limit analysis are compared to observed failure loads as reported in Tables 5 to 7 of Wright and Chiarito (1987). All of these tests terminated in flexural failure: the single diagonal tension crack reported in Model C2-3, Table 5 (Wright and Chiarito 1987) seems to have occurred well after attainment of the full flexural strength.

76. Several caveats are indicated in judging the validity of the comparisons:

a. In most of the specimens, predominantly the thin ones, actual applied load distribution varied significantly from that specified (Gerstle 1985). Applied loads always tended to readjust themselves toward hydrostatic compression, that is, the actual value of k at failure was always larger than that specified. In our calculations, we used the actual k value at failure rather than the specified k value.

b. The yield strength of the reinforcing wire D1 and D3 varied significantly according to test data,* but no correlation is available between strength and specimen. Computations for the affected specimens labeled with asterisk in Table 3 were carried out for maximum and minimum reported yield strengths; these values therefore constitute upper and lower bounds on

---

\* US Army Engineer Waterways Experiment Station. "WES Laboratory Data: Steel Reinforcing Report," Data Sheets dated 17 Feb 1984, 21 and 25 Jun 1983, and 7 and 12 Jul 1983, Vicksburg, Miss.

Table 3

Comparison of Strengths for WES Test Series

| Model | $k_{act}$** | $P_{cr}$ Experimental | $P_{cr}$ Strength | $P_{cr}$ Limit | $\dfrac{P_{cr}\ \text{Strength}}{P_{cr}\ \text{Limit}}$ | $\dfrac{P_{cr}\ \text{Experimental}}{P_{cr}\ \text{Strength}}$ | $\dfrac{P_{cr}\ \text{Experimental}}{P_{cr}\ \text{Limit}}$ |
|---|---|---|---|---|---|---|---|
| C 1-1* | 0.338 | 46.9 | { 34.0 / 34.8 | 35.8 / 36.4 } | 0.95 | 1.37 | 1.30 |
| C 2-1 | 0.313 | 38.5 | 31.2 | 32.4 | 0.97 | 1.23 | 1.19 |
| C 2-2 | 0.521 | 43.4 | 35.2 | 37.3 | 0.94 | 1.23 | 1.16 |
| C 2-3 | 0.267 | 36.5 | 31.3 | 32.8 | 0.95 | 1.16 | 1.11 |
| C 3-1 | 0.367 | 49.0 | 41.6 | 44.2 | 0.94 | 1.18 | 1.11 |
| C 4-1* | 0.376 | 27.3 | { 22.4 / 24.3 | 24.7 / 25.2 } | 0.94 | 1.16 | 1.10 |
| C 4-2* | | 34.1 | { 23.7 / 24.2 | 24.5 / 25.4 } | 0.96 | 1.43 | 1.37 |
| C 5-1 | 0.334 | 19.4 | 20.1 | 21.0 | 0.96 | 0.96 | 0.93 |
| C 5-2 | 0.578 | 28.5 | 21.6 | 22.7 | 0.95 | 1.32 | 1.25 |
| C 5-3 | 1.0 | 29.2 | 29.3 | 29.3 | 1.00 | 1.00 | 1.00 |
| C 5-4 | 0.321 | 17.5 | 16.1 | 16.7 | 0.96 | 1.09 | 1.05 |
| C 6-1 | 0.394 | 17.9 | 14.7 | 15.3 | 0.96 | 1.22 | 1.18 |
| C 6-2 | 0.508 | 20.0 | 14.5 | 15.6 | 0.93 | 1.37 | 1.28 |
| C 7-1* | 0.513 | 5.3 | { 4.5 / 5.0 | 5.2 / 6.5 } | 0.89 | 1.02 | 0.91 |
| C 8-1* | 0.495 | 7.3 | { 8.3 / 9.2 | 9.4 / 9.7 } | 0.92 | 0.83 | 0.76 |
| C 8-2* | 0.387 | 5.2 | { 4.8 / 5.8 | 5.4 / 6.3 } | 0.91 | 0.98 | 0.88 |
| C 8-3* | 0.637 | 11.5 | { 9.4 / 9.5 | 9.7 / 9.8 } | 0.97 | 1.20 | 1.18 |
| C 9-1* | 0.485 | 5.5 | { 6.6 / 7.0 | 6.8 / 7.1 } | 0.98 | 0.81 | 0.79 |

\* Upper and lower bounds on strength due to variations in steel yield strength.

\*\* Actual value of $k$ at failure for test specimen.

strength. The ratios of strengths given in Table 3 for these specimens are based on calculated average values.

c. The specimens of R/h = 4.1 were of thicknesses ranging from 2.00 to 2.25 in., with concrete cover about 1/2 in. thick. For these specimens, accuracy of steel placement becomes very critical; any slight deviation from values recorded in Table 1 of Wright and Chiarito (1987), which were used in the calculations, would lead to faulty predictions. It is quite possible that the gross overestimation of strength for Models C 8-1 and C 9-1 was due to this effect. Table 7 of Wright and Chiarito (1987) reported four hinges for these thin rings; therefore, plastic theory should apply.

77. Results of the comparison study are listed in Table 3 where observed strengths, predicted values of the jack load at the crown, $P_{cr}$, according to strength and limit analyses, and ratios of these values are given for all test specimens.

78. The same information is shown graphically in Figure 18, where the
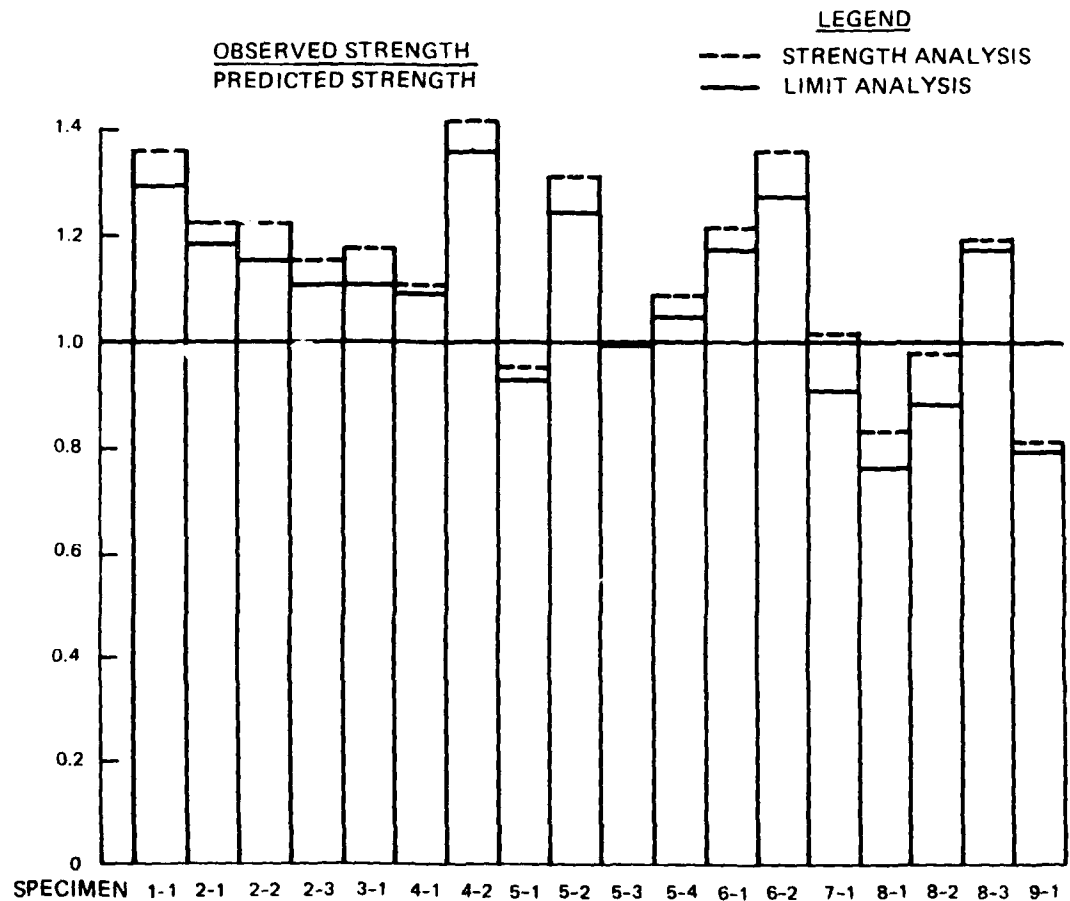


Figure 18. Comparison of predicted and observed strengths

39

ratio of observed to predicted strength is plotted for all specimens for both strength and limit theories. A value of unity indicates perfect agreement between theory and test result. Values above unity indicate a conservative, or safe, prediction, while values below unity denote an unsafe prediction.

79. It is noted that for the thick rings, predicted strengths are on the safe side, by factors up to 40 percent when calculated by strength method, and up to 30 percent when computed by limit analysis. Grave inconsistencies involving overestimated strength of up to 30 percent are noted for the thin rings. As mentioned before, inaccuracies due to unfavorable model scale could account for such inconsistencies.

## Influence of Experimental Inaccuracies on Ring Strength

80. Relatively wide deviations were observed between predicted and measured strengths for the WES ring specimens C 8-1, 8-2, 8-3, and 9-1, as shown in Table 3 and Figure 18. These were all thin rings with R/h ratio ranging from 3.9 to 4.5, and thickness h between 2.00 and 2.25 in.

81. Among factors possibly responsible for the mismatch are:

a. These thin rings required great accuracy in their preparation. Slight dimensional variations of the cross section might result in considerable strength variation.

b. There was uncertainty about the steel strength. Reported yield strength of the annealed wire varied from 58.6 to 76 ksi.

c. The actual load distribution applied to these relatively flexible rings deviated considerably from the specified distribution.

82. The relative importance of these variables has been assessed to understand possible reasons for the discrepancies. Because of restrictions imposed on the extent of this study, we have considered only one specimen, C 8-1, for which the ratio of measured to predicted failure load was 0.83 according to strength theory, and 0.76 according to limit analysis.

83. First, the effect of the cross-sectional parameters on the section strength has been considered: Specimen C 8-1 had the cross-sectional dimensions as specified in Table 1 of Wright and Chiarito (1987) and shown as insert a in Figure 19, indicates that the reinforcing cage had an eccentricity of 0.16 in., or about 3/16 in., with respect to the concrete section. The corresponding strength, assuming an average yield strength of 68.2 ksi (WES
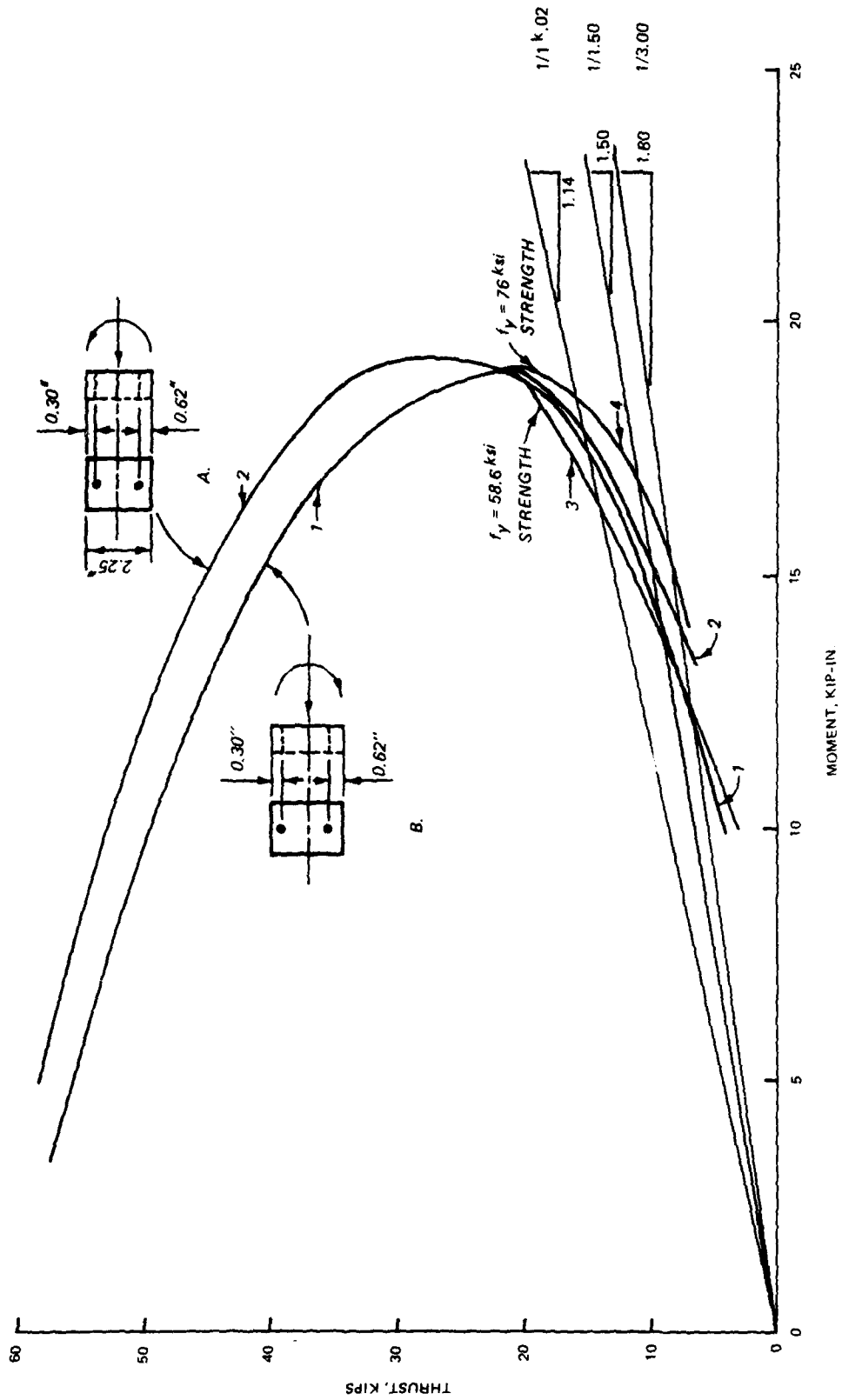
40

Figure 19. Effect of yield strength

41

Laboratory Data Sheets*), is shown by the strength envelope labeled 1 in Figure 19. Assume that the reinforcing cage is inserted in the forms with the opposite eccentricity, shown as insert b in Figure 19; that is, at 5/16 in. from that specified, the strength of the section will be as indicated by strength envelope 2 in Figure 19. The difference is no more than the scatter which might be expected among replicates.

## Effect of Different Yield Strengths

84. The effect of different yield strengths is shown by envelopes 3 and 4 in Figure 19. Envelope 3 results from assuming the lowest measured yield strength of 58.6 ksi, and envelope 4 results from assuming the highest value of 76 ksi. As might be expected, the difference shows up only in the region of tension failure. Again, the difference between envelopes 3 and 4 is moderate for the combination of axial force and moment expected in these rings.

85. Consider next the effect of load distribution on the ring strength. The recorded load distribution for specimen C 8-1 is plotted for increasing load to failure in Figure 20. It is seen that, as with the other thin rings, the actual load distribution varies considerably from the specified value of $k = 1/3$. Our earlier predictions were based on the value of $k = 1/2.02$ near failure. Another possible assumption might be an average value of $k = 1/2.5$, also shown in Figure 20.

86. The crown section of the ring is critical under all of these load ratios. The eccentricity at this section was computed from Equation 35, and the axial force at this section by intersection of the eccentricity lines with the strength envelopes (Figure 19). The crown jack load was determined by Equation 15.

87. Following this procedure, the failure loads at the crown were computed for three eccentricity lines and four strength envelopes, then entered in Table 1.

88. To assess the sensitivity of the failure load to the different parameters, Table 4 presents the ratio of the largest to the smallest load for different cross sections while holding the load distribution constant. Also,

---

* US Army Engineer Waterways Experiment Station, op. cit.
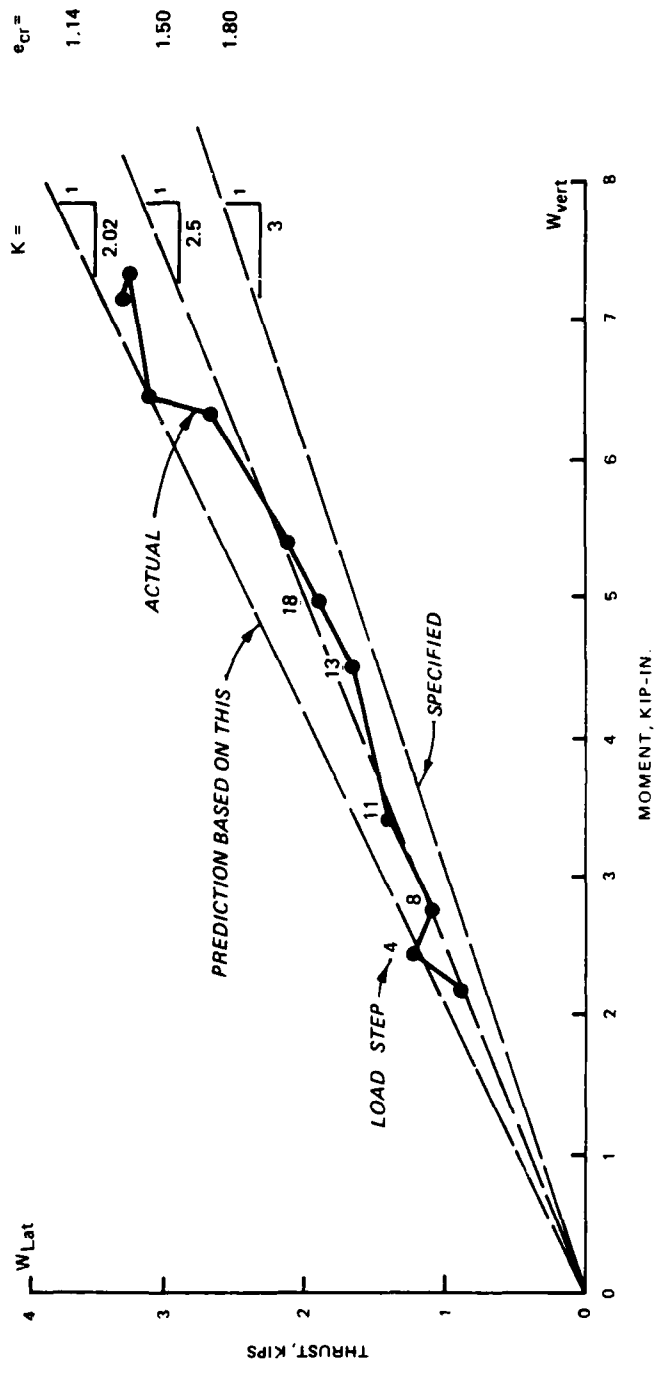
Figure 20. Effect of load distribution

the same ratio is recorded for different load distributions while holding the cross-sectional properties constant. The variation of cross-sectional properties causes a maximum variation of strength of 26 percent, while the variation of load distribution over a range of credible values causes strength variations of between 63 and 91 percent. The load distribution dominates in its significance.

Table 4

Sensitivity of Failure Load

| K | Strength Envelope $P_{cr}$, kips | | | | $\dfrac{P_{cr}\ max}{P_{cr}\ min}$ | $\dfrac{P_{cr}\ Experimental}{P_{cr}\ max}$ | $\dfrac{P_{cr}\ Experimental}{P_{cr}\ min}$ |
| | 1 | 2 | 3 | 4 | | | |
|---|---|---|---|---|---|---|---|
| 1/2.02 | 9.0 | 9.3 | 8.6 | 9.6 | 1.12 | 0.76 | 0.85 |
| 1/2.50 | 6.1 | 6.5 | 5.9 | 7.2 | 1.22 | 1.01 | 1.22 |
| 1/3.00 | 4.7 | 5.5 | 4.7 | 5.9 | 1.26 | 1.24 | 1.55 |

| $\dfrac{P_{cr}\ max}{P_{cr}\ min}$ | 1.91 | 1.69 | 1.83 | 1.63 | | | |
|---|---|---|---|---|---|---|---|

89. Table 4 also presents the ratios of the test strength of 7.3 kips of specimen C 8-1 to the predicted maximum and minimum strength for each value of load distribution. Observe the scatter around the value of unity denoting perfect prediction. The strength of these rings is extremely sensitive to the load distribution. A slight variation from the specified value will greatly affect the ring strength. The deviation of the applied loads from those specified during testing may account for the bulk of the difference between predicted and test results for these thin, flexible rings. Inaccuracies in construction and material strength may have played a lesser role.

90. In a larger sense, these flexible rings have a remarkable ability to readjust the load to a more favorable distribution, even under presumed load control, as in the WES tests. Similar behavior might be expected of flexible pipe in the ground. Analysis which includes soil-structure interaction will be needed to carry out realistic predictions of ring strength under such conditions.

## PART V: DESIGN OF CIRCULAR REINFORCED CONCRETE PIPE CULVERTS

91. Following the observations of Part IV, we will base the design of reinforced concrete pipe culverts on the strength approach according to ACI (1983), which combines ultimate section strength with elastic structure analysis. Other combinations of section and structure strength calculations, as outlined in Part IV, are possible but will not be pursued here for the sake of conciseness.

92. In the following design procedure and examples, only the EM 1110-2-2902 loading (Headquarters, Department of the Army 1969) will be specified. Other doubly symmetric loadings are possible but will not be considered in following text.

### Longhand Design Method

93. The longhand design method outlined here is based on the following premises:

a. Known, doubly symmetric applied loads, such as the EM 1110-2-2902 loading (Headquarters, Department of the Army 1969).

b. Nondimensional section strength envelopes plotting axial force versus moment applied jointly are available.

c. Equilibrium of axial force and moment at the critical crown and springing sections can be represented by radial lines of slope $1/e$ , as demonstrated in Figures 6 through 10.

d. Shear strength and possibility of slabbing failure are to be checked separately.

### Strength Envelopes

94. For design purposes, the strength envelopes as shown in Figures 5 through 10 are nondimensionalized in terms of the dimensionless axial force $n = N/(f_c'bh)$ , the dimensionless moment $m = M/(f_c'bh^2)$ , the reinforcing index $\omega = (A_s f_y)/(bhf_c')$ , and the cross-sectional parameter $\gamma = (h - 2d')/h$ . where

$f_c'$ = compressive strength of concrete

$b$ = width of section

$h$ = overall depth of section

$A_s$ = area of flexural reinforcement in tension

45

$f_y$ = yield strength of reinforcing steel

$\gamma$ = dimensionless cross-sectional parameter used in development of nondimensional strength envelope

$d'$ = distance from extreme compression fiber to centroid of compression reinforcement

95. A set of dimensionless strength envelopes for values of $\gamma$ ranging from 0.5 to 0.8 is shown in Figures 21 through 24. Since the section strength is sensitive to the value of $\gamma$, careful interpolation is necessary between strength values. These curves are valid only for rectangular cross sections of equal reinforcing on both sides. Note that in these curves, $\omega$ is defined as the total reinforcing index. The tensile reinforcing index would be half this value. No material strength factor is contained in these curves.

## Elastic Analysis

96. For the EM loading specified in the following examples, the results of equilibrium Equation 5 and of elastic analysis Equation 25 are nondimensionalized as:

$$n_{sp} = \frac{N_{sp}}{f'_c bh} = \frac{wR}{f'_c bh} \tag{39}$$

$$n_{cr} = \frac{N_{cr}}{f'_c bh} = k \cdot \frac{wR}{f'_c bh} \tag{40}$$

$$m_{sp} = m_{cr} = \frac{M_{sp}}{f'_c bh^2} = \frac{M_{cr}}{f'_c bh^2} = (1 - k) \frac{wR^2}{4f'_c bh^2} \tag{41}$$

97. From these axial forces and moments, the slopes of the nondimensional radial eccentricity lines can be established for springing and crown:

$$\frac{h}{e_{sp}} = \frac{n_{sp}}{m_{sp}} = \frac{4}{1 - k} \cdot \frac{1}{(R/h)} \tag{42}$$

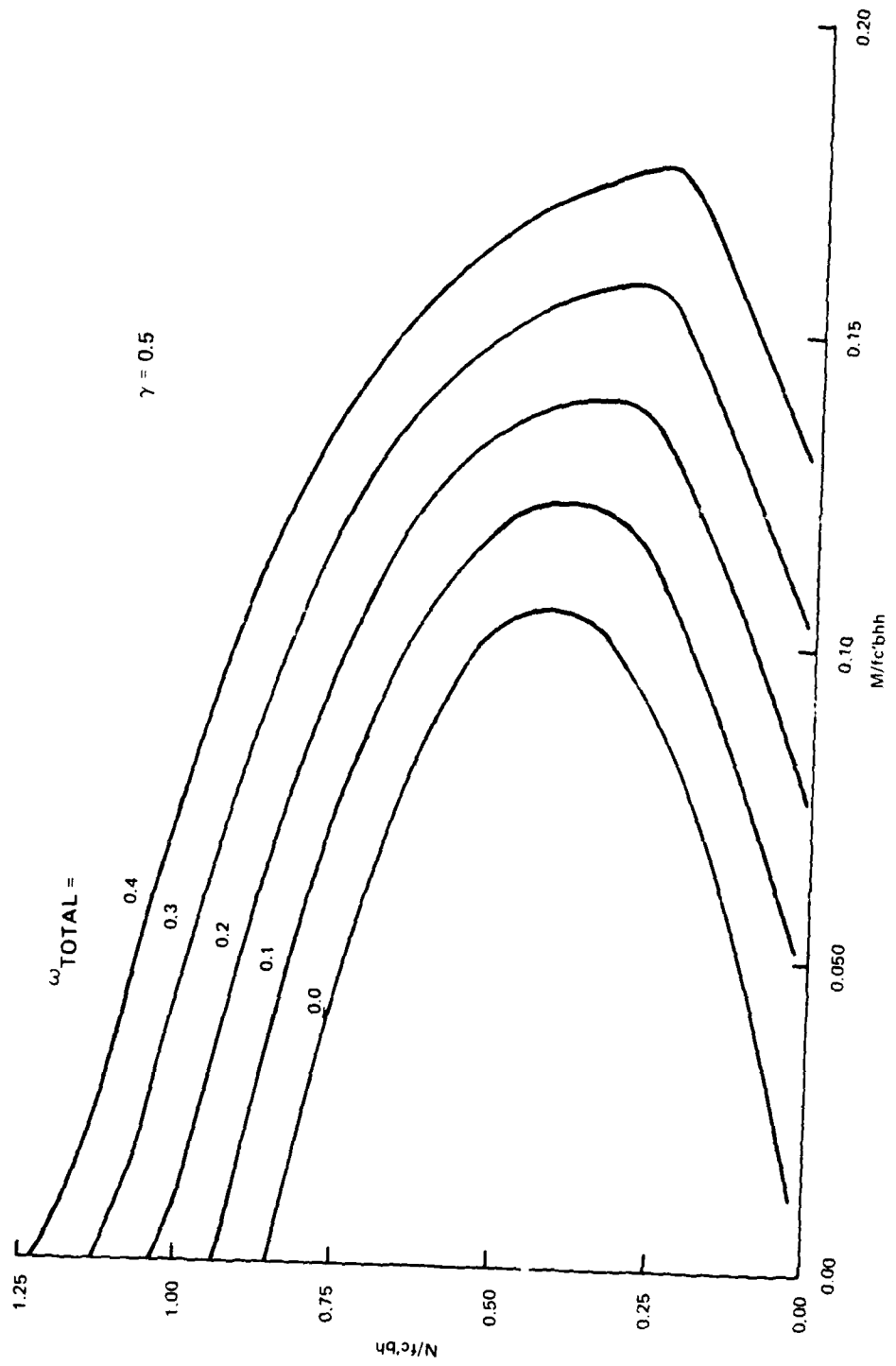$$\frac{h}{e_{cr}} = \frac{n_{cr}}{m_{cr}} = \frac{4k}{1 - k} \cdot \frac{1}{(R/h)} \tag{43}$$

46

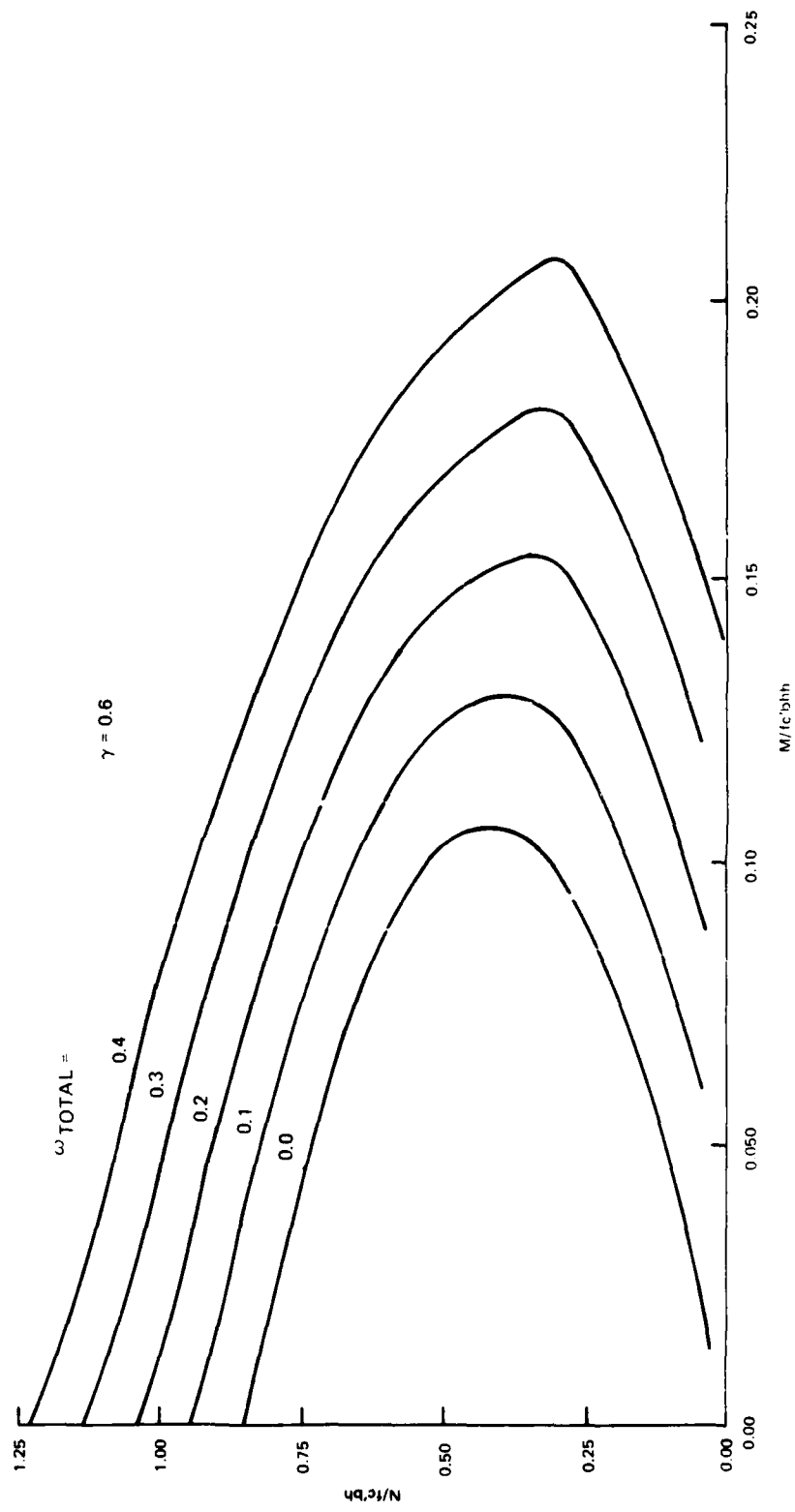Figure 21. Strength curves for $\gamma = 0.5$

Figure 22. Strength curves for $\gamma = 0.6$
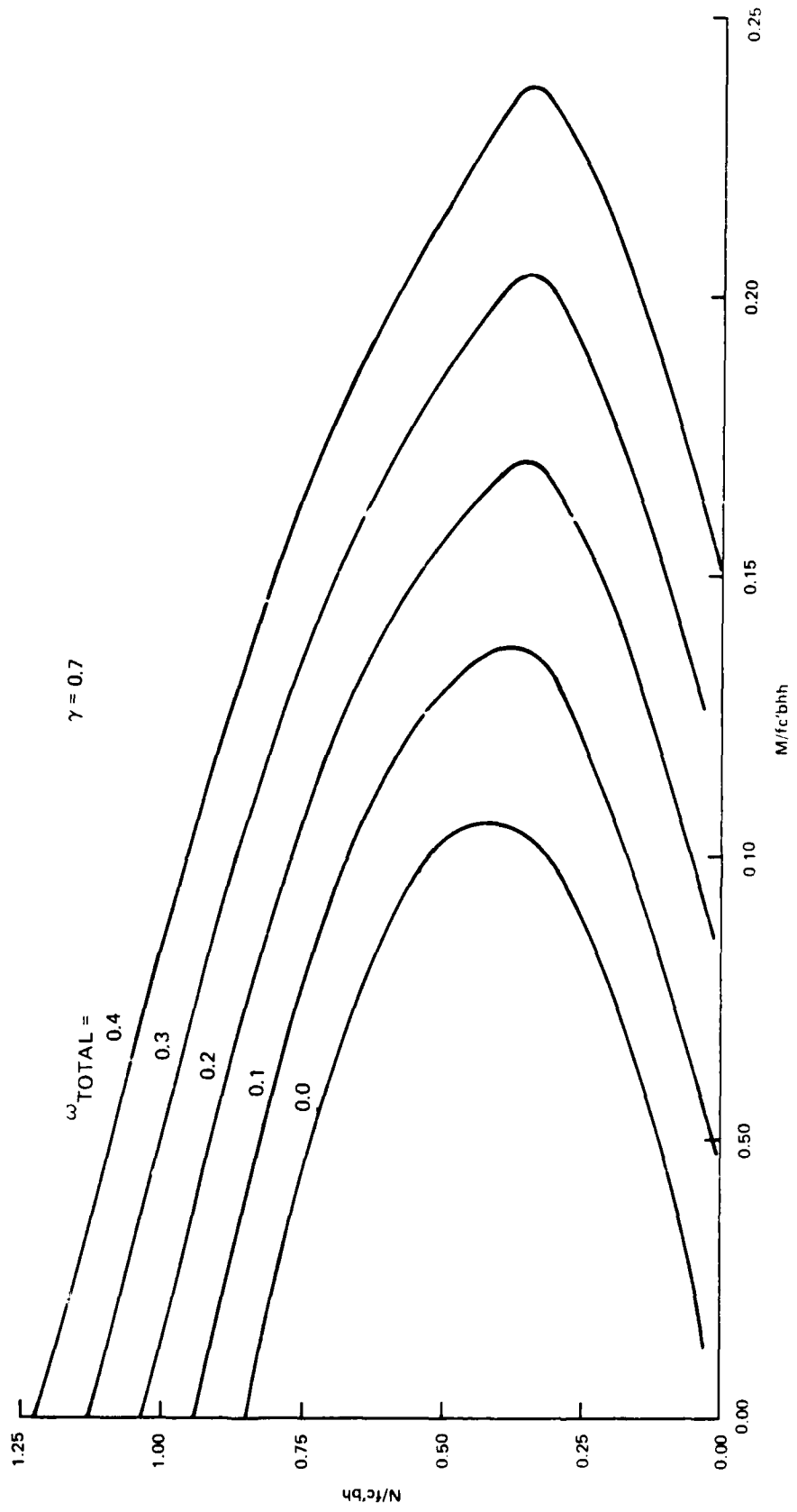
Figure 23. Strength curves for $\gamma = 0.7$

49
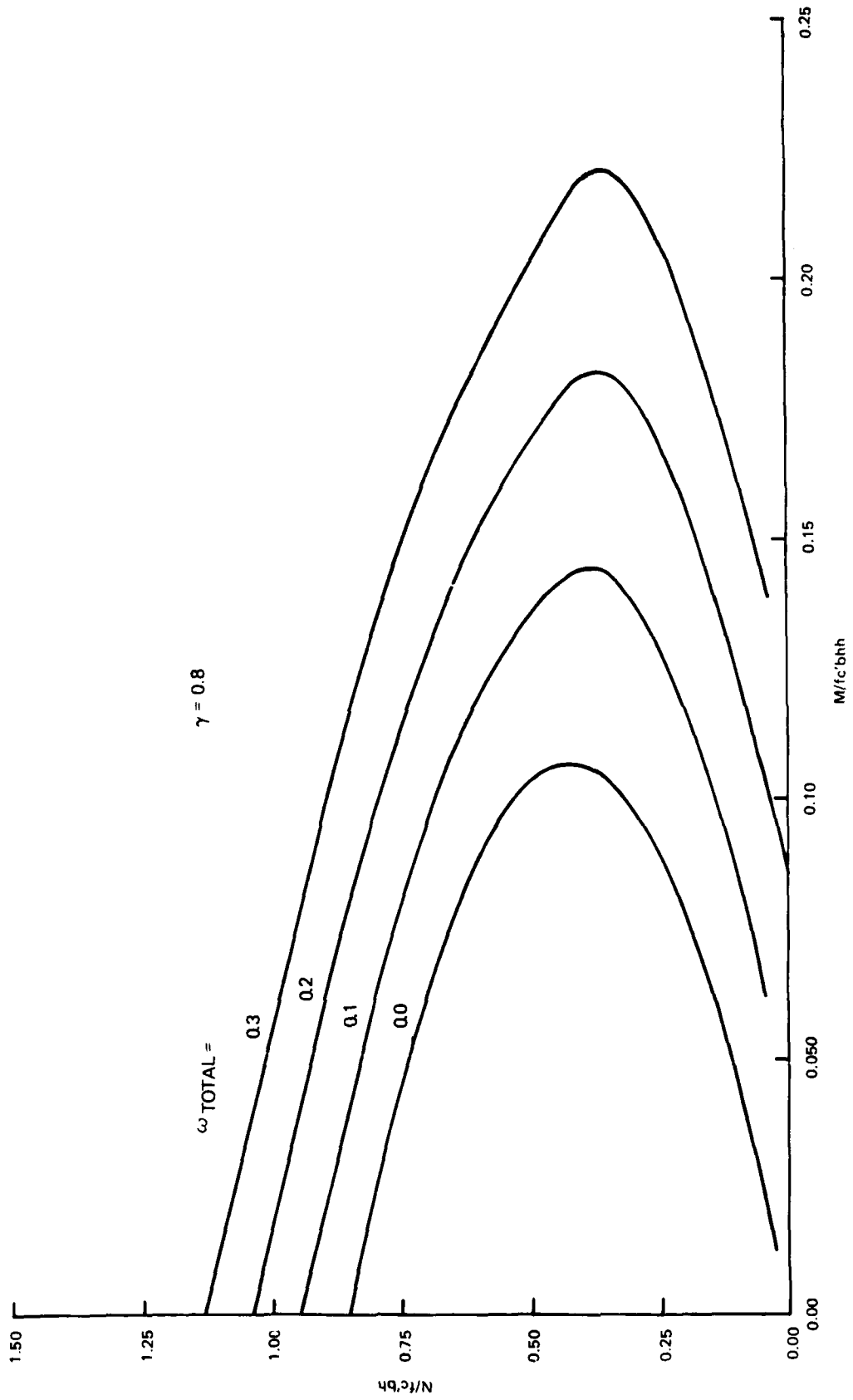
Figure 24.  Strength curves for  $\gamma = 0.8$

98. In any case, a well-designed pipe must satisfy the strength condition of the appropriate strength envelope, the internal equilibrium (and continuity) condition of Equations 42 and 43, and the axial force which is in equilibrium with the applied load according to Equations 39 and 40. The intersection of two straight lines, one radial, one horizontal, with the strength envelope provides the desired solution, as illustrated in the following examples.

99. Two failure modes are possible: with equal moments at springing and crown according to Equation 41, the eccentricity line for the springing section intersects the strength envelope first, indicating compression failure at this section, as shown in Figure 25a, or the eccentricity line for the crown section intersects the strength envelope first as shown in Figure 25b,



a. Springing critical                          b. Crown critical

Figure 25. Strength design of rings

indicating tension failure (tensile yielding of the inside steel) at the crown section. Equations 42 and 43 indicate that for thick rings (R/h small) the former is likely to happen, for sufficiently thin rings (R/h large), the latter may occur.

## Design Procedure

100. With loads and pipe radius, as well as material strengths speci-
fied, two different design situations can be visualized:

Case 1. Given: Pipe thickness $h$

Required: Reinforcing $A_{so} = A_{si} = (1/2)A_{st}$
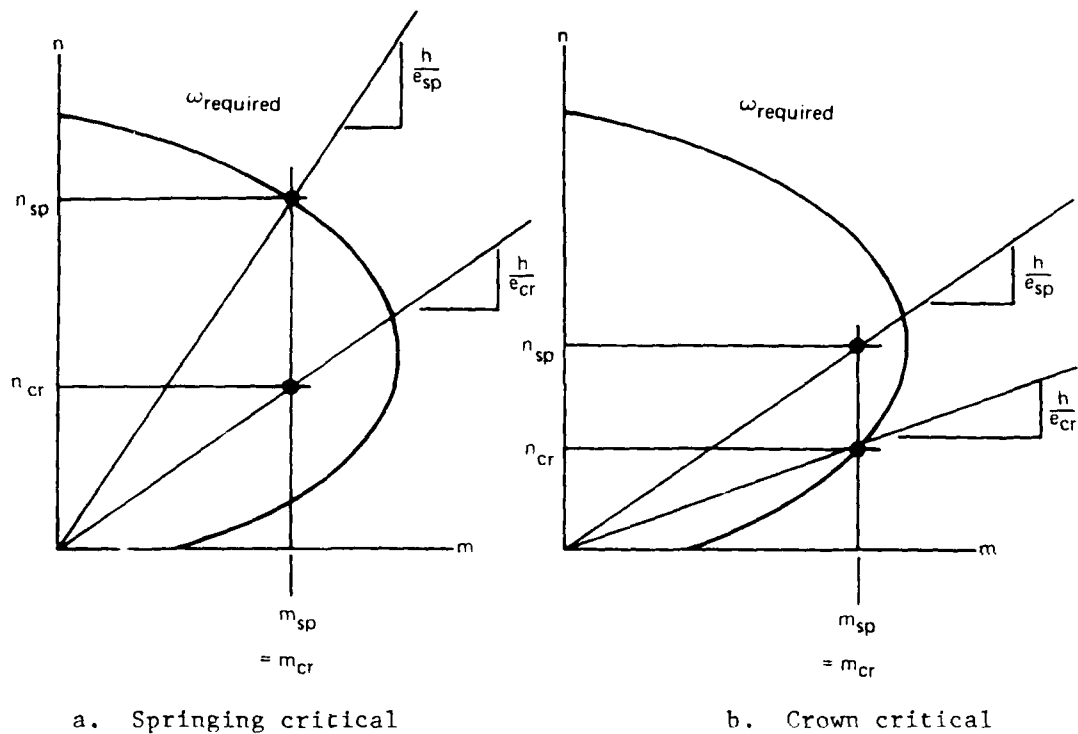
where

$A_{si}$ = steel area of inner cage, inches squared/feet

$A_{so}$ = steel area of outer cage

$A_{st}$ = total area of reinforcement in section (inner and outer cages)

or

Case 2. Given: Specified steel reinforcing index $\omega = \dfrac{A_{st}f_y}{bhf'_c}$

Required: Thickness $h$

where $\omega$ is reinforcing index, dimension term used in development
of nondimensional strength envelopes.

101. An example will be given for each of these cases. No load or
resistance factors are considered here, so the specified loads should be
considered ultimate values.

Case 1

102. In this case, with concrete cover specified, the appropriate value
of $\gamma$ can be computed to select the proper set of interaction envelopes (or
interpolate between given values) and draw the eccentricity lines of slopes
$h/e_{sp}$ and $h/e_{cr}$ according to Equations 42 and 43. The nondimensional axial
section forces, $n_{sp}$ and $n_{cr}$ , are computed for the specified loads by
Equations 39 and 40 and projected horizontally on the dimensionless section
strength plot. The intersection of these lines with the corresponding
eccentricity lines defines the reinforcing index required at spring and crown
sections.

103. Since the strength envelopes are calculated for equal inside and
outside reinforcing, this design requirement should be satisfied.

Availability of a computer program which generates data for unequal inside and outside reinforcement seems useful for economical design of pipe structures.

104.   In the example design of Case 1, the dimensions and material strengths are those of specimen G-1 of Heger, Nawy, and Saba (1963).

Given:   Inside diameter = 72 in.

Wall thickness = 7 in.

Concrete cover = 1 in.

Factored load, vertical = 24 k/ft$^2$

Factored load, horizontal = 12 k/ft$^2$

$f'_c$ = 4.8 ksi

$f_y$ = 88 ksi

Required:   Reinforcement

R = 39.5 in.;   R/h = 5.64 ;   $\gamma$ = 0.71 $\approx$ 0.7 ;

k = 12/24 = 0.5

where $\gamma$ is dimensionless cross-sectional parameter used in development of nondimensional strength envelopes.

Keep all units in inches; per foot length of pipe:

w = 2.00 k/in.

b = 12 in.

From Equation 39:   $n_{sp} = \dfrac{wR}{f'_c \cdot bh} = 0.196$

From Equation 40:   $n_{cr} = k \cdot \dfrac{wR}{f'_c \cdot bh} = 0.098$

From Equation 41:   $\dfrac{h}{e_{sp}} = \dfrac{4}{1-k} \cdot \dfrac{1}{(R/h)} = 1.418$

53

From Equation 42: $\dfrac{h}{e_{cr}} = \dfrac{4k}{1-k} \cdot \dfrac{1}{(R/h)} = 0.709$

Enter graph for $\gamma = 0.7$ (Figure 26):

Springing lines intersect at $\omega_{sp} = 0.18$ ($\omega_{sp}$ is reinforcing index

for springing section)

Crown lines intersect at $\omega_{cr} = 0.27$ ($\omega_{cr}$ is reinforcing index

for crown section)

Crown section controls:

$\rho_{\text{Total req'd}} = \omega \dfrac{f'_c}{f_y} = 0.0147$ ($\rho$ is tensile reinforcement ratio)

$A_{S\ \text{Total req'd}} = 0.0147 \cdot 12 \cdot 7 = 1.24$ in.$^2$/ft

$A_{Si} = A_{So} = 0.62$ in.$^2$/ft for continuous ring reinforcement

Spring section:

$\dfrac{\omega_{sp}}{\omega_{cr}} = \dfrac{2}{3}$ for noncontinuous reinforcement

Possibly, a better design might be a combination of:

continuous inside steel area = 3/2 outside steel area

but this case is not covered by strength envelopes which are limited to equal steel inside and outside.

Case 2

105. In this case, a value of h has to be assumed, allowing the computation and plotting of the equilibrium lines of slope $h/e_{sp}$ and $h/e_{cr}$ according to Equations 42 and 43. The horizontal axial force lines according to Equations 39 and 40 are also drawn. If these lines for the critical
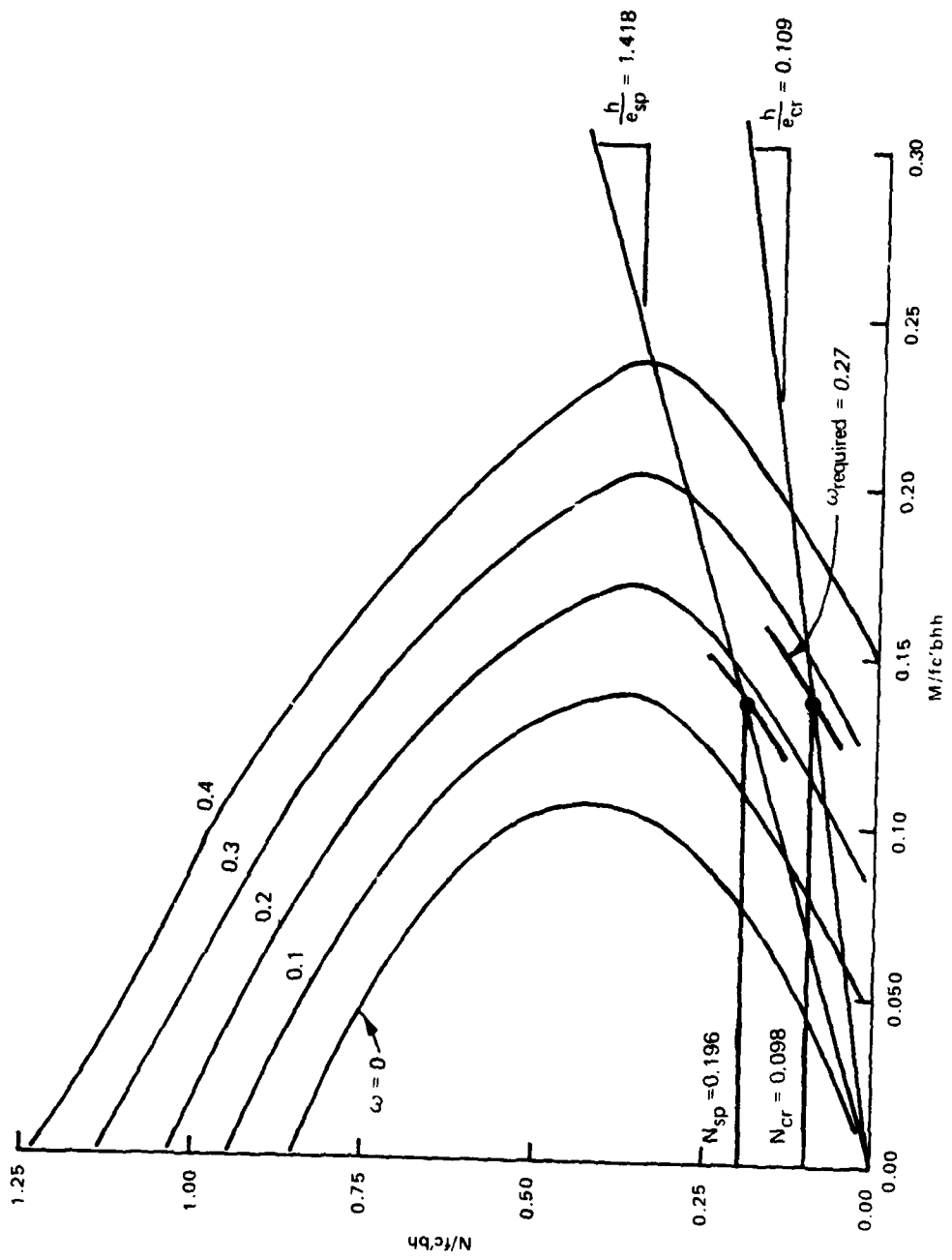
Figure 26. Example, Case 1

55

section intersect on the desired ω strength envelope, the assumed value of h is correct. If not, a new value of h will have to be assumed and the process repeated, as shown in the following example.

106. In the example design of Case 2, the diameter and material properties of the preceding example are used, but the earth pressure is varied to demonstrate compression failure.

Given: Inside diameter = 72 in.

Concrete cover = 1 in.

Desired total steel ratio $\rho_{Total}$ = 0.011

$f'_c$ = 48 ksi

$f_y$ = 88 ksi

Factored load, vertical = 60 k/ft$^2$

Factored load, horizontal = 40 k/ft$^2$

Required: Wall thickness h .

Assume h = 12 in.; R = 42 in.; R/h = 3.5 ; γ = 0.83 ; k = 0.67 :

$$\omega_{req'd} = \rho \frac{f_y}{f'_c} = 0.2$$

Per foot length of pipe:

w = 5.00 k/in.

b = 12 in.

From Equation 39: $n_{sp} = \frac{wR}{f'_c \cdot bh} = 0.304$

From Equation 40: $n_{cr} = k \cdot \frac{wR}{f'_c \cdot bh} = 0.203$

56

From Equation 41: $\dfrac{h}{e_{sp}} = \dfrac{4}{1-k} \cdot \dfrac{1}{(R/h)} = 3.43$

From Equation 42: $\dfrac{h}{e_{cr}} = \dfrac{4k}{1-k} \cdot \dfrac{1}{(R/h)} = 2.29$

107. The trial calculations can be set up in tabular form (Table 5), using the nondimensionalized strength curves of Figures 21 through 24; obtain $n_{sp}$ and $n_{cr}$ from Equations 39 and 40, $h/e_{sp}$ and $h/e_{cr}$ from Equations 42 and 43. Figure 27 presents the nondimensionalized curves for the 8-, 9-, and 12-in. sections.

Table 5

Case 2 Trial Calculations

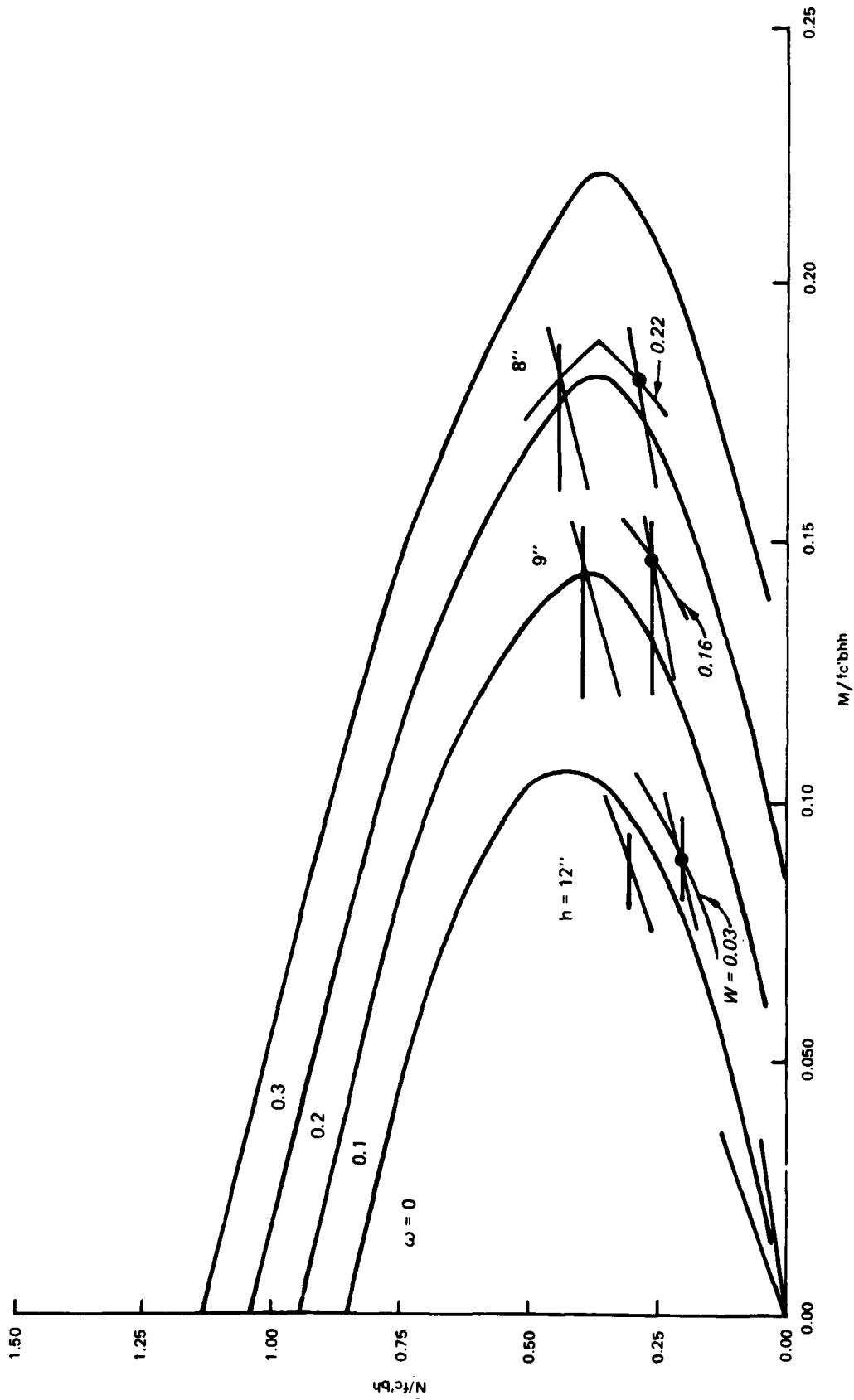| Assumed $h$, in. | $R$ in. | $\gamma$ | $R/h$ | $n_{sp}$ | $n_{cr}$ | $h/e_{sp}$ | $h/e_{cr}$ | $\omega_{req'd}$ |
|---|---|---|---|---|---|---|---|---|
| 12 | 42 | 0.83 | 3.5 | 0.304 | 0.203 | 3.43 | 2.29 | 0.03 |
| 9 | 40.5 | 0.78 | 4.5 | 0.391 | 0.261 | 2.67 | 1.78 | 0.16 |
| 8 | 40 | 0.75 | 5.0 | 0.434 | 0.289 | 2.40 | 1.60 | 0.22 |

Figure 27. Example, Case 2

# PART VI: SHEAR STRENGTH OF RINGS

## Background

108. Shear strength of reinforced concrete culvert pipe has been of concern for some time. Heger (1963) and Heger and McGrath (1982b) have proposed two different empirical formulations for shear strength of ring sections, based on test results of rings under three-edge bearing tests, as well as other experimental evidence.

109. While shear strength of curved reinforced concrete members under combinations of axial force, shear force, and moment may be of both basic and practical interest, its importance in concrete pipe buried in the ground can be questioned. No evidence of shear failure in buried concrete pipe has been apparent.

110. Garner (1986) has studied the shear aspects of the WES test series. None of the specimens of this series failed in shear, although they were of relatively thick cross section, generally considered to be shear-critical, and subject to a wide range of load distributions. However, Heger's method (1963) did predict shear failure for these specimens, and a critical study of this strength formulation is warranted.

## Helpful Computations

111. The following computations are intended to clarify the question of criticality of shear in both the WES test specimens as well as buried culvert pipe, in general.

## Procedure

112. A circular reinforced concrete pipe as shown in Figure 28, of radius-thickness ratio $R/h$, of equal circular reinforcement inside and outside, total reinforcement index $\omega_t = (A_{st} f_y)/(h f_c')$ per unit length is considered. No web reinforcement is provided.

113. Two loading conditions will be considered: the radial load shown

59
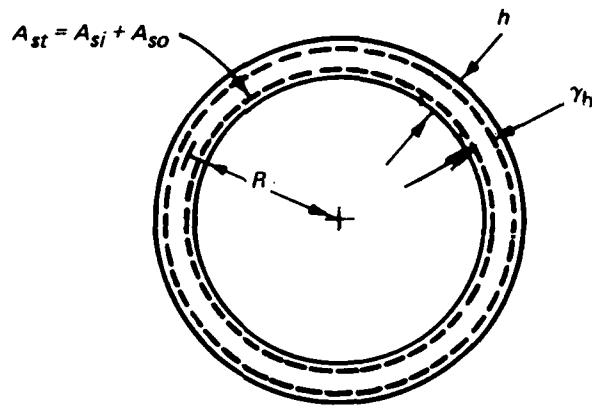
Figure 28. Culvert pipe section

in Figure 29a, varying sinusoidally as applied in the WES test series:

$$p = \frac{w}{2} [(1 + k) - (1 - k) \cos 2\theta]$$

and the EM 1110-2-2902 (Headquarters, Department of the Army 1969) loading consisting of uniform vertical load $w$ , and lateral load $kw$ , as shown in Figure 29b. To determine conditions under which the pipe is likely to fail in shear and those under which axial-flexural failure is critical, follow this procedure:

a. Determine the load $w_s$ under which shear failure will occur, following the methods of Heger (1963), which had previously been considered by Garner (1986), and Heger and McGrath (1982b).
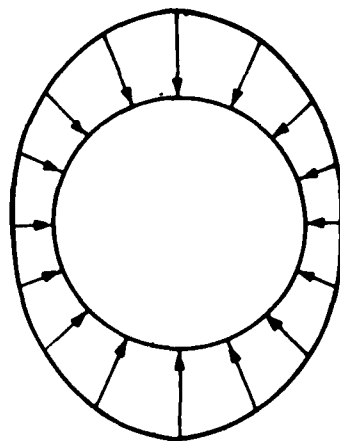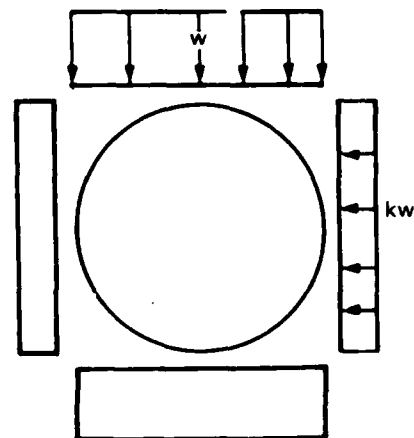


a. Test loading                    b. EM loading

Figure 29. Loading conditions

60

<u>b</u>.  Determine the load  $w_f$  under which flexural failure will
occur.  Following earlier work (Part IV), use the strength
method, which combines ultimate section strength with elastic
structure analysis.

<u>c</u>.  Compare shear and flexural strength by setting up the ratio
$w_f/w_s$ .  If larger than unity, shear failure is predicted; if
less than unity, flexural failure should occur.

114.  The ratio  $w_f/w_s = 1$  will be plotted for a range of ring propor-
tions  R/h , load distributions  k , and reinforcing indices  $\omega$ , to compare
criticality of shear and flexure for a full range of conditions.

## Shear Strength

115.  The shear strength of curved members as in reinforced concrete
pipe has been investigated over many years by Heger (1963) and Heger and
McGrath (1982a, b, c).  Two different methods proposed by these authors will
be followed.  Garner (1986) used only the Heger (1963) work to analyze the WES
test ring data, stating "although the ACI equations predict shear failure for
the 16-point load tests, none of the models failed primarily in shear."  It is
of interest to check whether the Heger and McGrath (1982b) formulation might
be more successful in predicting the failure mode of these rings.

116.  The details of the shear strength prediction according to Heger
(1963) and Heger and McGrath (1982b) will be relegated to Appendix C, in order
not to interrupt the flow of the presentation.  Overall, the sequence of
determination of the shear strength  $w_s$  is as follows:

<u>a</u>.  Determine the shear strength  $V_b$  at the critical section
according to Heger (1963) or Heger and McGrath (1982b).

<u>b</u>.  Determine the internal forces  V ,  N , and  M  at the criti-
cal section for the specified loading condition as a function
of the applied load  w .

<u>c</u>.  Equate the shear force  V  at the critical section to the
shear strength  $V_b$  and solve for the applied load  $w_s$  which
would lead to shear failure.

## Axial-Flexural Strength

117.  The graphical method outlined in Part III is used to determine the
flexural strength of the rings under both test (radial) loading and EM

61

loading. To conform to the nondimensional character of the investigation, use the appropriate nondimensional n-m strength envelopes of Part V, using the strength method, which combines the ultimate section strength for $\epsilon_u = 0.003$ with elastic structure analysis.

118. To limit the number of variables, assume the cross-sectional parameter $\gamma = (h - 2d')/h = 0.7$ , which is a reasonable average value. The reinforcing index $\omega$ varies from 0.03 to 0.11 for the WES test specimens, and is assumed to range from 0.05 to 0.15 for real culvert pipe in ground. R/h values ranging from 2 to 10, and load ratios ranging from $k = 0$ to $k = 0.8$ are considered.

119. Because the shear strength according to Heger is a function of $\sqrt{f_c'}$ , but the flexure strength depends on $f_c'$ itself, a value for the concrete strength must be assumed. The analysis has been carried out for rings having an $f_c'$ value of 5 ksi and an $f_y$ value equal to 60 ksi .

120. With the axial force $N_{sp}$ or $N_{cr}$ at the critical section known, the flexural failure load $w_f$ can be computed by Equations 3 or 5 for the test or EM loading.

## Failure Mode

121. With $w_s$ and $w_f$ known for various values of ring and load parameters R/h and $k$ , the contours $w_s/w_f = 1$ can be plotted for different values of the reinforcing index $\omega$ . Such a plot is shown in Figure 30, in which the vertical axis represents the ring proportion R/h , the horizontal axis, and the load distribution $k$ . The contours $w_s/w_f = 1$ for $\omega = 0.1$ are shown for two shear strength methods, Heger (1963) and Heger and McGrath (1982b), and for two loading conditions, the radial test loading and the EM loading.

122. Any ring with parameters above the respective contour should fail in flexure, and any ring with parameter combination below the contour should fail by shear, according to the adopted failure criteria.

123. The following conclusions can be drawn from a study of Figure 30:

    a. Thicker rings, under loading approaching hydrostatic, are more likely to fail in shear. Thinner rings, under more nonuniform load distribution, are more likely to fail in an axial-flexural mode.

62
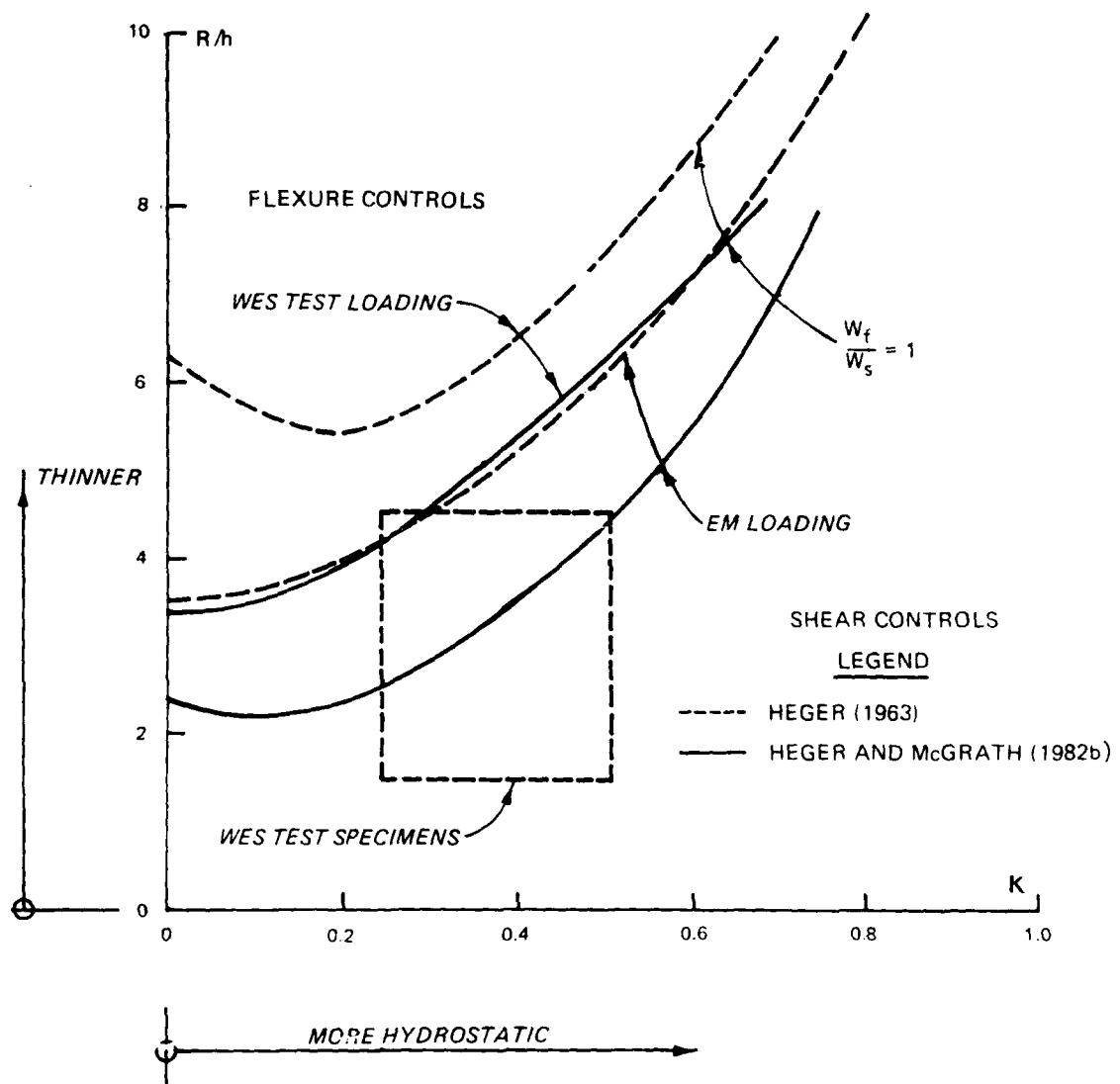
Figure 30. Flexural versus shear failure

b. The WES test (radial) loading is more likely to lead to shear failure than the EM loading.

c. For all cases, Heger (1963) predicts greater shear-criticality than Heger and McGrath (1982b).

124. The range of parameters for the WES test specimens is also indicated in Figure 30 as a rectangular box. Although Heger (1963) predicts shear failure for all these specimens (as noted by Garner (1986)), each one failed in flexure. In view of this apparent inadequacy of Heger's (1963) method, all further comparisons will draw on the Heger and McGrath (1982b) procedure.

63

125. The empirical formulation of the shear strength of the WES test specimens according to Heger and McGrath (1982b), as outlined in Appendix C, was implemented for values of $\omega = 0.05$ , $0.07$ , and $0.09$ , reflecting the levels of reinforcing of these rings. The results are shown plotted in Figure 31. It appears that the amount of flexural reinforcing has only a minor influence on the failure mode.

126. The location of the 18 test specimens, divided into four groups according to the reinforcing indices matching those of the computed
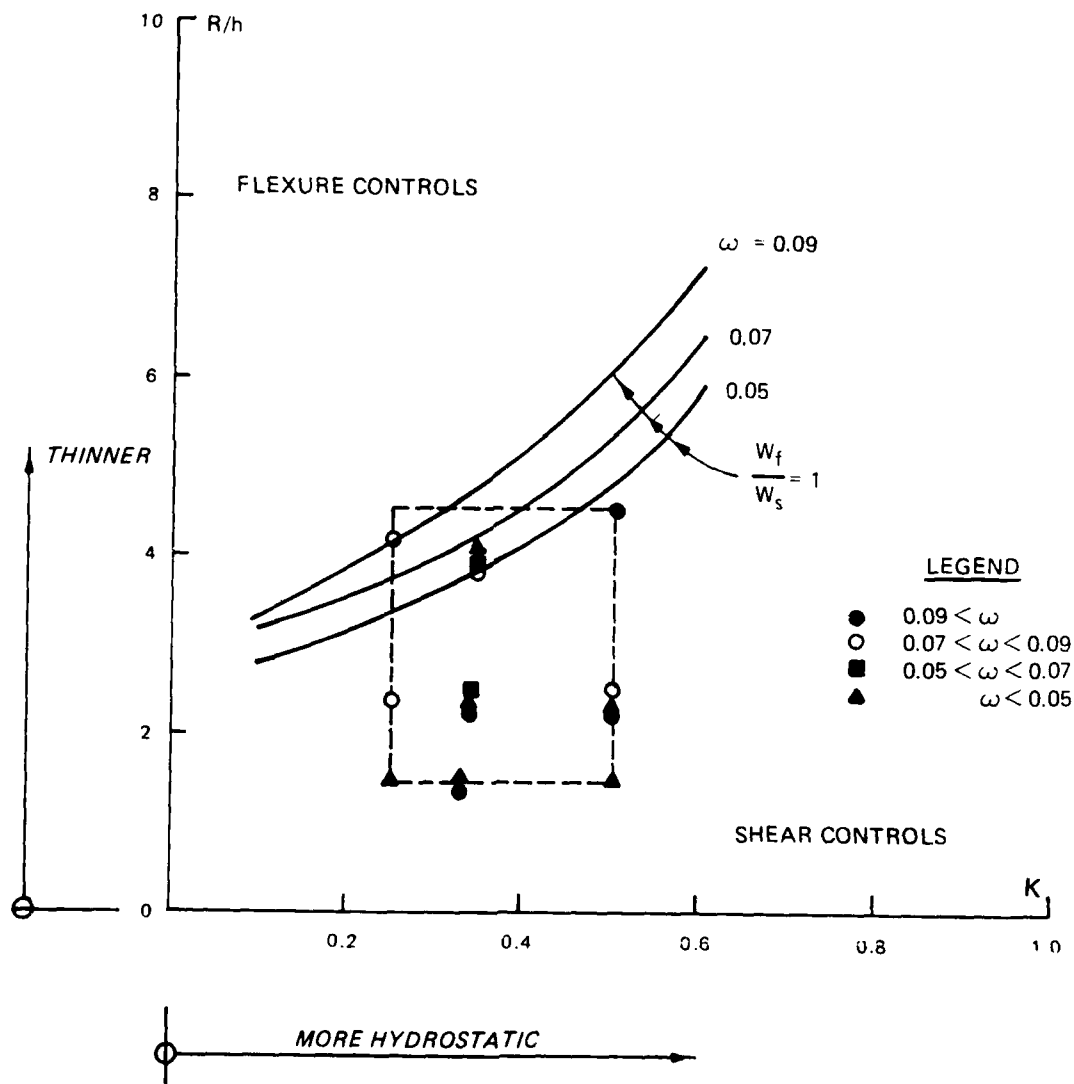


Figure 31. Predicted and observed failure mode for WES tests

contours, is also shown by different symbols on this plot. If these points appear below the respective contours, shear failure is predicted according to Heger and McGrath (1982b); if above, flexural failure.

127. Heger and McGrath (1982b) predict shear failure for all of these specimens with the exception of Models C7-1 and C8-2, and, in fact, none of these specimens failed in shear. Heger and McGrath (1982b) underestimated the shear strength of these rings by a considerable margin.

## Likelihood of Shear Failure of Pipe in Ground

128. To assess the shear failure of circular culvert pipe in ground due to soil pressure, pipe of proportion $R/h$ ranging from 5 to 10 is considered. The load distribution factor $k$, for various backfill conditions and soil types, according to EM 1110-2-2902 (Headquarters, Department of the Army 1969), Sec. 4, might vary from 0.10 to 1.0, whereby it is unlikely that the latter, hydrostatic condition, would be critical for design of circular culvert pipe.

129. The reinforcing index $\omega$ for real culvert pipe might range from 0.05 to 0.1, and Figure 32 shows the $w_f/w_s = 1$ contours for these values plotted according to Heger and McGrath (1982b), along with the field $R/h$ and $k$, for real culverts.

130. It is seen that according to Heger and McGrath (1982b), only relatively thick, heavily reinforced culverts under loads verging on the hydrostatic might fail in shear. Since such loading conditions are unlikely to be critical for design, shear failure in the ground appears unlikely.

131. Further, it was shown in the preceding section that the contours according to Heger and McGrath (1982b) are too high. If lowered according to the comparisons with the WES test results as shown in Figure 31, then it appears that the entire field of realistic circular culverts is located in the axial-flexural failure range.

132. It can be concluded that shear failure of circular culvert pipe under soil pressure is quite unlikely.

## Shear Strength of Rings in Three-Edge Bearing

133. Because the Heger (1963) and Heger and McGrath (1982b) formulations have been calibrated using three-edge bearing test results, and because

65
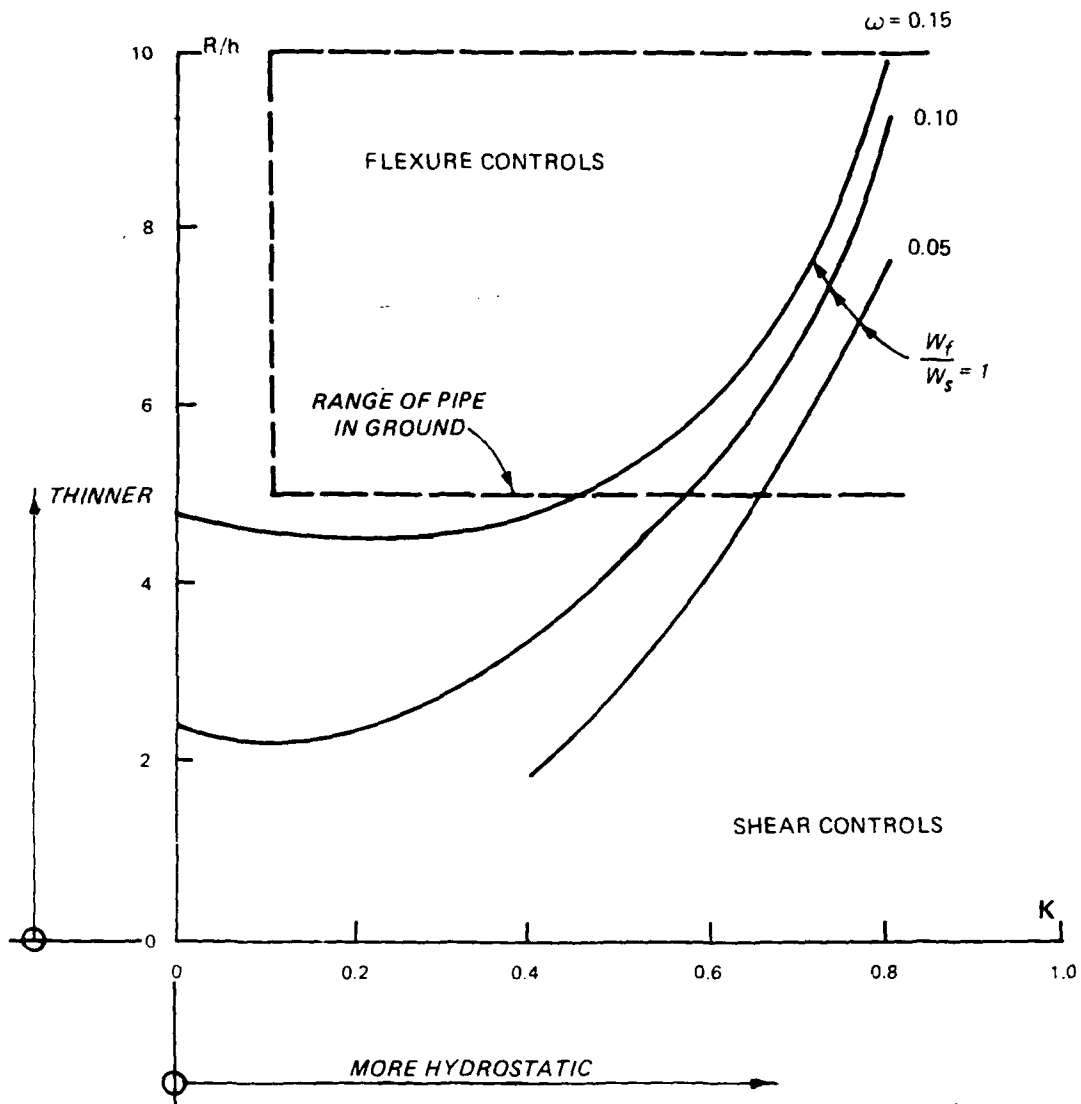
Figure 32.  Failure mode for pipe in ground

these formulations do not seem effective in predicting the shear strength of rings under distributed loadings, it seems appropriate to study the three-edge bearing test conditions and results.  To determine possible causes for these discrepancies, the test data of Heger, Nawy, and Saba (1963) were studied.

134.  The tenuousness of relation between pipe strength in three-edge bearing and in the ground was pointed out by Heger and McGrath (1982c) as follows:

> "(The three-edge bearing test) does not always provide an accurate basis for determining the in-ground strength of the pipe..., due to differences...between in-ground loading conditions and three-edge loading conditions."

66

135. The approach used in this technical report, which uses a rational method for the determination of the axial-flexural strength and the best available formulation for the shear strength, could be expected to provide understanding of conditions and modes of failure, irrespective of loading condition. Accordingly, the same method used in a previous section will be used to analyze some of the three-edge bearing tests of Heger, Nawy, and Saba (1963) to compare them to observed failure modes.

### Failure Modes for Three-Edge Bearing and Distributed Loads

136. To analyze for flexural or shear failure, proceed in this manner:

    a. Follow the strength approach of Part IV for determination of the axial-flexural strength, using nondimensional formulation.

    b. Follow Heger and McGrath (1982b) as previously outlined to determine the shear strength, on a nondimensional basis.

    c. By comparing the results of a and b, predict criticality of flexural or shear failure for rings of given characteristics: because the load distribution factor k is not a variable in this case, attention has been focused on the ring slenderness $R/h$ and the reinforcing index $\omega$ .

137. The critical section in flexure is at the loaded crown section, where the axial force is zero, so the section is in pure bending. The location $\theta$ of the critical section for shear, according to Equation C-6, is given for the assumed average value of $\gamma = 0.7$ by the transcendental equation

$$\frac{2}{\pi} \frac{1}{\cos \theta} - \tan \theta = \frac{2.55}{(R/h)} \qquad (44)$$

The shear strength of the section at points defined by this equation was calculated according to Heger and McGrath (1982b), using the procedure outlined in Appendix C. The average values, $\gamma = 0.7$ , $f'_c = 5$ ksi, and $f_y = 89$ ksi, have been assumed representing values of Tables 1 and 2 according to Heger, Nawy, and Saba (1963). Steel inside and outside was assumed equal in area to that of the inside steel at the critical section for flexure. This approximation seems insignificant.

138. The ratio of flexural to shear strength $P_f/P_s$ was computed, and the contour $P_f/P_s = 1$ entered onto the plot of Figure 33. Any ring in

67
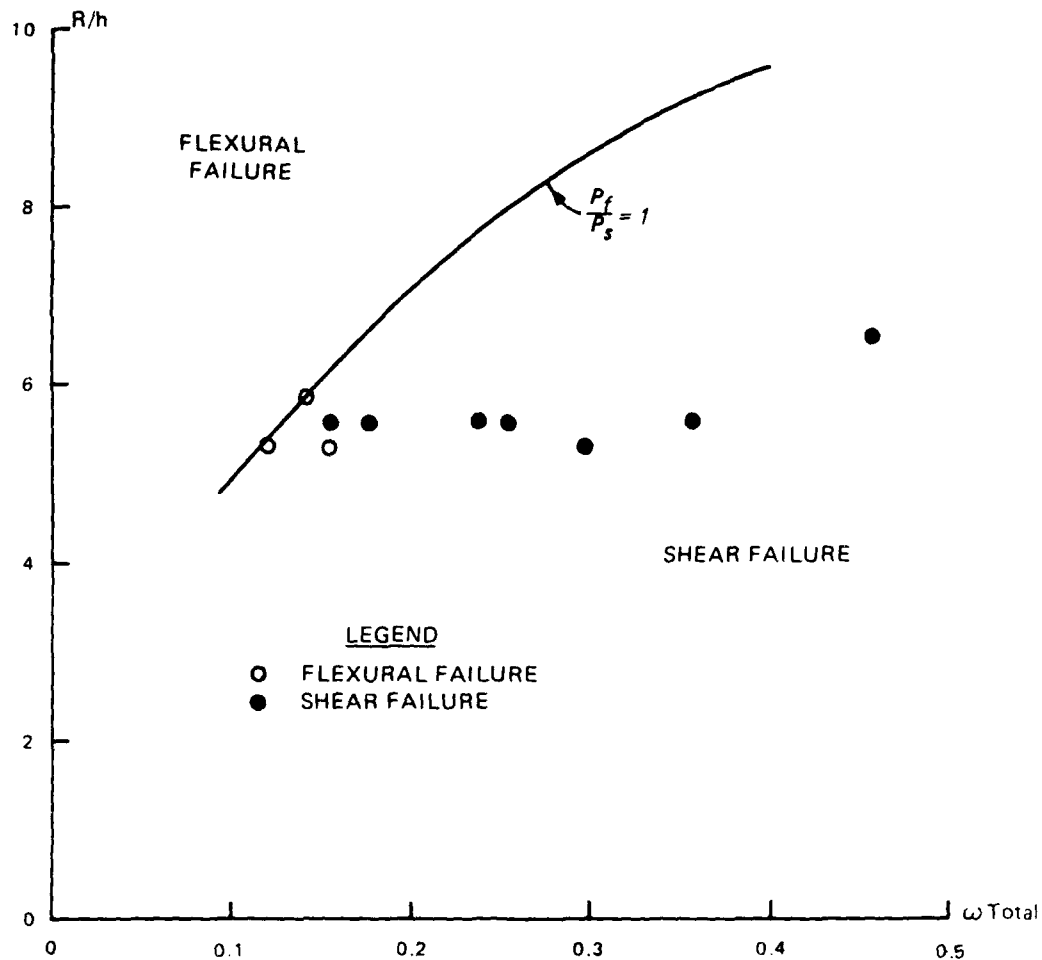
Figure 33. Predicted and observed failure modes for
three-edge bearing tests

three-edge bearing above this contour should, according to these predictions, fail in flexure; below this contour, fail in shear.

139. On the same plot, the test results have been entered from Table 4 of the paper by Heger, Nawy, and Saba (1963), which summarizes a test series conducted at the Massachusetts Institute of Technology on rings. These are indicated by two different symbols in Figure 33. All specimens except two are well within the range in which shear failure should be expected. Three specimens which are on, or near the dividing line between expected shear and flexural failure, did fail in flexure. It appears that American Society for Testing Materials culvert types unreinforced against shear, with all but minimal hoop reinforcing will always fail in shear, as reported by Heger, Nawy,

and Saba (1963). Indeed, those specimens within this range which were reported in the same study to have failed in flexure were supplied with shear reinforcing. Further, the reported failure loads of these rings were reasonably close to those predicted by the Heger and McGrath (1982b) method. This should have been expected since they were used to calibrate this prediction method.

140. Still unresolved is why the Heger and McGrath (1982b) formulation does in fact seem to be able to predict the shear strength of pipes under three-edge bearing, but not under distributed loads. Two possible reasons are:

   a. In pipe under three-edge bearing, sections of maximum shear are also sections of maximum moment, whereas in pipe under distributed loading (test or EM), the section of maximum shear corresponds to the section of zero moment, and vice versa. Thus, it is possible that there is little relation between the shear strength of pipe under three-edge bearing, and that of pipe in the ground.

   b. Further, the critical section in Heger and McGrath (1982b) defined by Equation C-6 was based on beam test results of Kani, Huggins, and Wittkopp (1979). This approach simply states that if a point load is applied too closely to the beam support, transfer of load to the support takes place by compressive arch action rather than by flexural shear leading to diagonal tension. Rings under distributed loading (or three-edge loading, for that matter) respond quite differently and their critical sections may also be located elsewhere.

## Suggestion for Shear Test Program

141. The results of the preceding sections indicate that currently available methods for prediction of shear strength do not seem particularly effective for assessing the shear capacity of pipe sections under distributed loading. This is not surprising since these are empirical equations based on test data from a variety of specimens under quite different combinations of geometry and loading.

142. In view of the fact that so far, rational analysis of shear strength of even straight, prismatic, reinforced concrete beams has not been very successful, it appears that empirical approaches based on test results of appropriate specimens must be relied on for better information. In the following paragraph, one approach is suggested.

143. Refer to the test program of Heger and McGrath (1982a) on radial tension strength, which deals with one third of an 84-in.-diam pipe section,

69

subtending 120 deg, supported and loaded for constant moment and zero shear at midspan. The same specimen, under different arrangement of load and supports as shown in Figure 34a, will have a region of constant shear and variable moment in its central region, as shown in Figures 34b and 34c.

144. With shear reinforcement provided over all but the portion of the specimen expected to fail in shear, shear failure under a range of M/V ratios could be investigated with such an arrangement. Small axial forces will also be present in the specimen. Independent control of axial forces will be more complex.

145. If shear strength of culvert sections is of concern (in spite of the question of relevance raised in a preceding section), then it appears that a purposeful, carefully designed series of tests may be necessary. Such a test program will require considerable planning and investment.

a. Test setup

b. Shear on tranverse section

c. Moment, K - in.

42 in.

8.75"

$P$

0.06P

1.94P

2' - 0 1/2 in.    2' - 4 in.    2' - 0 1/2 in.

0.95P

0.50P

0.03P    0.06P

0.90P    0.90P

0.95P

1.5P

24.5P

27.2
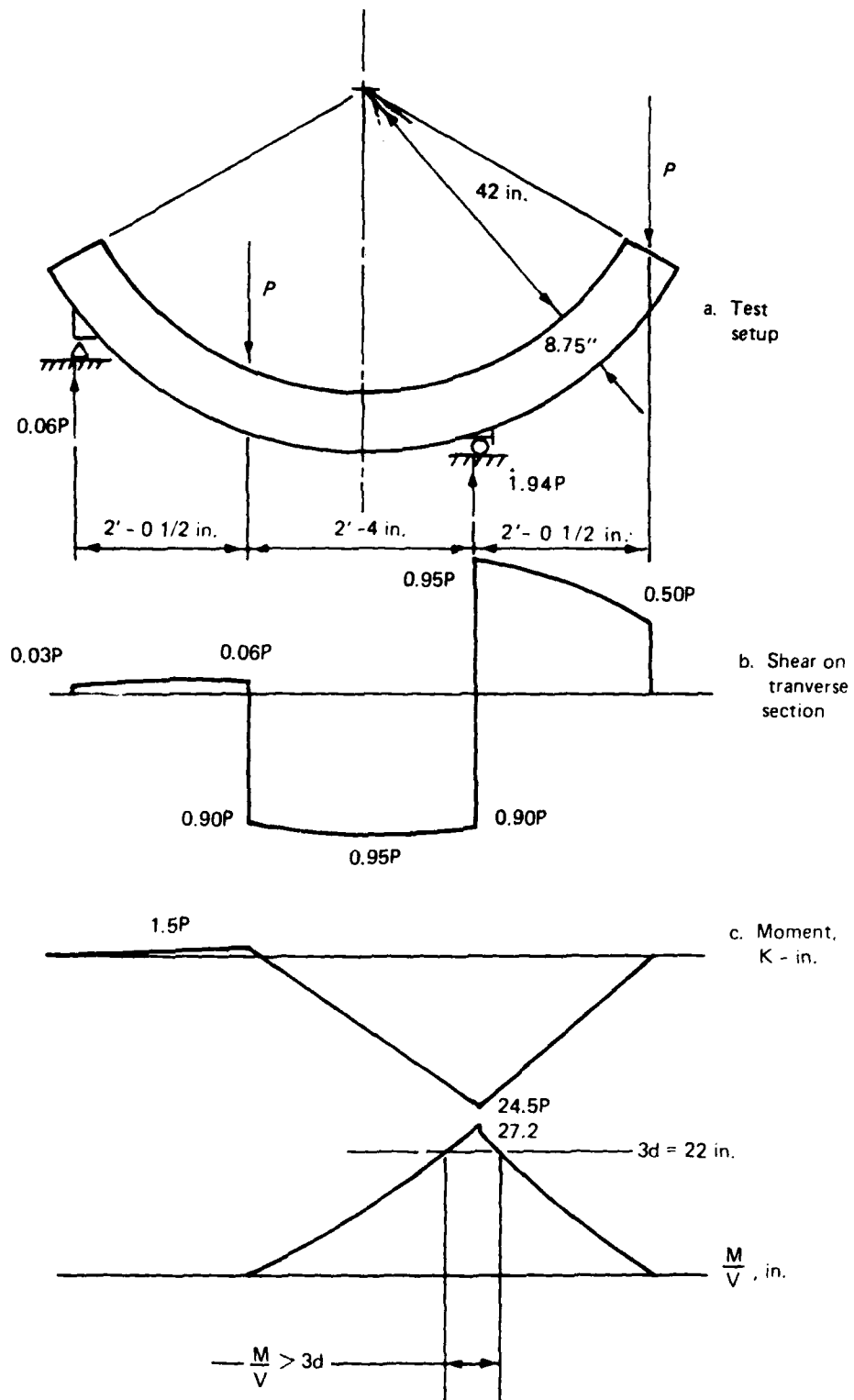
3d = 22 in.

$\dfrac{M}{V}$ , in.

$\dfrac{M}{V} > 3d$

Figure 34.  Ring shear test

# PART VII: SUMMARY, CONCLUSIONS, AND RECOMMENDATIONS

## Summary

146. In an effort to gain maximum benefit from the results of the WES ring test program, various experimental and analytical aspects of circular reinforced concrete culvert sections were studied. Among these were analyses of the flexural strength of these specimens according to elastic and plastic theories (Parts II and III), and comparison with test results (Part IV). Also in Part IV are studies of the effects of various basic material and structure assumptions on analysis results. Part V deals with design aspects of circular rings, whereby a graphical longhand method was stressed. This approach can be used in practice but, more importantly, also provides an outline for a computer-based design procedure to be implemented in future work. Part VI considers problems of shear strength of reinforced concrete rings without shear reinforcement under various loading conditions and points out a number of discrepancies to be resolved by future studies.

147. Among aspects which were not considered in this work were:

    <u>a</u>. Crack width limitations.

    <u>b</u>. Radial tension problems, or "slabbing."

    <u>c</u>. Most importantly, the interaction between soil and structure. All analyses of pipe in the ground were carried out using the soil pressures prescribed in EM 1110-2-2902 (Headquarters, Department of the Army 1969). In fact, the soil provides not only the load, but also the constraint which prevents uncontrolled deformations of the pipe, therefore contributing to the pipe strength.

## Conclusions

148. Some of the major conclusions from the study are:

    <u>a</u>. Plastic or elastic analyses of ring sections under distributed loads are practical, convenient tools for strength determination. For radial or EM 1110-2-2902 (Headquarters, Department of the Army 1969) loadings on circular rings, elastic analysis is even simpler than plastic analysis. Sufficient rotation capacity is available for full redistribution of moments.

    <u>b</u>. Purely elastic theory at both section and structure level (the "working stress" approach) underestimates the flexural strength of rings by a wide margin.

72

c. The choice of crushing strain of concrete has only a minor influence on the ultimate section strength. An ultimate strain of 0.003 in./in., corresponding to ACI 318 (1983), is recommended.

d. The strength method, which combines ultimate section strength with elastic structure analysis, is recommended for pipe design. It follows well known concepts, is convenient, and will produce results slightly on the conservative side of fully plastic analysis. Elastic analysis also provides a basis for future inclusion of soil-structure interaction.

e. Comparison with results of the WES test series indicates flexural reserve strength beyond that predicted by either strength or plastic analysis for thick rings, but unsafe predictions for the thin rings. Possible explanations are offered for these discrepancies.

f. Prediction of shear strength of rings according to Heger (1963) or Heger and McGrath (1982b) is satisfactory for rings in three-edge bearing, but is highly conservative for shear strength determination of these rings under distributed loading. Possible explanations are offered for these discrepancies.

g. Calculations indicate that shear strength may never be of concern for circular concrete pipe in the ground.

## Recommendations for Further Work

149. The following recommendations are intended for logical continuation of the work done so far, with the aim of arriving at a better understanding of the behavior and strength of circular concrete culvert pipe in the ground. A full understanding will permit optimal design of safe and economical pipe.

a. Computerized flexural design methods, based on the principles outlined in this report, should be developed and implemented. Harter, Bircher, and Wilson (1980) provide a solid foundation for this work.

b. In view of the apparent inadequacy of currently available methods for prediction of shear strength of pipe sections, a complete, well-thought-out study of shear strength, with both analytical and experimental phases, seems indicated. Part VI contains some suggestions along these lines.

c. The loading conditions in EM 1110-2-2902 do not seem realistic. Since pipe strength depends primarily on the soil pressure experienced by the pipe during its lifetime, a complete understanding of the soil-structure interaction is necessary. Modern computer methods permit such analyses. Currently available tools (Olander 1950; Heger, Liepins, and Selig 1985)

73

should be studied for applicability, and procedures laid out which incorporate these effects in analysis and design. This requires cooperation of structural, geotechnical, and computer engineers, and a long-term commitment, but will be necessary for rational assessment of pipe safety.

# REFERENCES

American Concrete Institute. 1983. "Building Code Requirement for Reinforced Concrete," ACI 318-83, Detroit, Mich.

_____. 1985. "Design Handbook," Vol 2, Detroit, Mich.

Anderson, R. H., Haelsig, R. T., and Reifel, M. D. 1966 (Mar). "Structural Behavior of Ring Sections under Nonuniform External Pressure," Technical Report No. AFWL-TR-65-145, Air Force Weapons Laboratory, Kirtland Air Force Base, N. Mex.

Chiarito, Vincent, and Mlakar, Paul. 1984 (Sep). "Strength Design of Reinforced Concrete Hydraulic Structures; Load-Moment Characteristics of Reinforced Concrete Circular Conduits," Technical Report SL-80-4, Report 4, US Army Engineer Waterways Experiment Station, Vicksburg, Miss.

Garner, S. B. 1986 (Jan). "Shear and Radial Tension Capacity of Circular Conduit Models" (In-House Report), US Army Engineer Waterways Experiment Station, Vicksburg, Miss.

Gerstle, K. H. 1974. Basic Structural Analysis, Prentice-Hall, Englewood Cliffs, N. J.

_____. 1985 (Aug). "Analytical Study of WES Ring Tests," Structural Research Series 8504, Civil, Environmental, and Architectural Engineering Department, University of Colorado, Boulder, Colo.

Harter, M. M., Bircher, B. F., and Wilson, H. B. 1980 (Feb). "User's Guide: Computer Program for Design/Review of Curvilinear Conduits/Culverts," Instruction Report K-80-1, US Army Engineer Waterways Experiment Station, Vicksburg, Miss.

Headquarters, Department of the Army. 1969. "Design of Miscellaneous Structures, Conduits, Culverts, and Pipes," Engineer Manual 1110-2-2902, Washington, DC.

Heger, F. J. 1963 (Nov). "Structural Behavior of Circular Reinforced Concrete Pipe - Development of Theory," Journal, American Concrete Institute, Vol 60, p 1567.

Heger, F. J., Liepins, A. A., and Selig, E. T. 1985 (Aug). "SPIDA: An Analysis and Design System for Buried Concrete Pipe," International Conference on Advances in Pipeline Engineering, Madison, Wisc.

Heger, F. J., and McGrath, T. J. 1982a. "Radial Tension Strength of Pipe and Other Curved Flexural Members," Journal, American Concrete Institute, Vol 80, p 33.

_____. 1982b. "Shear Strength of Pipe, Box Sections, and Other One-Way Flexural Members," Journal, American Concrete Institute, Vol 79, p 470.

Heger, F. J., and McGrath, T. J. 1982c. "Design Method for Reinforced Concrete Pipe and Box Sections," Report to Technical Committee of American Concrete Pipe Association, Cambridge, Mass.

Heger, F. J., Nawy, E. G., and Saba, R. B. 1963 (Oct). "Structural Behavior of Circular Concrete Pipe Reinforced with Welded Wire Fabric," Journal, American Concrete Institute, Vol 60, p 1389.

Hodge, P. G., Jr. 1959. Plastic Analysis of Structures, McGraw-Hill, New York.

Kani, M. W., Huggins, M. W., and Wittkopp, R. R. 1979. "Kani on Shear in Reinforced Concrete," University of Toronto Press, Toronto, Ont., Canada.

Olander, H. C. 1950. "Stress Analysis of Concrete Pipe," Engineer Monograph No. 6, US Bureau of Reclamation, Denver, Colo.

Park, R., and Paulay, T. 1975. Reinforced Concrete Structures, Wiley, New York.

Wright, Stephen, and Chiarito, Vincent. 1987 (Apr). "Strength Design of Reinforced Concrete Hydraulic Structures; Experimental Study on the Ultimate Behavior of Model Reinforced Concrete Circular Conduits," Technical Report SL-80-4, Report 5, US Army Engineer Waterways Experiment Station, Vicksburg, Miss.

# APPENDIX A: ELASTIC ANALYSIS OF RINGS

(Equations and figures cited in this appendix can be found
in the main text by the corresponding numbers, and refer-
ences are listed in the References section at the end of
the main text.  Symbols used in this appendix are defined
in the Notation, Appendix D.)

## Equilibrium

(From Figure 2):   On element of unit length:

$$Y = w \cdot \sin \theta \qquad\qquad X = kw \cdot \cos \theta$$

$$Y_N = w \cdot \sin^2 \theta \qquad\qquad X_N = kw \cdot \cos^2 \theta$$

$$Y_T = w \cdot \sin \theta \cos \theta \qquad\qquad X_T = kw \cdot \sin \theta \cos \theta$$

$$p_N = Y_N + X_N = w \, (\sin^2 \theta + k \cdot \cos^2 \theta)$$

$$= \frac{w}{2} \left[ (1 + k) - (1 - k) \cos 2\theta \right] \qquad\qquad (1)$$

$$p_T = Y_T - X_T = w \, (\sin \theta \cos \theta - k \sin \theta \cos \theta)$$

$$= \frac{w}{2} \, (1 - k) \sin 2\theta \qquad\qquad (2)$$

US Army Engineer Waterways Experiment Station (WES)

Test loading:   Due to $p_N$  only

(From Figure 4b)

Axial forces at Springing (SP) and Crown (CR) (Compression is +):

$$\Sigma F_y = 0 : \quad N_{sp}^N = \int_{\theta=0}^{\pi/2} p_N \sin \theta \cdot R d\theta$$

$$= \frac{wR}{2} \int_{0}^{\pi/2} \left[ (1 + k) - (1 - k) \cos 2\theta \right] \sin \theta d\theta$$

$$= \frac{wR}{3} \, (2 + k) = \frac{8}{3\pi} \, P_{cr} \, (2 + k) \qquad\qquad (3a)$$

A2

$$\Sigma F_x = 0 : \quad N_{cr}^{N} = \int_{\theta=0}^{\pi/2} P_N \cos \theta \cdot Rd\theta$$

$$= \frac{wR}{2} \int_{0}^{\pi/2} (1 - k) \sin 2\theta \cos \theta d\theta$$

$$= \frac{wR}{3} (2k + 1) = \frac{8}{3\pi} P_{cr} (2k + 1) \qquad (3b)$$

(From Figure 4b):

$$\overset{\curvearrowright}{\Sigma M}_{o} = 0 : (N_{cr} - N_{sp})R + M_{cr} + M_{sp} = 0 :$$

$$(M_{sp} + M_{cr}) = (N_{sp} - N_{cr})R$$

$$= \frac{wR^2}{3} (1 - k) = \frac{8}{3\pi} P_{cr}R(1 - k) \qquad (7)$$

EM 1110-2-2902 (Headquarters, Department of the Army 1969) loading: Due to $P_N + P_T$ (From Figure 4a)

$$\Sigma F_y = 0 : \quad N_{sp}^{T} = \int_{\theta=0}^{\pi/2} P_T \cos \theta \cdot Rd\theta$$

$$= \frac{wR}{2} \int_{0}^{\pi/2} (1 - k) \sin 2\theta \cos \theta d\theta = \frac{wR}{3} (1 - k) \qquad (4a)$$

A3

$$\Sigma F_x = 0 : \quad N_{cr}^T = - \int_{\theta=0}^{\pi/2} p_T \sin \theta R d\theta$$

$$= - \frac{wR}{2} \int_0^{\pi/2} (1 - k) \sin 2\theta \sin \theta d\theta = \frac{wR}{2} (k - 1) \qquad (4b)$$

Adding resultants of $p_N$ and $p_T$ (EM loading):

$$N_{sp} = N_{sp}^N + N_{sp}^T = wR \qquad (5a)$$

$$N_{cr} = N_{cr}^N + N_{cr}^T = \underline{kw \cdot R} \qquad (5b)$$

From Figure 4a:

$$\overset{+}{\Sigma} M_{sp} = 0 : \quad M_{cr} + M_{sp} + N_{cr} \cdot R - wR(1 + k) \frac{R}{2} = 0$$
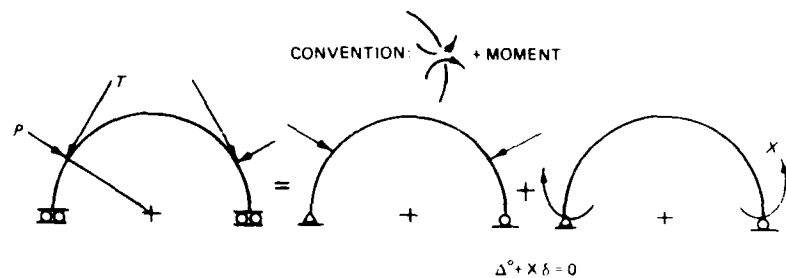
$$(M_{sp} + M_{cr}) = \frac{wR^2}{2} (1 - k) \qquad (6)$$

Elastic Analysis

Procedure:

1. Use Force Method

$$\therefore X = \frac{-\Delta^{\circ}}{\delta}$$



CONVENTION: + MOMENT

$\Delta^{\circ} + X\delta = 0$

2. Use Symmetry: a. Compute $X$ due to symmetric point loads $P$, $T$

b. Integrate over $\frac{\pi}{2}$: $P = p_N \cdot ds$

$T = p_T \cdot ds$

A4

3.  Compute effects of normal loads $p_N$ and tangential loads $p_T$, separately.

4.  Compute  M  and  N  at  SP  and  CR  sections

### Normal Load Components

Concentrated load  P  at  $\theta$
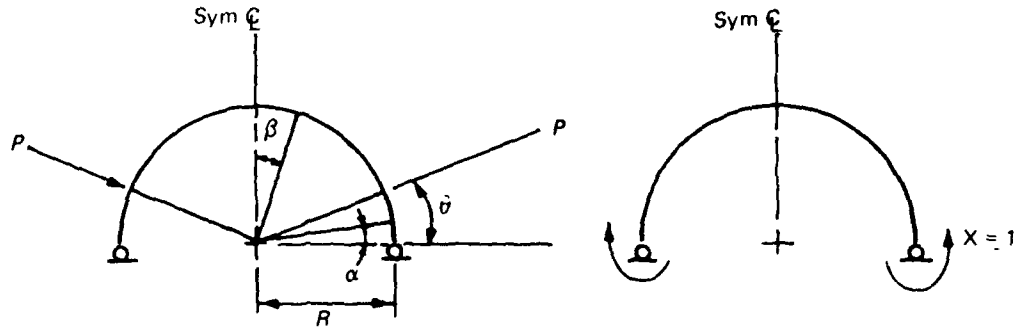


$$M = PR(1 - \cos \alpha) \, , \quad \alpha \leq \theta \qquad\qquad m = 1 \, , \quad 0 \leq \theta \leq \frac{\pi}{2}$$

$$M = PR (\sin \theta - \cos \theta \cos 3) \, , \quad \beta \leq \left(\frac{\pi}{2} - \theta\right)$$

By  VW :

$$\Delta^\circ = \int_{\theta=0}^{\pi/2} \frac{Mm}{EI} \cdot Rd\theta = \frac{PR}{EI} \left(\frac{\pi}{2} \sin \theta - 1\right)$$

$$\delta = \int_{\theta=0}^{\pi/2} \frac{m^2}{EI} \cdot Rd\theta = \frac{R}{EI} \cdot \frac{\pi}{2}$$

$$X = - \frac{\Delta^\circ}{\delta} = PR\left(\frac{2}{\pi} - \sin \theta\right) = M_{sp}$$

A5

and

$$M = PR\left(\frac{2}{\pi} - \sin \theta \cos \alpha\right) , \quad \alpha \leq \theta$$

$$M = PR\left(\frac{2}{\pi} - \cos \theta \cos \beta\right) , \quad \beta \leq \frac{\pi}{2} - \theta$$

Moment at SP and CR:

$$M_{sp} = M(\alpha = 0) = PR\left(\frac{2}{\pi} - \sin \theta\right)$$

$$M_{cr} = M(\beta = 0) = PR\left(\frac{2}{\pi} - \cos \theta\right)$$

Due to $\quad p_N = \frac{w}{2}\left[(1 + k) - (1 - k) \cos 2\theta\right]$

$$= w(a - b \cos 2\theta) : \quad \text{in which} \quad a = \frac{1}{2} (1 + k)$$

$$b = \frac{1}{2} (1 - k)$$

$$P = p_N R d\theta = w(a - b \cos 2\theta)R d\theta$$

Integrating over quarter ring:

$$M_{sp} = \int_{\theta=0}^{\pi/2} w(a - b \cos 2\theta)\left(\frac{2}{\pi} - \sin \theta\right)R^2 d\theta = -\frac{wR^2}{6} (1 - k)$$

$$M_{cr} = \int_{\theta=0}^{\pi/2} w(a - b \cos 2\theta)\left(\frac{2}{\pi} - \cos \theta\right)R^2 d\theta = +\frac{wR^2}{6} (1 - k) \quad\quad (24)$$

Moments due to WES test loading are equal

A6

## Tangential Load Components

Concentrated load  T  at  θ
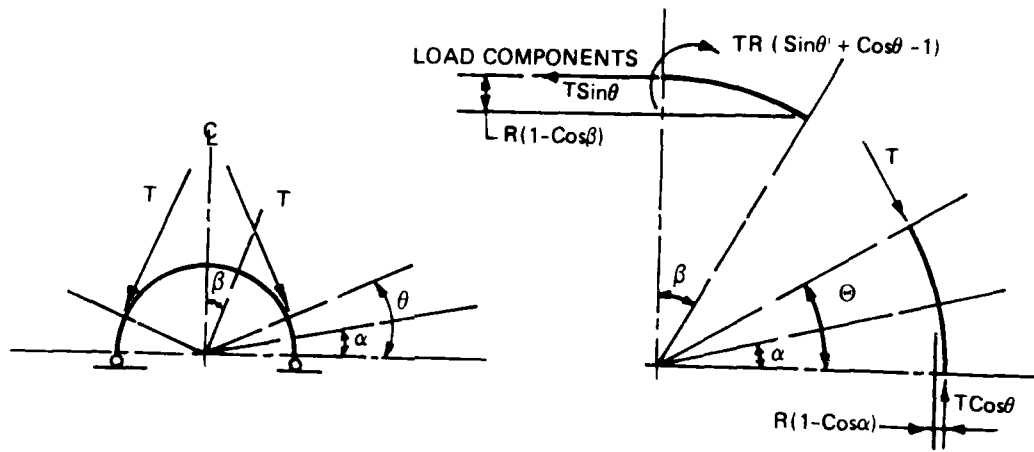


$M = TR \cos \theta \, (1 - \cos \alpha) \, , \quad \alpha \leq \theta$

$M = TR(\cos \theta + \sin \theta \cos \beta - 1) \, , \quad \beta \leq \dfrac{\pi}{2} - \theta'$

Due to redundant  X = 1 :  (as before)

m = 1

By  VW :

$$\Delta^\circ = \int_{\theta=0}^{\pi/2} \frac{Mm}{EI} \cdot Rd\theta = \frac{TR^2}{EI}\left[\theta + \frac{\pi}{2} \, (\cos \theta - 1)\right]$$

$$\delta = \int_{\theta=0}^{\pi/2} \frac{m^2}{EI} \cdot Rd\theta = \frac{R}{EI} \cdot \frac{\pi}{2}$$

A7

$$X = -\frac{\Delta^\circ}{\delta} = TR\left(1 - \cos\theta - \frac{2}{\pi}\theta\right) = M_{sp}$$

$$M = TR\left(1 - \cos\theta\cos\alpha - \frac{2}{\pi}\theta\right), \quad \alpha \leq \theta$$

$$M = TR\left(\sin\theta\cos\beta - \frac{2}{\pi}\cdot\theta\right), \quad \beta \leq \frac{\pi}{2} - \theta$$

Moment at SP and CR:

$$M_{sp} = M(\alpha = 0) = TR\left(1 - \cos\theta - \frac{2}{\pi}\theta\right)$$

$$M_{cr} = M(\beta = 0) = TR\left(\sin\theta - \frac{2}{\pi}\theta\right)$$

Due to $p_T = \frac{w}{2}(1-k)\sin 2\theta = w \cdot b \sin 2\theta$ :

$$\text{where} \quad b = \frac{1}{2}(1-k) ,$$

$$T = wb \sin 2\theta \cdot Rd\theta$$

Integrating over quarter ring:

$$M_{sp} = \int_{\alpha=0}^{\pi/2} (wb \sin 2\theta)\left(1 - \cos\theta - \frac{2}{\pi}\theta\right)R^2 d\theta = -\frac{1}{12}wR^2(1-k)$$

$$M_{cr} = \int_{\beta=0}^{\pi/2} (wb \sin 2\theta)\left(\frac{2}{\pi} - \cos\theta\right)R^2 d\theta = +\frac{1}{12}wR^2(1-k)$$

Due to EM 1110-2-2902 loading:  Add results due to  P  and  T  loading:

$$M_{sp} = wR^2(1-k)\left(-\frac{1}{6} - \frac{1}{12}\right) = -\frac{1}{4}wR^2(1-k)$$

$$M_{cr} = wR^2(1 - k)\left(+ \frac{1}{6} + \frac{1}{12}\right) = + \frac{1}{4} wR^2(1 - k) \tag{25}$$

Moments due to EM 1110-2-2902 loading are equal.

APPENDIX B:  HINGE ROTATION OF RINGS

(The equations cited in this appendix can be found in the
main text by the corresponding numbers, and the references
are listed in the References section at the end of the main
text.  Symbols used in this appendix are defined in the
Notation, Appendix D.)

## Plastic Hinge Rotation

Assume plastic hinge rotation occurs at SP

Hinge rotation $\theta_{sp} = 2\Delta°$ ,

$\Delta°$ due to $\Delta P$ at $\theta$ : From Appendix A:

$$\Delta° = \frac{\Delta PR^2}{EI}\left(\frac{\pi}{2} \sin\theta - 1\right) ;$$

Due to distributed test loading: $\Delta P = \Delta p_N = \Delta w(a - b \cos 2\theta)Rd\theta$ , and

$$\Delta° = \frac{\Delta wR^3}{EI} \int_{\theta=0}^{\pi/2} (a - b\cos 2\theta)\left(\frac{\pi}{2}\sin\theta - 1\right)d\theta$$

$$= \frac{\Delta wR^3}{EI} \cdot \frac{\pi}{12}(1 - k) , \quad \text{since} \quad \Delta w = \frac{8}{\pi R} \cdot \Delta P_{cr}$$

$$\theta_{sp} = \frac{\Delta wR^3}{EI} \cdot \frac{\pi}{6}(1 - k) = \frac{\Delta P_{cr}R^2}{EI} \cdot \frac{4}{3}(1 - k) \tag{33}$$

Hinge rotation at SP due to <u>Test Loading</u> for $P_{cr} > \frac{3\pi}{4} \frac{M_o}{R} \frac{1}{1 - k}$

$\Delta°$ due to $\Delta T$ at $\theta$ : From Appendix A:

$$\Delta° = \frac{\Delta TR^2}{EI}\left[\theta + \frac{\pi}{2}(\cos\theta - 1)\right]$$

B2
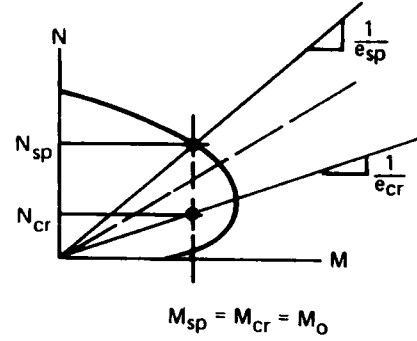
Due to distributed tangential loading: $\Delta T = \Delta p_T = \Delta w \cdot b \sin 2\theta \cdot Rd\theta$ ;

$$\Delta^\circ = \frac{\Delta w R^3}{EI} \int_{\theta=0}^{\pi/2} (b \sin 2\theta) \cdot \left[\theta + \frac{\pi}{2}(\cos\theta - 1)\right] d\theta$$

$$= \frac{\Delta w R^3}{EI}(1 - k) \cdot \frac{\pi}{3}$$

Due to EM 1110-2-2902 (Headquarters, Department of the Army 1969) load:

$$\Delta^\circ = \Delta_N^\circ + \Delta_T^\circ = \frac{\Delta w R^3}{EI}(1 - k) \cdot \frac{5\pi}{12}$$

$\therefore$ Hinge rotation due to EM load is:

$$\theta_{sp} = 2\Delta_o = \frac{\Delta w R^3}{EI}(1 - k) \cdot \frac{5\pi}{6} \tag{34}$$

Hinge rotation at springing due to <u>EM 1110-2-2902 Loading</u> for $w > \dfrac{M_o}{R^2}\dfrac{4}{1-k}$

## Plastic Hinge Rotation at SP for Specimen 2-1, WES Test Loading

From Wright and Chiarito (1987) and as shown in Table 1:

$R = 7.47$ in., $k = \dfrac{1}{3}$

From Wright and Chiarito (1987) and as shown in Tables 3 and 4:

$$\left.\begin{array}{l} E_s = 28.1 \times 10^3 \text{ ksi} \\[2ex] E_c = 4.19 \times 10^3 \text{ ksi} \end{array}\right\} \ n = 6.7$$

where

$E_s$ = modulus of elasticity of steel

$E_c$ = initial elastic concrete modulus

I OF UNCRACKED SECTION



$A_s = 0.10$ in$^2$

B = 5.27 in.

1.75" 1.75"

H = 5.0 in.
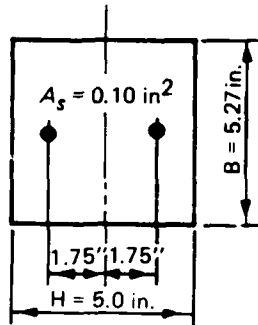
$$I_T = \frac{1}{12} \cdot 5.27 \cdot 5.00^3$$

$$+ \; 6.7 \cdot 0.10 \cdot 1.75^2 \cdot 2$$

$$= 59.0 \text{ in.}^2$$

$$EI = 4.19 \cdot 10^3 \cdot 59$$

$$= 247 \cdot 10^3 \text{ k-in.}^2$$

From Equation 33 for test loading, with $\Delta P_{cr}$ = 28.8 k – 27.8 k = 1.0 k :

$$\theta_{sp} = \frac{4}{3} (1 - k) \frac{\Delta PR^2}{EI} = \underline{0.20 \cdot 10^{-3} \text{ rad}}$$

Rotation capacity at  SP  for Specimen 2.1, WES Test Loading

For $M_{sp}$ = 55 k-in.,  $N_{sp}$ = 57 k:   c = 4.2 in.

$$\phi_u = \frac{\varepsilon_u}{C} = \frac{0.003}{4.2} = 0.71 \cdot 10^{-3} \text{ rad/in.}$$

$$\theta_u = \phi_u \cdot H = 0.71 \cdot 10^{-3} \cdot 5.0 \text{ in.} = \underline{3.5 \cdot 10^{-3} \text{ rad}}$$

APPENDIX C:  SHEAR AND FLEXURAL STRENGTH OF RINGS

(The references cited in this appendix are listed in the
References section at the end of the main text.)

1. In this appendix, calculations in support of the analyses presented in Part VI, "Shear Strength of Rings," will be shown in this sequence:

  a. Two formulations for the shear strength of rings, by Heger (1963) and Heger and McGrath (1982b). The procedure leading to the shear strength values $w_s$ used in Part VI is also outlined.

  b. Procedure and sample calculations for the calculation of the flexural strength $w_f$ for these rings, using methods established earlier in Part III.

## Shear Strength According to Heger and McGrath

### Heger (1963)

2. This approach is based on principal tension stress as affected by the radial stresses in the curved member, calibrated by reference to ACI shear strength. The nominal shear strength

$$v_{b_i} \equiv \frac{V_b}{bd} = \frac{1}{Z}\left[ 1.9\ \sqrt{f'_c} + 2,500\ \rho \cdot \frac{V \cdot d}{Mm} \right] \qquad (C-1)$$

where

  $v_b$ = nominal shear strength of section, pounds/square foot

  $Z$ = correction factor for the initial curvature of the member

  $d$ = distance from extreme compression fiber to centroid of tension reinforcement

and the expression in brackets is from "Building Code Requirements for Reinforced Concrete," Sec. 11.3 (ACI 1983).

3. A simplified expression for the curvature factor $Z$ is

$$Z = 0.9\left(1 + \frac{g}{r_s}\right) + 0.45\ \frac{Mm}{V \cdot r_s} \qquad (C-2)$$

where

  $g$ = distance from center line of section to compressive resultant force

  $r_s$ = radius to inner steel cage

  $Mm = M_u - \frac{4h - d}{8} \cdot N_u$

  $M_u$ = ultimate moment acting on a cross section of width $b$, foot-pounds/foot

$N_u$ = ultimate thrust acting on a cross section of width $b$ , pounds/foot

4. After introduction of some empirical constants, Equation C-1 simplifies (Heger 1963) to

$$v_b \equiv \frac{V_b}{bd} = 1.53\sqrt{f'_c} + 320\,\frac{A_{Si}}{D_i} \tag{C-3}$$

where

$A_{Si}$ = steel area of inner cage, inches squared/feet

$D_i$ = inside diameter of pipe, feet

5. In terms of the nondimensional quantities (R/h), $\gamma$ , and $\omega$ used earlier in our work, for equal steel inside and outside, and considering $b$ = unity , Equation C-3 becomes

$$\frac{V_b}{\sqrt{f'_c}\cdot R} = \left[0.77 + 480\omega\,\frac{\sqrt{f'_c}}{f_y}\cdot\frac{1}{\left(\frac{R}{h}-\frac{1}{2}\right)}\right]\frac{(1+\gamma)}{R/h} \tag{C-4}$$

6. Assuming $\gamma = 0.7$ , $f'_c = 5{,}000$ psi, $f_y = 60{,}000$ psi as average values, Equation C-4 becomes

$$\frac{V_b}{\sqrt{f'_c}\cdot R} = \left[1.31 + 0.963\,\frac{\omega}{\left(\frac{R}{h}-\frac{1}{2}\right)}\right]\frac{1}{R/h} \tag{C-5}$$

Equation C-5 was used for the shear strength according to Heger (1963) in these calculations.

Heger and McGrath (1982b)

7. Heger and McGrath's study postulated that the critical section for diagonal tension failure of a member under shear force $V$ and moment $M$ would be at the point where

$$\frac{M}{V} = 3d \tag{C-6}$$

8. At this critical section, the "basic" shear strength is

C3

$$v_b = \frac{V_b}{bd} = (1.1 + 60\rho)\ \sqrt{f'_c} \qquad\qquad (C\text{-}7)$$

9.  Correction factors $F_N$ and $F_C$ account for the effects of thrust N and initial curvature R/d :

$$v_b = \frac{V_b}{bd} = \frac{(1.1 + 60\rho)\ \sqrt{f'_c}}{F_N F_C} \qquad\qquad (C\text{-}8)$$

in which

$$F_N = 1 - 0.12\ \frac{N}{V} \geq 0.75 \qquad\qquad (C\text{-}9)$$

and

$$F_C = \left(1 + \frac{d}{2R}\right)\ \text{for tension inside} \qquad\qquad (C\text{-}10a)$$

$$= \left(1 - \frac{d}{2R}\right)\ \text{for tension outside} \qquad\qquad (C\text{-}10b)$$

10.  Two additional correction factors of Heger are neglected here.  For b = unity , Equation C-7 can be nondimensionalized:

$$\frac{V_b}{\sqrt{f'_c}\cdot R} = \frac{1.1 + 60\omega \cdot \dfrac{f'_c}{f_y}}{F_N F_C} \cdot \frac{(1 + \gamma)}{2(R/h)} \qquad\qquad (C\text{-}11)$$

Equation C-11 was used to compute the shear strength according to Heger and McGrath (1982b) in our calculations, whereby care is necessary to distinguish between Equations C-10a and C-10b for $F_C$ .

## Internal Forces

11. To find the applied load $w_s$ under which shear failure occurs, we must equate the internal shear at the critical section to the shear strength $V_b$ as computed in the preceding sections. For this reason we must compute the internal forces due to the two loading conditions considered. From elastic analysis (Part III):

Test (radial) loading

$$N = \frac{wR}{2} \left[ (1 + k) + \frac{1}{3} (1 - k) \cos 2\theta \right] \tag{26}$$

$$V = \frac{wR}{3} (1 - k) \sin 2\theta \tag{27}$$

$$M = \frac{wR^2}{6} (1 - k) \cos 2\theta \tag{28}$$

EM loading

$$N = \frac{wR}{2} \left[ (1 + k) + (1 - k) \cos 2\theta \right] \tag{29}$$

$$V = \frac{wR}{2} (1 - k) \sin 2\theta \tag{30}$$

$$M = \frac{wR^2}{4} (1 - k) \cos 2\theta \tag{31}$$

12. These forces must be evaluated at the critical section, located at an angle $\theta_c$ .

13. For Heger (1963), the maximum shear occurs at $\theta_c = 45°$. For Heger and McGrath (1982b), Equation C-6 defines the critical section, in which M and V are inserted from Equations 27 and 28 for the test loading, and from Equations 30 and 31 for the EM loading. In either case

C5

$$\frac{M}{V} = \frac{R}{2} \cdot \frac{\cos 2\theta_c}{\sin 2\theta_c} = 3d$$

or

$$\cot 2\theta_c = \frac{6d}{R} = \frac{3(1 + \gamma)}{(R/h)} \qquad (C-12)$$

14. For given $\gamma$ and $R/h$, the location of this critical section can be determined from Equation C-12, and the appropriate forces computed from Equations 26 through 31.

15. These computations were carried out for an appropriate range of $R/h$ and $k$, and the shear force $V$ equated to the shear strengths according to Equations C-5 or C-11 in order to arrive at the shear strength $w_s/\sqrt{f'_c}$.

## Axial-Flexural Strength

16. The graphical method, suitably computerized for computation purposes, as outlined in Parts III and IV, was used for the determination of the flexural strength $w_f$ of the rings. The axial force at the critical section, which could be either at the crown or at the springing, is determined by the intersection of the radial line of appropriate slope (e/h) with the strength envelope. The corresponding load $w_f$ is then determined by elastic analysis, using the following relations.

Test loading

17. Using Equations 35 and 36, and nondimensionalizing by dividing through $h$, we obtain the nondimensionalized eccentricities for springing and crown sections:

$$\left(\frac{e}{h}\right)_{sp} = \frac{1}{2}\left(\frac{1 - k}{2 + k}\right) \cdot \frac{R}{h} \qquad (C-13)$$

$$\left(\frac{e}{h}\right)_{cr} = \frac{1}{2}\left(\frac{1 - k}{2k + 1}\right) \cdot \frac{R}{h} \qquad (C-14)$$

C6

18. The nondimensional flexural failure load is found from the non-dimensional axial force $n = N/(f'_c \cdot bh)$ at either springing or crown by statics, using Equation 3:

$$\frac{w_f}{f'_c} = \frac{3}{2 + k} \cdot n \cdot \frac{1}{R/h} \quad \text{if the springing section is critical} \qquad (C-15)$$

or

$$\frac{w_f}{f'_c} = \frac{3}{(2k + 1)} \cdot n \cdot \frac{1}{R/h} \quad \text{if the crown section is critical} \qquad (C-16)$$

EM 1110-2-2902 loading

19. Proceeding similarly, the nondimensional eccentricities for the EM loading are from Equations 37 and 38:

$$\left(\frac{e}{h}\right)_{sp} = \frac{1}{4}(1 - k) \cdot \frac{R}{h} \qquad (C-17)$$

$$\left(\frac{e}{h}\right)_{cr} = \frac{1}{4}\left(\frac{1 - k}{k}\right) \cdot \frac{R}{h} \qquad (C-18)$$

and the failure loads are computed from the nondimensional axial force $n = N/(f'_c \cdot bh)$ , using Equation 5:

$$\frac{w_f}{f'_c} = n \cdot \frac{1}{R/h} \quad \text{if the springing section is critical} \qquad (C-19)$$

or

$$\frac{w_f}{f'_c} = k \cdot n \cdot \frac{1}{R/h} \quad \text{if the crown section is critical} \qquad (C-20)$$

Ratio is $w_f/w_s$ since the shear strength $w_s$ according to Heger is proportional to $\sqrt{f'_c}$ , but the flexural strength $w_f$ is a function of $f'_c$ , the ratios differ for different concrete strengths.

20. In calculating, the ratio in terms of the concrete strength $f'_c$ is given by $w_f/f'_c \Big/ w_s/\sqrt{f'_c}$ , therefore the actual ratio

$$\frac{w_f}{w_s} = \sqrt{f'_c} \cdot \frac{w_f/f'_c}{w_s/\sqrt{f'_c}}$$

All calculations were carried out for concrete strength, $f'_c = 5,000$ psi.

APPENDIX D:  NOTATION

| | |
|---|---|
| $A_s$ | Area of flexural reinforcement in tension |
| $A_{si}$ | Steel area of inner cage, inches, squared/feet |
| $A_{so}$ | Steel area of outer cage |
| $A_{st}$ | Total area of reinforcement in section (inner and outer cages) |
| $b$ | Width of section |
| $c$ | Distance from extreme compression fiber to the neutral axis |
| $d$ | Distance from extreme compression fiber to centroid of tension reinforcement |
| $d'$ | Distance from extreme compression fiber to centroid of compression reinforcement |
| $D_i$ | Inside diameter of pipe, feet |
| $e_{avg}$ | Eccentricity based on averages of moment and thrust values at crown and springing |
| $e_{cr}$ | Eccentricity at crown |
| $e_{sp}$ | Eccentricity at springing |
| $E_u$ | Ultimate compression strain |
| $E_c$ | Initial elastic concrete modulus |
| $E_s$ | Modulus of elasticity of steel |
| $f'_c$ | Compressive strength of concrete |
| $f_y$ | Yield strength of reinforcing steel |
| $F_c$ | Correction factor for effects of initial curvature |
| $F_N$ | Correction factor for effects of thrust |
| $g$ | Distance from center line of section to compressive resultant force |
| $h$ | Overall depth of section |
| $k$ | Ratio of lateral earth pressure to vertical earth pressure |
| $k_{act}$ | Actual value of $k$ at failure for test specimen |
| $m$ | Nondimensionalized moment |
| $m_{sp}$ | Nondimensionalized moment at springing |
| $m_{cr}$ | Nondimensionalized moment at crown |
| $M_{avg}$ | Average of internal moments at springing and crown acting on a cross section of width $b$, ft-lb/ft |
| $M_{cr}$ | Internal moment at crown acting on a cross section of width $b$, ft-lb/ft |
| $M_{sp}$ | Internal moment at springing acting on a cross section of width $b$, ft-lb/ft |
| $M_u$ | Ultimate moment acting on a cross section of width $b$, ft-lb/ft |
| $n$ | Nondimensionalized axial force |
| $n_{cr}$ | Nondimensionalized axial force at crown |

| | |
|---|---|
| $n_{sp}$ | Nondimensionalized axial force at springing |
| $N_{avg}$ | Average of internal thrust at springing and crown acting on a cross section of width $b$, lb/ft |
| $N_{cr}$ | Internal thrust at crown acting on a cross section of width $b$, lb/ft |
| $N_{sp}$ | Internal thrust at springing acting on a cross section of width $b$, lb/ft |
| $N_u$ | Ultimate thrust acting on a cross section of width $b$, lb/ft |
| $p_N$ | Radial pressure acting on a unit length of ring |
| $p_T$ | Tangential traction acting on a unit length of ring |
| $P_{cr}$ | Concentrated crown load in a 16-point test loading, lbs |
| $P_f$ | Flexural strength of conduit defined as distributed load on conduit at failure in flexural mode |
| $P_s$ | Shear strength of conduit defined as distributed load on conduit at failure in shear mode |
| $r_s$ | Radius to inner steel cage |
| $R$ | Outer radius of conduit |
| $v_b$ | Nominal shear strength of section, $lb/ft^2$ |
| $V_b$ | Shear strength at critical section, lb |
| $w$ | Uniform vertical pressure |
| $X$ | Resultant of horizontal forces acting on ring due to earth pressures |
| $X_N$ | Normal component of horizontal forces acting on ring due to earth pressures |
| $X_T$ | Tangential component of horizontal forces acting on ring due to earth pressures |
| $Y$ | Resultant of vertical forces acting on ring due to earth pressures |
| $Y_N$ | Normal component of vertical forces acting on ring due to earth pressures |
| $Y_T$ | Tangential component of vertical forces acting on ring due to earth pressures |
| $Z$ | Correction factor for initial curvature of member used in American Concrete Institute 318-83 equation for strength |
| $\alpha, \beta$ | Rectangular stress block constants |
| $\gamma$ | Dimensionless cross-sectional parameter used in development of nondimensional strength envelopes |
| $\epsilon$ | Strain |
| $\theta_u$ | Rotation capacity |
| $\rho$ | Tensile reinforcement ratio |
| $\phi_u$ | Ultimate curvature |

$\omega$     Reinforcing index, dimension term used in development of nondimensional strength envelope

$\omega_{cr}$     Reinforcing index for crown section

$\omega_{sp}$     Reinforcing index for springing section

$\omega_t$     Total reinforcing index accounting for inside and outside circular reinforcement